3D Biofabrication of Cell-laden Alginate Hydrogel Structures

Atabak Ghanizadeh Tabriz

Submitted for the Degree of Doctor of Philosophy

Heriot-Watt University

Institute of Mechanical, Process and Energy Engineering

June 2017

Abstract

Biofabrication has been receiving a great deal of attention in tissue engineering and regenerative medicine either by manual or automated processes. Different automated biofabrication techniques have been used to produce cell-laden alginate hydrogel structures, especially bioprinting approaches. , These approaches have been limited to 2D or simple 3D structures, however. In this thesis, a new extrusion-based bioprinting technique and a new simple, manual 3D biofabrication method are presented to culture cells in 3D. These methods do not rely on any complex fabrication methods. The bioprinting technique was developed to produce more complex alginate hydrogel structures. This was achieved by dividing the alginate hydrogel cross-linking process into 3 stages: primary calcium ion cross-linking for printability of the gel, secondary calcium cross-linking for rigidity of the alginate hydrogel immediately after printing and tertiary barium ion cross-linking for the long-term stability of the alginate hydrogel in the culture medium. Simple 3D structures including tubes were first printed to ensure the feasibility of the bioprinting technique. Complex 3D structures, such as branched vascular structures, were subsequently printed successfully. The static stiffness of the alginate hydrogel after printing was 20.18 ± 1.62 kPa which was rigid enough to sustain the integrity of the complex 3D alginate hydrogel structure during the printing. The addition of 60 mM barium chloride was found to significantly extend the stability of the cross-linked alginate hydrogel from 3 days to beyond 11 days without compromising the cellular viability. The results based on cell bioprinting suggested that the viability of U87-MG cells was 92.94 ± 0.91 % immediately after bioprinting. Cell viability was maintained above 88 ± 4.3 % in the alginate hydrogel over a period of 11 days.

On the other hand, the manual biofabrication approach developed in this thesis enabled the fabrication of scalable 3D cell-laden hydrogel structures easily, without complex machinery. The technique could be carried out using only apparatus available in a typical cell biology laboratory. The fabrication method would involve micro coating cell-laden hydrogels covering the surface of a metal bar by dipping into cross-linking reagent $CaCl_2$ or $BaCl_2$, to form hollow tubular structures. This method could be used to form single- or multi-layered tubular structures. This fabrication method has incorporated the use alginate hydrogel as the primary biomaterial and secondary biomaterial could be added depending on the desired application. The feasibility of this method has been demonstrated by showing the cell survival rate and normal

responsiveness of cells within these tubular structures using mouse dermal embryonic fibroblast cells and human embryonic kidney 293 cells containing a tetracycline responsive red fluorescence protein (tHEK cells). By adjusting the fabrication protocol, complex hollow alginate hydrogel structures could be generated.

Acknowledgments

I would like to thank the Almighty God to put me on this path to complete this thesis with his blessings and guidance.

I would like to express my deepest gratitude to my supervisor, Professor Will Shu throughout the 4 years of my PhD for being patient, passionate and helpful on my progress. He was not only a supervisor helping me in an academic aspect but he was like a brother to me constantly giving me valuable life lessons to be always motivated in life which helped me to gain valuable experiences.

I would like to thank my parents Mr. Akbar Ghanizadeh Tabrizi and Mrs. Forough Parvaneh Davtalabi who have always been supporting me emotionally and financially and were there for me all the time. Without their help and support I would not be where I am now.

I am very grateful to be granted the scholarship by Heriot Watt University to support my studies throughout the four years of the PhD.

ACADEMIC REGISTRY
Research Thesis Submission

Name*:*	Atabak Ghanizadeh Tabriz		
School:	School of Engineering and Physical Sciences		
Version: *(i.e. First, Resubmission, Final)*	Final	Degree Sought:	PhD Mechanical Engineering

Declaration

In accordance with the appropriate regulations I hereby submit my thesis and I declare that:

1) the thesis embodies the results of my own work and has been composed by myself
2) where appropriate, I have made acknowledgement of the work of others and have made reference to work carried out in collaboration with other persons
3) the thesis is the correct version of the thesis for submission and is the same version as any electronic versions submitted*.
4) my thesis for the award referred to, deposited in the Heriot-Watt University Library, should be made available for loan or photocopying and be available via the Institutional Repository, subject to such conditions as the Librarian may require
5) I understand that as a student of the University I am required to abide by the Regulations of the University and to conform to its discipline.
6) I confirm that the thesis has been verified against plagiarism via an approved plagiarism detection application e.g. Turnitin.

* *Please note that it is the responsibility of the candidate to ensure that the correct version of the thesis is submitted.*

Signature of Candidate*:*		Date:	

Submission

Submitted By *(name in capitals):*	
Signature of Individual Submitting:	
Date Submitted:	

For Completion in the Student Service Centre (SSC)

Received in the SSC by *(name in capitals):*			
Method of Submission *(Handed in to SSC; posted through internal/external mail):*			
*E-thesis Submitted (**mandatory for final theses)***			
Signature:		Date:	

Table of Contents

List of figures

Abbreviations

2D	Two dimensional
3D	Three dimensional
ABS	Acrylonitrile butadiene styrene
AM	Additive manufacturing
bECs	Bovine aortic endothelial cells
CAD	Computer aided design
dSMCs	Canine smooth muscle cells
DOD	Drop-on-Demand
ECACC	European Collection of Cell Cultures
ECM	Extracellular matrix
EDTA	Ethylenediaminetetraacetic acid
EGFP	Enhanced green fluorescent protein
FBS	Fatal bovine serum
FDM	Free deposition modelling
HAFSCs	Human amniotic fluid-derived stem cells
hES	Human Embryonic stem cells
hMSC	Human mesenchymal stem cells
HMVEC	Human dermal microvascular endothelial cells
LIFT	Laser-induced forward transfer
MAPLE DW	Matrix-assisted pulsed laser evaporation direct writing
MDCKII	Madin-Darby canine kidney cells
MEM	Minimum essential medium
NEAA	L-Glutamine, non-essential amino acids

NHS	National Health Service
PBS	Phosphate buffered solution
PCL	Polycaprolactone
PDMS	Polydimethylsiloxane
PLA	Polylactic acid
PMMA	Poly (methyl methacrylate)
RP	Rapid prototyping
SEM	Scanning electron microscope
SFF	Solid free-form fabrication
TE	Tissue engineering
tHEK	Human embryonic kidney cells
U-87-MG	Glioblastoma
UV	Ultraviolet

LIST OF PUBLICATIONS BY THE CANDIDATE

1. A. Ghanizadeh Tabriz, W. Shu. 3D bioprinting of Organ-like alginate hydrogel structures, *Biofabrication Conference,* Pohang University, South Korea (2014), Sep 28th – Oct 1st

2. A. Ghanizadeh Tabriz, A.H. Hermida, N.R. Leslie, W. Shu. Three-dimensional bioprinting of complex cell laden alginate hydrogel structures. *Biofabrication* 7(4) 045012. (2015)

3. A. Ghanizadeh Tabriz, G.M. Mills, A.H. Hermida, N.R. Leslie, J.J. Mullins , J.A. Davis, W. Shu. 3D Biofabrication of cell-laden hydrogel for tissue engineering, *IMPEE conference,* Heriot Watt University, UK (2015)

4. Z.E. Dieseru, **A. Ghanizadeh Tabriz**, W. Shu. 3D printing and mechanical characterisation of microstructure tissue scaffolds. *Proceedings of the Institution of Mechanical Engineers, Part H: Journal of Engineering in Medicine* (In preparation)

5. A. Ghanizadeh Tabriz, G.M. Mills, A.H. Hermida, N.R. Leslie, J.J. Mullins , J.A. Davis , W. Shu Rapid fabrication of cell-laden alginate hydrogel structures by dip coating. *Frontiers in Bioengineering and Biotechnology 5(2017)*

Chapter 1- Introduction & Literature Review

1.1 Introduction

Tissue engineering is rapidly developing biomedical field, which is defined as "an interdisciplinary field that applies the principles of engineering and life sciences toward the development of biological substitutes that restore, maintain, or improve tissue function or a whole organ" [1]. The field of tissue engineering was once considered as a subfield of biomaterials. But as the importance of this field became better understood and recognised, it is now considered to be an individual field on its own.

Biofabrication as an emerging field that focuses on the use of biological cells, biological matters and biomaterials in order to produce biological systems. The combination of biofabrication and tissue engineering bring out the field of bioprinting and bioassembly. These involve either direct spatial arrangements of cells and biomaterials or automated process of cell assembly containing building blocks [2].

3D printing is recognised as Solid Freeform Fabrication (SFF), Additive Manufacturing (AM) and Rapid Prototyping (RP). A common application in the engineering world and various industries is to create a new prototype before releasing the original product. The prototype would be useful in order to make further improvements to the product. 3D printing could also be used directly for developing final products. 3D printing is a layer by layer fabrication process where the layers are laid on top of each other until a 3D structure is formed. The resolution of the part is based on two aspects. One is vertical resolution (Z resolution) which is the smallest achievable layer thickness. Another is horizontal resolution which is the smallest feature size that can be made through the XY plane. The 3D printing process can be performed by means of different technologies. 3D printing technologies used in bioprinting field could be classified as follows: Inkjet based, valve based, extrusion based and laser based bioprinting [3].

Foundation studies of tissue engineering (TE) include the investigation of cell and tissue coalescence phenomena [4, 5], tissue affinity [6], cell adhesion [7] and the fluidity of embryonic tissue [8]. These fundamentals are necessary and essential to enable the process of tissue regeneration for tissues such as liver tissue [8], skin tissue [9], nerve [10] or any other tissues. Based on these fundamentals, cell aggregation and blood vessels can be assembled without use of synthetic polymers [11] using engineered

spheroids [12]. A better understanding of these fundamentals is therefore needed to enable further development and progress in tissue engineering.

The main goal of tissue engineering is the fabrication of synthetic tissue and organs to replace or repair damaged tissue or organ. The main motivation for this is the current crisis of organ shortage for medical transplantation. It was reported in 2012 that in the USA only 26,246 transplantations were performed, while 112,905 patients were still on the waiting list for organs [13]. This means more than 75% of patients were not given their treatment due to organ shortage. A report from National Health Service (NHS) from the United Kingdom in 2011/2012 states that only 3960 organ transplants were performed while 3676 other registered patients were on the waiting list [14]. To make the problem worse, transplantations are not always successful due to organ rejection or infection. These numbers do not reflect the situation less affluent countries where it could be much worse.

Conventional scaffold-based fabrication technologies such as phase separation [15, 16], melt moulding [17, 18], fibre networking [19, 20], gas foaming [21-24], freeze drying [25, 26] and particle leaching [27-29] have been used for tissue regeneration and tumour models. However, the conventional scaffold-based approaches do not provide full control over the inner and outer geometry of the structure. This results in a heterogeneous structure with varying permeability and porosity due to the lack of control over the mechanical properties of the scaffold. Rapid Prototyping (RP) technologies, a more design-dependent method, could possibly overcome the control over mechanical properties, porosity and permeability of the scaffolds.

In recent years, organ printing has emerged as a new area in tissue engineering to tackle some of the problems with organ fabrication. Organ printing differs from conventional tissue engineering, which is mainly based on manual and labour-intensive methods of fabricating scaffold or tissue.

Organ printing makes use of automated Solid Freeform Fabrication (SFF) technology (e.g. 3-dimensional fabrication) where cells and scaffold materials are deposited layer by layer until a 3D structure is formed. The recent progress based on bioprinting using

different RP technologies will be discussed in detail in the literature review later in this chapter.

The literature review of this thesis will cover 3D printing, 3D bioprinting and some of the hydrogel materials used for TE. A background based on different 3D printing technologies will be briefly described in this chapter. 3D bioprinting techniques and the use of different bio-inks for live cell printing into programmable patterns will be discussed. Each 3D bioprinting technique including their advantages and disadvantages will be described in detail. Finally, the conclusions will cover the outcome of the literature review and breakdown of each chapter for completion of this thesis.

1.2 Inkjet based printing

Inkjet based printing is used to assist tissue engineering. These are normal printers that are available off–the-shelf. The first ever commercially available Inkjet printer was introduced by Siemens in 1951 as a medical strip chart recorder [30]. Inkjet printers work based on two different mechanisms: drop-on-demand (DOD), as shown in Figure 1.1, and continuous ejection mechanism, shown in figure 1.2. In drop-on-demand systems, electrical signals are used to control the ejection of an individual droplet. In continuous-drop systems, ink emerges continuously from a nozzle under pressure. The jet then breaks up into a train of droplets, the direction of which is controlled by electrical signals [31]. Ejection of the droplets is caused by the pressure pulses created by thermal, piezoelectric or acoustic actuators. Both mechanisms have the capability to be operated with droplets ranging from 15 to several hundred microns [32]. Inkjet printing technology in the bioprinting field was first developed by Wilson and Boland in 2003 at the Bioengineering Department in Clemson University USA. Wilson and Boland's method was designed to dispense protein and viable cell solutions such as bovine aortal endothelial cells and smooth muscle cell line. Viability assays indicated roughly 75% of cells were viable after this bioprinting process [33]. Cell viability is usually defined by the number of live cells over the total number of cells.

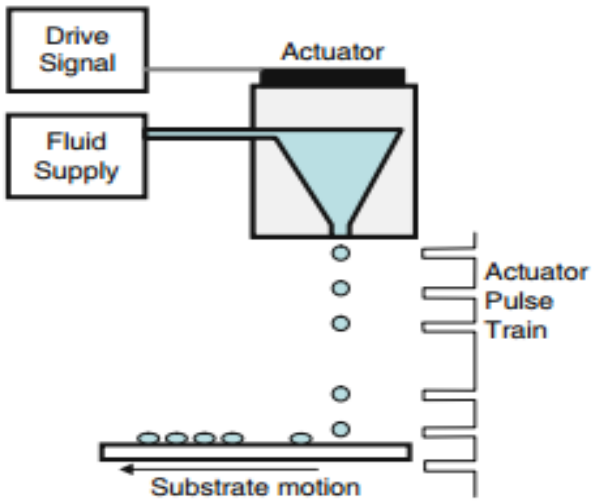

Figure 1.1 *– Inkjet printing by Drop-On-Demand mechanism [34]*

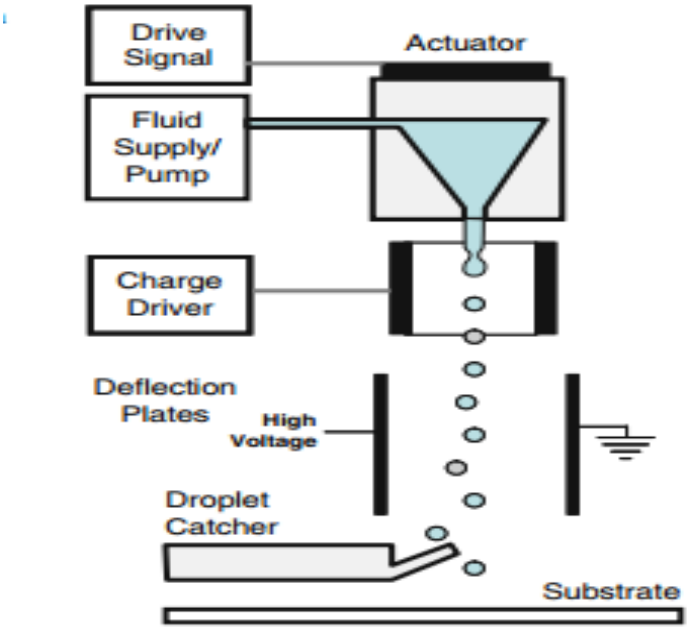

Figure 1.2 *– Inkjet printing by continues ejection mechanism [34]*

The same team in Clemson University have applied thermal inkjet printing to fabricate microvasculature. The concept is to remove the ink from the cartridges, sterilise them and replace the ink with endothelial cells and thrombin as its bio-ink. A fibrinogen substrate is used as the bio-paper and where the cells in the bio-ink are deposited, a fibrin channel will form on the substrate as shown in Figure 1.3 [35]. Fibrin is polymerized using fibrinogen and thrombin solutions [36] and plays a key role for

natural wound healing. Fibrin could be taken from the patient's own blood [37] and it has been widely used as a scaffold material for tissue engineering such as chondrocytes [38] skeletal muscle cells [39] and smooth muscle cells [40].

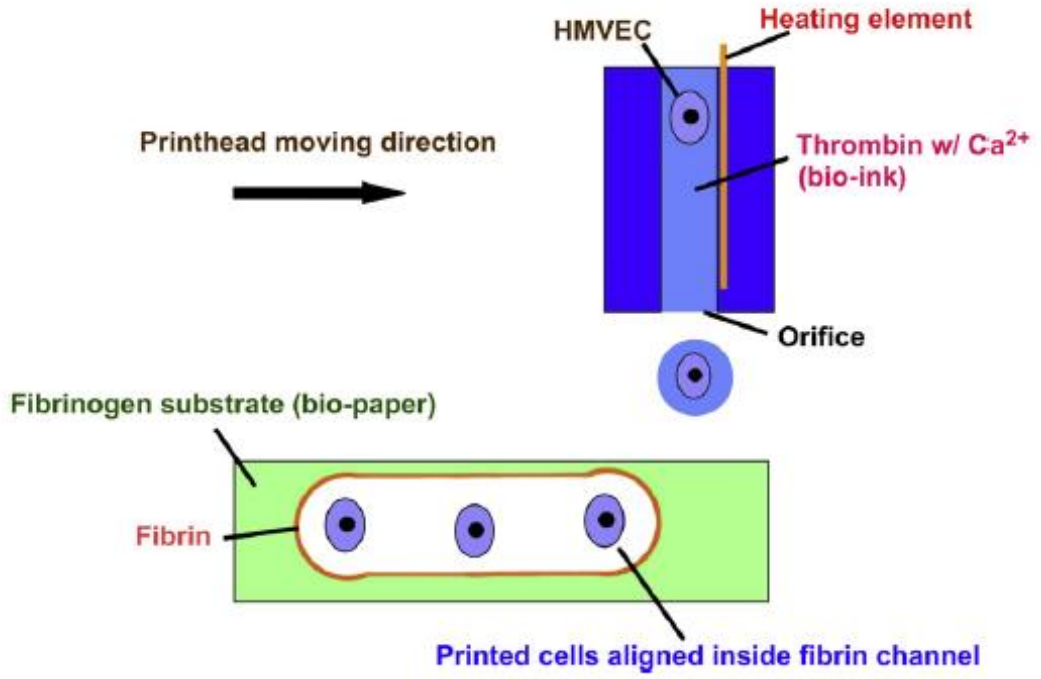

Figure 1.3 *– Schematic drawing for simultaneous dispositions of HMVEC and fibrin channels scaffolds using inkjet printing [35].*

Another research group from Wake Forest Institute for Regenerative Medicine in the USA has used thermal inkjet printing to construct a complex heterogeneous tissue containing multiple cell types. Cartridges were emptied and each of them was filled with different cells mixed with calcium chloride. The cell types used were canine smooth muscle cells (dSMCs), bovine aortic endothelial cells (bECs) and human amniotic fluid-derived stem cells (hAFSCs). Each cell type was printed into a pie-shaped structure in different locations (Figure 1.4 and Figure 1.5) and was delivered into a sodium alginate-collagen composite. The reaction between the calcium chloride and sodium alginate-collagen resulted in the rapid formation of the gel. Since the structure had a thickness, the inkjet printer was modified by adding a vertical axis motion. The heterogeneous construction was evaluated *in vivo* and *in vitro* where the cells remained viable with normal proliferation rates, phenotypic expression and physiological function. The viability of the printed constructs was evaluated at day 1, 4 and 7 after culturing [41].

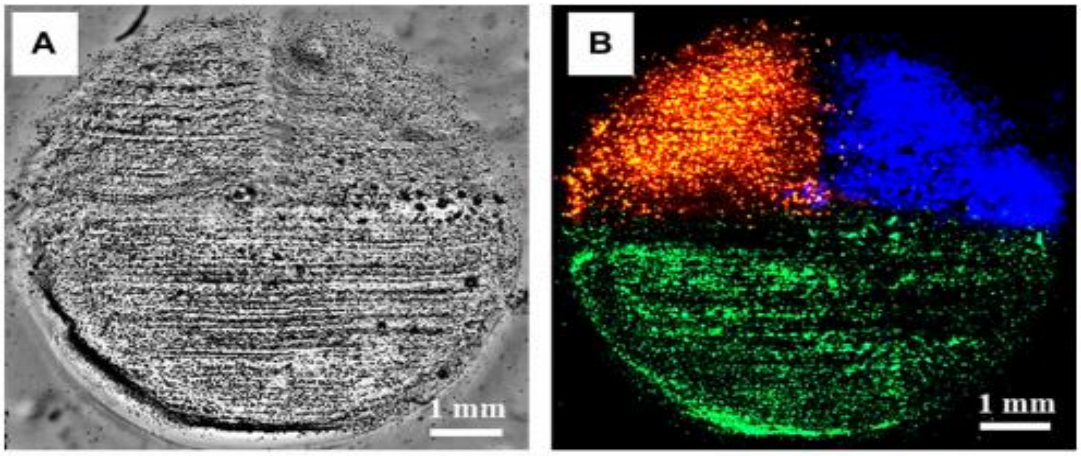

Figure 1.4 *– Light (A) and fluorescence (B) microscopic top views of a complete 3D multi-cell "pie" construct before implantation. The cells that appear green are bECs labelled with PKH 26 dyes; the cells that appear blue are hAFSCs tagged with CMHC dyes; the cells that appear red are dSMCs labelled with PKH 67 dyes. Different cells were located onto their predetermined locations after printing [41].*

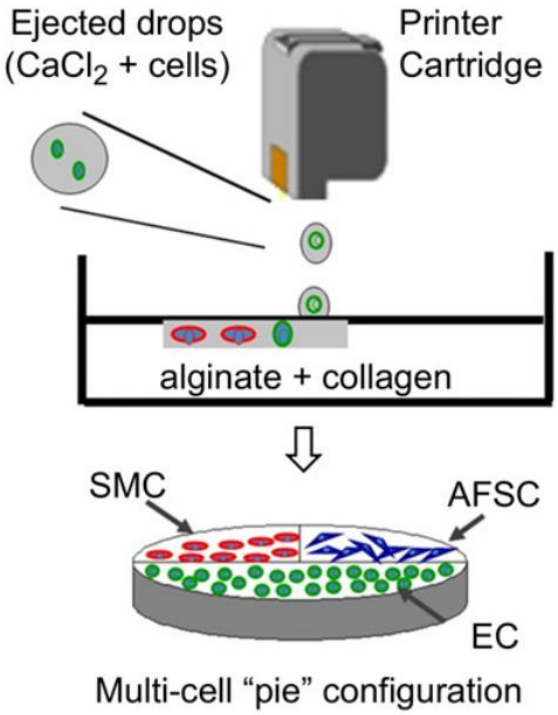

Figure 1.5 *– Schematic drawing of applying inkjet printing to fabricate multi-cell heterogeneous tissue constructs[41].*

A research group from the University of Toyama in Japan developed a piezoelectric inkjet printer to bioprint alginate hydrogel tubular structures. The custom-made Inkjet 3D bioprinter used a piezoelectric type inkjet head where sodium alginate solutions at 0.8 % weight to volume ratio (w/v) were inkjet-printed into a cross-linking reagent of

2% (w/v) $CaCl_2$ bath prepared in hyaluronan or polyvinyl alcohol (PVA) at 0.5 % or 15 % respectively. The cross-linked alginate micro beads generated by this approach ranged from 26 µm to 38 µm in diameter. In order to produce tubular structures, the print head would move in a circular motion to print a 2D ring structure in the $CaCl_2$ bath. This process would be repeated several times to generate alginate hydrogel tubular structures as shown in Figure 1.6. [42]

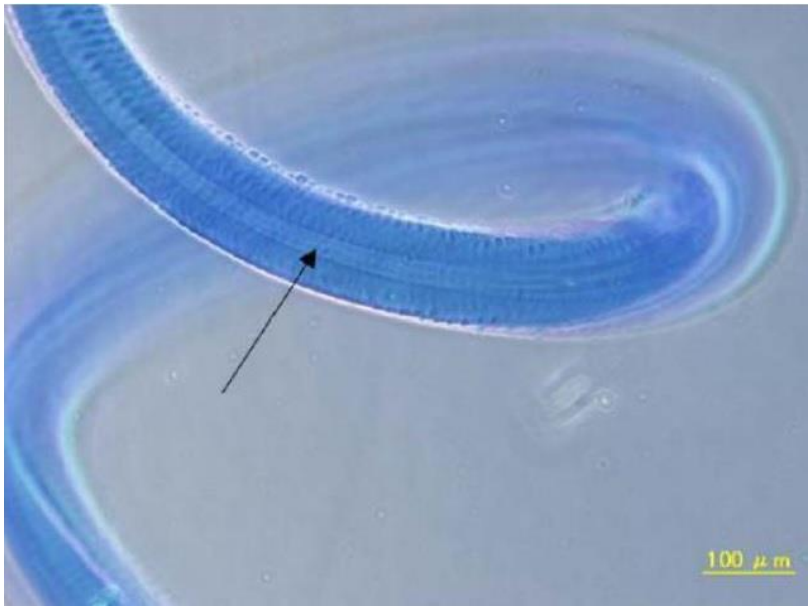

Figure 1.6 *– A hollow alginate hydrogel tubular structure printed by Inkjet head using pizo type inkjet head [42].*

Despite being capable of printing viable cells with suitable resolution, inkjet bioprinting technologies are not sufficiently well adopted to build up 3D cell-laden structures. This is due to the inability of inkjet printing to print viscous material that would result in less favourable mechanical properties of the cell-laden structures [43]. In general alginate hydrogel at concentrations of less than 2% (w/v) is recommended for use in inkjet-based bioprinting [44-46].

1.3 Laser-based bioprinting

Laser-based printing was first commercially available in 1976 when IBM created a nozzle-free dispensing system called IBM 300. [47] The first ever laser based printer to print 2D cell patterns was developed in 1999 by Odde and Renn [48].

The laser-based technologies that are mainly used in bioprinting field are laser-induced forward transfer (LIFT) and matrix-assisted pulsed laser evaporation direct writing (MAPLE DW). These techniques (shown in Figure 1.7) work in similar manners where a laser transparent ribbon is placed underneath a layer glass or quartz. A cell solution suspended in a culture medium with either glycerol or hydrogels is coated onto the bottom of the ribbon. Cell solutions usually have a concentration of around 1×10^8 cells/mL depending upon the cell type, where the coated solution on the ribbon ranges from 10 μm to 100 μm thick [49, 50]. The receiving substrate is usually placed from a distance of 30 μm to 1000 μm from the ribbon [51]. To dispense the cells a laser pulse is directed at the ribbon, causing the formation of a bubble. The shock waves caused by the formation of the bubble eventually force the cells to be dispensed towards the substrate. Laser-based printing is the only nozzle-free dispensing approach. It has a higher dispensing resolution compared to the other bioprinting technologies, making it a superior bioprinting technology to print single cells. For example, mammalian cells could be printed onto a hydrogel substrate as individual cells [52], which could allow bioprinting of the smallest parts of certain human body organs or tissues. Laser fluence and the biomaterial during printing will have a direct effect on cell viability however. A study from Chrisey and his co-workers from Clemson University used the LIFT technique to bioprint NIH 3T3 fibroblast cells suspended in 1% (w/v) alginate solution in the medium and $CaCl_2$ cross-linking reagent for 2 minutes and 10 minutes [53]. The study indicated that higher laser fluence resulted in lower cell viability. This is due to shear stresses/strains developed during jet/droplet formation [54] and landing [55, 56].

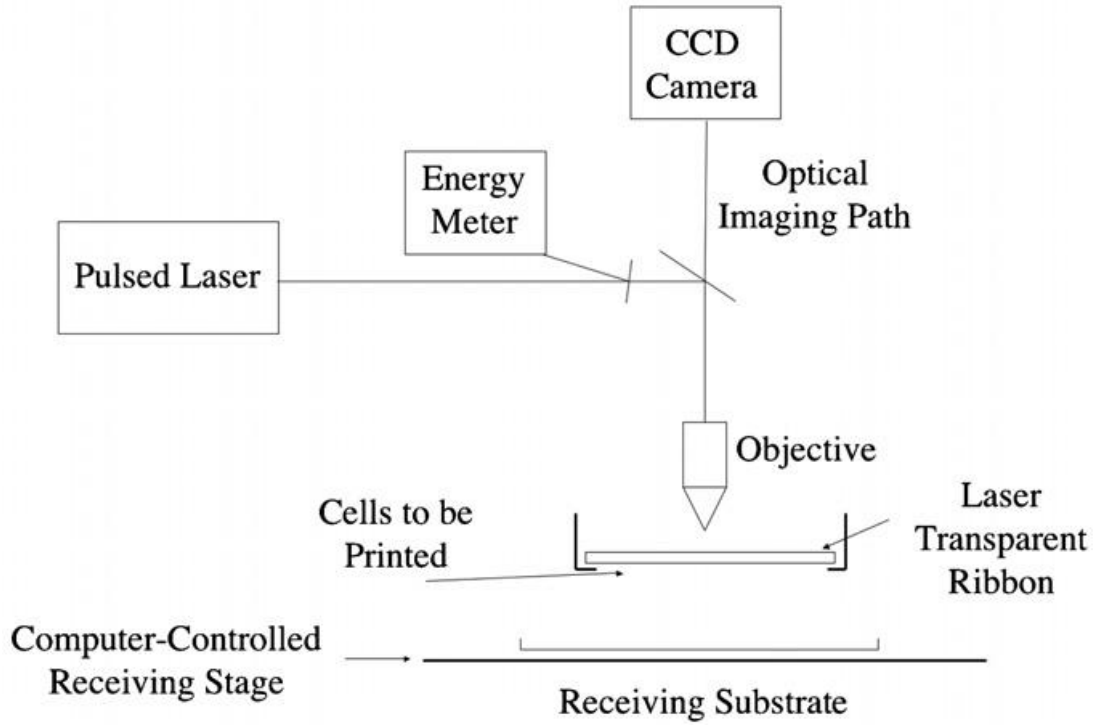

Figure 1.7 *– Working principle of laser-induced forward transfer (LIFT), and matrix-assisted pulsed laser evaporation direct writing (MAPLE DW) [57]*

Laser-based bioprinting is a capable of printing higher viscosity biomaterials compared with inkjet-based bioprinting. This makes it a superior technology for printing structures with better mechanical properties. For instance, the department of biomedical engineering at Renseeler Polytechnic Institute has used 8% (w/v) alginate as a popular hydrogel material to create cell-encapsulated microbeads [58, 59]. Human breast cancer cells (ATCC, Manassas, VA) suspended in a 2% alginate and 10% gelatine composition were dispensed using LDW into a 2% (w/v) calcium chloride solution to cross-link the beads as shown in Figure 1.8. Cells encapsulated with the microbeads had a viability of 89.6%, decreasing to 84.3% after five days of culture. This makes this technology suitable for drug discovery applications [59].

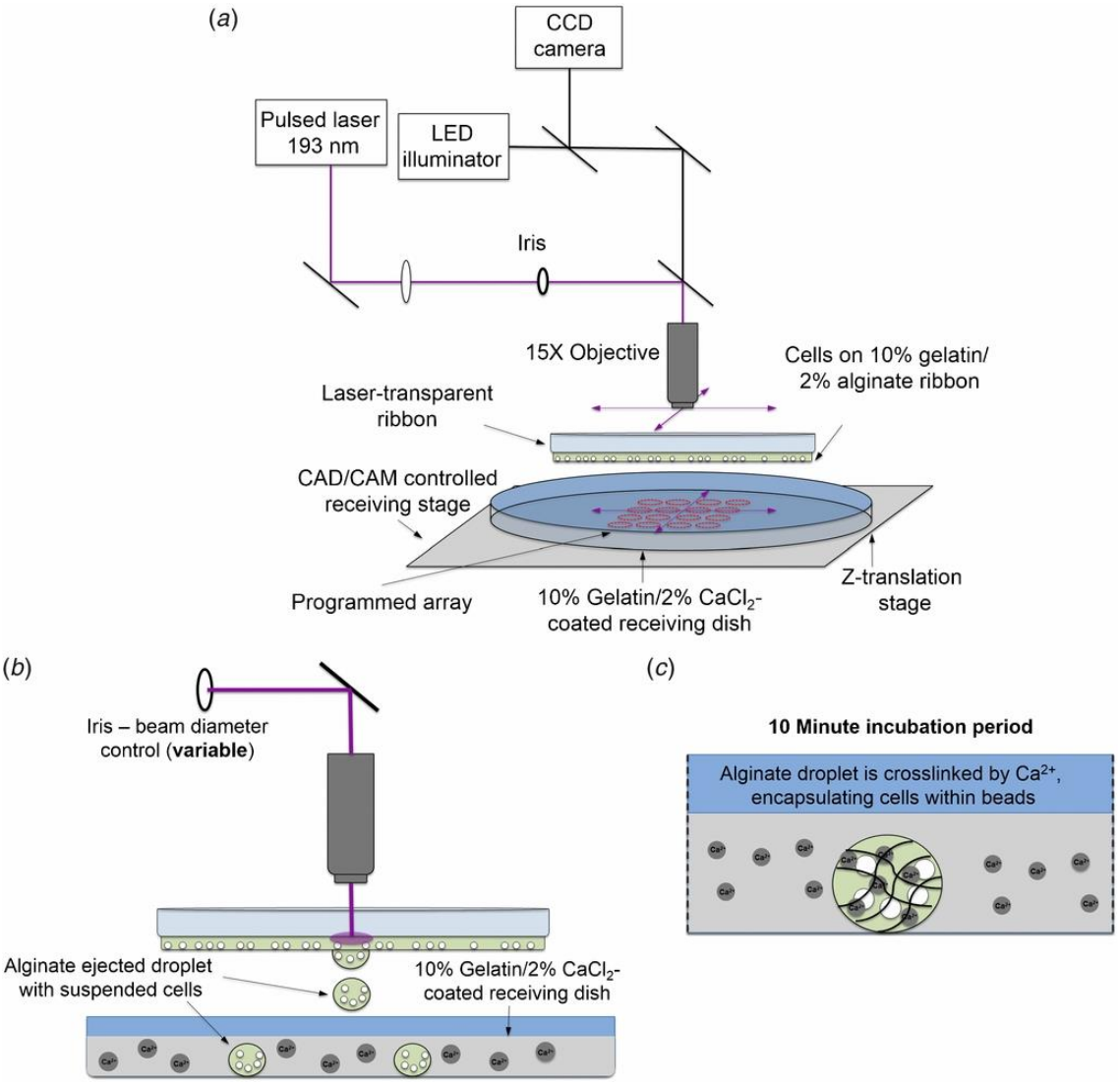

Figure 1.8 *– Schematic drawing of laser-based bioprinting of encapsulated human breast cancer cells in alginate-gelatine microbeads cross-linked with 2% $CaCl_2$ for 10 minutes [60].*

With the ability to print more viscous materials by laser-based printing it is possible to print more rigid structures, generating structures with greater complexity compared to printing in 2D or 3D with limited aspect ratio. The team at Renseeler Polytechnic Institute has used laser-based printing to produce alginate tubular structures with 2%, 4%, 6% and 8% alginate hydrogel. In this approach, the ribbon containing the alginate hydrogel is placed 1 mm above the $CaCl_2$ solution with 2% concentration. The alginate beads are deposited through the laser pulse into the moving platform, which is submerged in the $CaCl_2$ solution to cross-link the alginate hydrogel. [61] This process repeats several times while the moving platform is further submerged into the cross-linking bath until the tube structures are formed. The study showed that tubular structures printed with higher alginate concentrations under the same laser power of

1437 ± 28 mJ cm^{-2} created rings with better uniformity and printing resolution. In their recent studies (figure 1.9), the team at Renseeler Polytechnic Institute used a lower alginate hydrogel concentration of 2% rather than 8% as this gave better diffusion of oxygen, nutrient, and wastes [62]. Mouse fibroblast cells were suspended in 2% alginate bio-ink and printed into a 2% $CaCl_2$ solution with cell culture medium at 1:1 (v/v) [63]. However, the cell viability was around 60% immediately after printing. This indicates that this approach is not still suitable for printing highly viable cells in 2% alginate, which is a mid-range viscosity bio-ink.

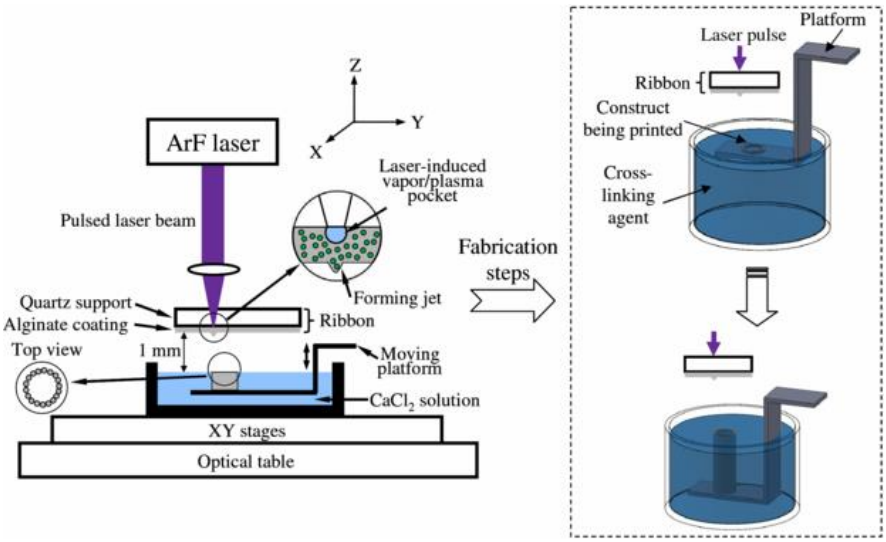

Figure 1.9 *– Schematic drawing of the laser based printing setup to printing hydrogel tabulator structures [60].*

1.4 Valve based printing

Valve based printing is a relatively new technique emerging in the last decade in which the bioprinting world has been under development. Valve-based printing works in a similar manner to inkjet-based printing, where droplets are dispensed from a reservoir through a nozzle using static air pressure. The bio-ink is dispensed once the voltage-controlled valve is activated [64, 65]. The droplet size is determined by the nozzle diameter, air pressure and valve opening time [66].

Valve based bioprinting was first developed by Demirci and his co-workers. The cell types to verify the feasibility of this novel technology were mammalian cells: AML-12 hepatocytes, NIH-3T3 fibroblasts, HL-1 cardiomyocytes, mouse embryonic stem cells and RAJI cells. All printed cell types had a viability over 89%, indicating this novel technology is very gentle on cells [65].

In 2013 Shu and his co-workers described a microvalve based printing method for bioprinting human embryonic stem cells to form cell aggregates.[67] This was the first time human embryonic stem cells were printed, opening up tremendous applications in stem cell studies in the future. The human embryonic stem cells (hES) cells were printed under various air pressures ranging from 4 PSI to 23 PSI. Cell viability was over 70 % after 24 hrs of culture and over 80% after 72 hrs of culture after bioprinting for all the pressures.

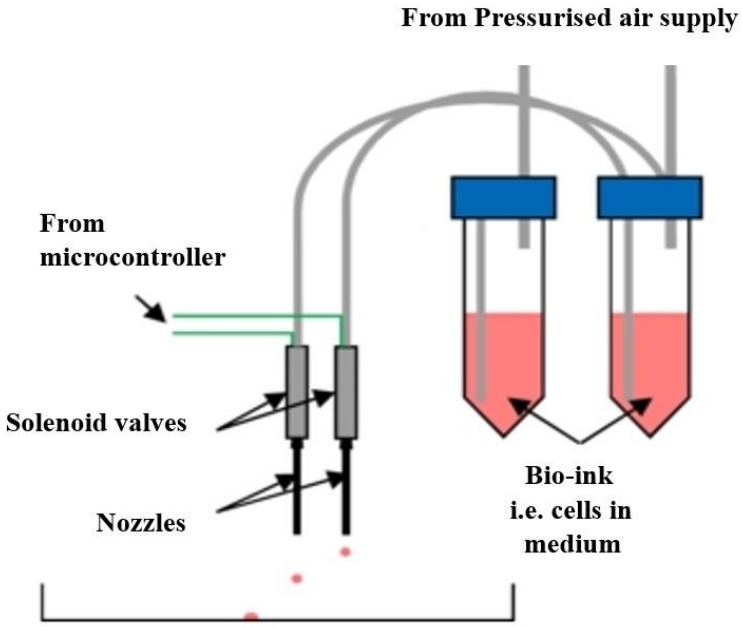

Figure 1.10 *– Schematic of valve-based printing compatible to bioprint viable hES cells [66]*

The same techniques have also been used to bioprint a novel DNA hydrogel material with live cells in millilitre-range structures [68]. It is reported that pluripotent stem cells could be differentiated into hepatocyte-like cells for 3D mini-liver generation [69]. Similar to inkjet based printing, valve based printing is currently limited to printing highly viscous materials despite being very gentle on cells, especially embryonic stem cells. It is therefore difficult to generate larger 3D structures with a degree of complexity [69].

1.5 Extrusion-based bioprinting

Extrusion-based printing works in a different manner compared with the other printing methods explained in this chapter. Instead of ejecting droplets into a pre-designed format, materials are continuously deposited as filaments through a nozzle layer by layer until a 3D structure is constructed. Extrusion-based printing is derived from fused deposition modelling (FDM), which was developed in the 1980s by Scott Crump. The first commercially available FDM printer was created in 1990 by Stratasys [70]. FDM usually works by extruding plastic or metals via heat; softer materials such as ceramic are extruded by mechanical pressure.

Extrusion-based systems in bioprinting all work in a similar manner, where hydrogel/ bio-inks are extruded via pressurised air, rotary screw or by a piston (as shown in Figure 1.11). Extrusion-based systems using pressurised air can dispense a variety of materials such as pure liquids [71] pastes [72] and semi-molten polymers [73]. The main disadvantage of this approach is the inability to extrude highly viscous material due to the limitation of air pressure [74]. Piston-driven and screw-driven depositions allow the printing of more viscous materials, making these a more suitable approach for the printing of 3D structures with more onerous mechanical properties.

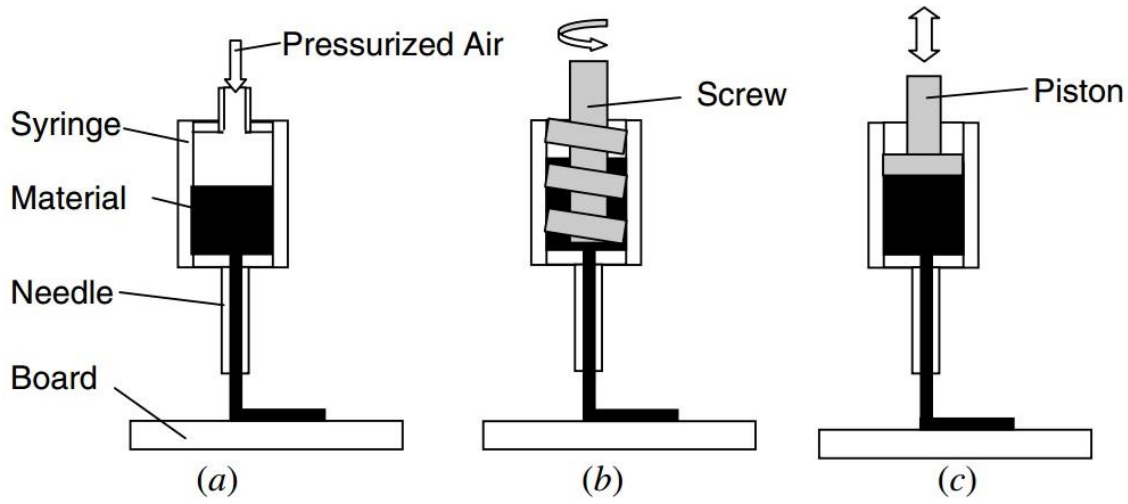

Figure 1.11 *– extrusion based printing with different mechanisms. (a) Extruded filaments via pressurised air, (b) rotary system and (a) mechanical piston.*

Using higher viscosity materials will result in 3D structures with better mechanical properties. However, due to the higher shear stress and surface tension applied to the materials/bio-inks during their extrusion [75-79] there is a risk of damage to the plasma membrane, reducing cell viability [80, 81]. For this reason there are various research groups developing new and novel approaches based on extrusion-based 3D printing to construct 3D cell-laden structures.

Extrusion based printing has been used to successfully demonstrate the ability to print scaffolds for bone generation in the field of hard tissue engineering [82, 83]. The majority of recent works on soft tissue printing are limited to 2D or very simple 3D structures with limited aspect ratio, however.

Sun and his co-workers developed a new extrusion-based technology to bioprint Hela cells to create a 3D cancer model *in-vitro* to evaluate cancer studies in 2D [84, 85]. The bio-ink used for this method was a composition of 10% gelatine, 1% sodium alginate and 2% fibrinogen. The composition was then loaded into a syringe at 25 ^{o}C and extruded at 10 ^{o}C. A lower temperature was used to keep the gelatine in the gel state. 3% $CaCl_2$ solution was used to cross-link the alginate and the alginate was then submerged into a 20 U mL^{-1} thrombin for 15 minutes to cross-link the fibrinogen. This technology, despite being able to support tumour growth within the printed bio-ink as well as human embryonic stem cells [86], is not able to print 3D structures taller than 3 mm [87].

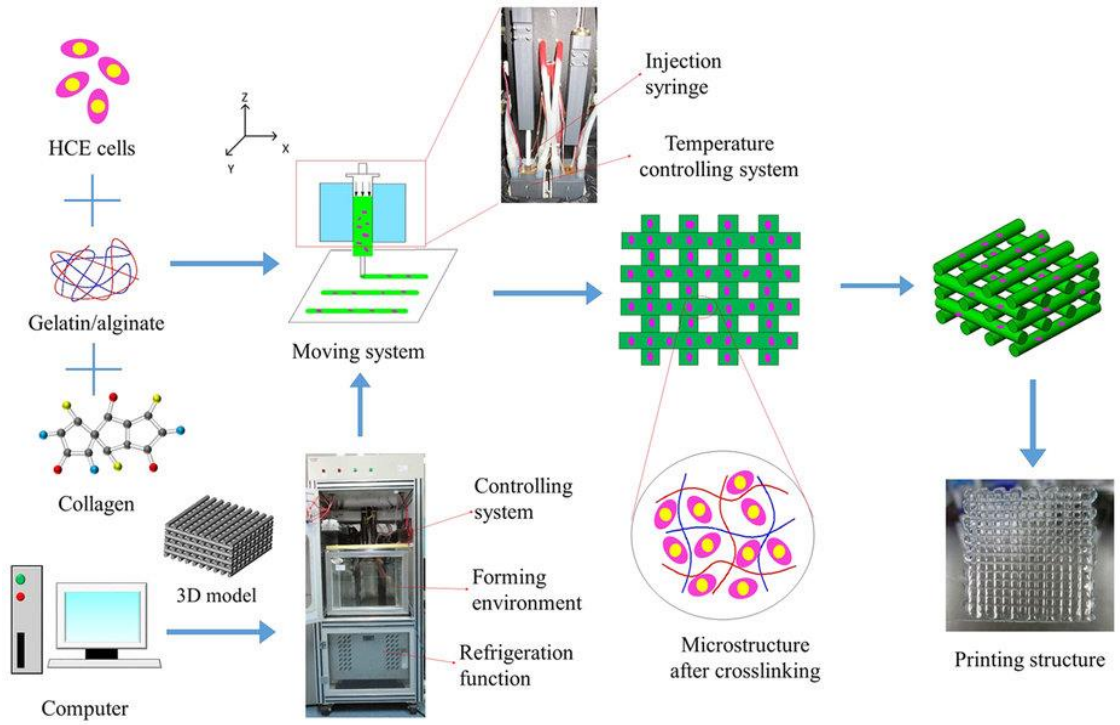

Figure 1.12 *– Schematic drawing of 3d printing setup to bioprint suspended Hela cells, HES cells and human corneal epithelial cells in alginate alginate/gelatin composition [85].*

A research group from Department of Dental Materials and Biomaterials Research at RWTH University Hospital developed a new technique to print 3D cell-laden hydrogel structures. The method incorporates the use of high density fluid to support the integrity of printed cell-laden hydrogel as shown in Figure 1.13 [88]. The bio-ink consisted of human mesenchymal stem cells (hMSC) at a concentration of 1×10^7 cells/mL suspended in 1.5% (w/v) agarose. The cell-laden hydrogel is deposited layer by layer to form a 3D structure in a fluorocarbon reservoir, a high density hydrophobic fluid to support the cell-laden hydrogel. The printing technique is gentle on cells while keeping the cell viability over 90% after both 24 hrs and 21 days of culture. Despite the method being capable of printing highly viable cells into a 3D structure, there is a limitation on the complexity of the structures: they are limited to simple tube structures as shown in Figure 1.14.

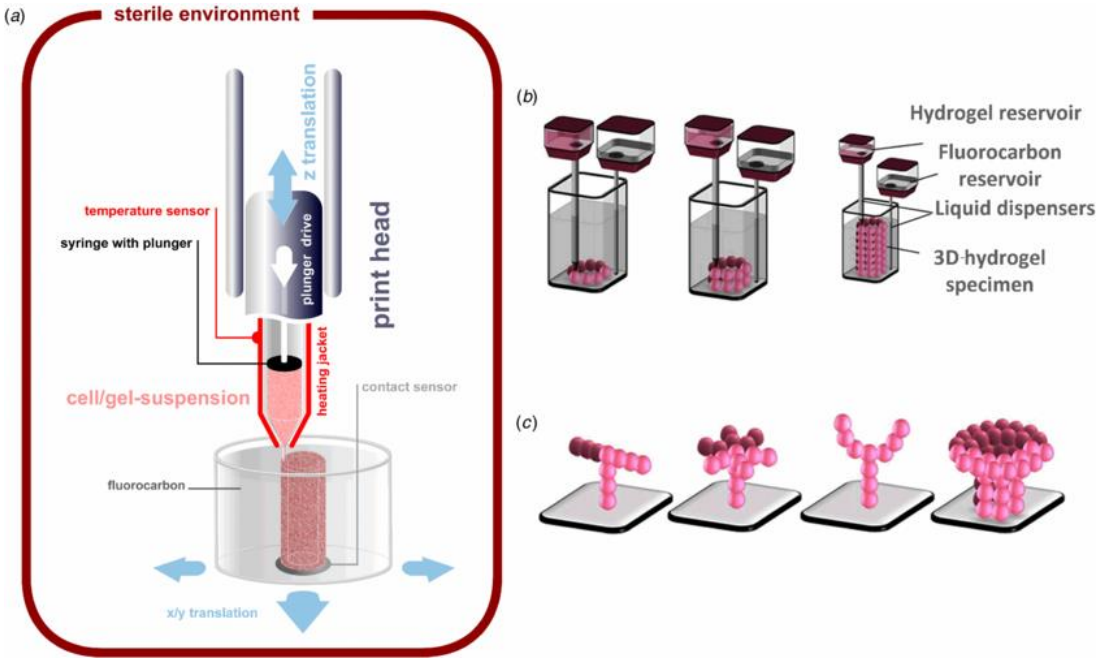

Figure 1.13 *– Schematic drawing of 3D bioprinting cell-laden hydrogel mechanically supported by high-density fluorocarbon liquid [88].*

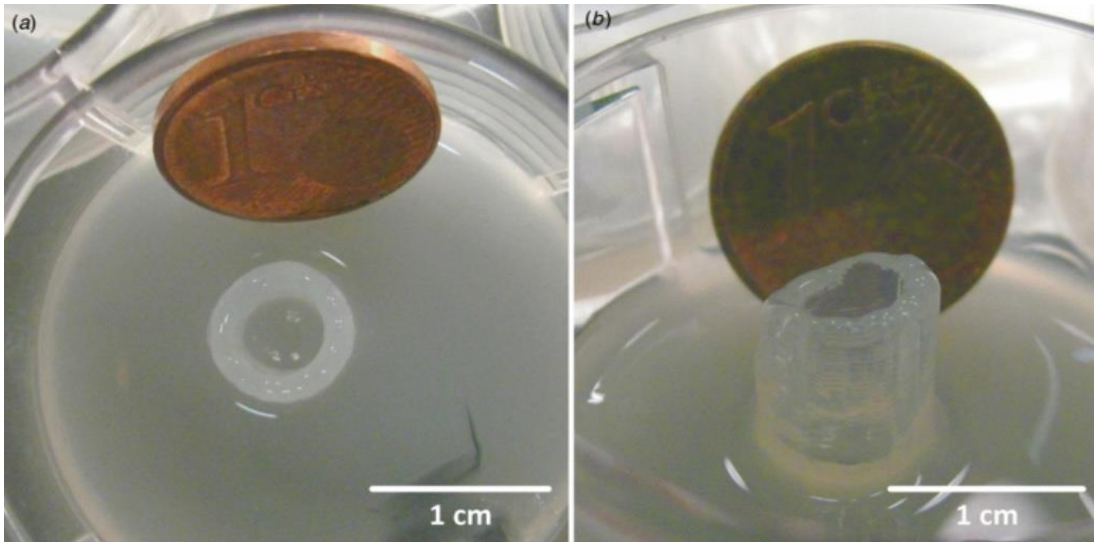

Figure 1.14 *– 3D printed cell-laden hydrogel ring construct submerged in fluorocarbon. (a) Top and (b) side view of the construct [88].*

Several research groups have incorporated the use of printed support material to create 3D cell-laden hydrogel structures. For example, Butcher and co-workers [89] from Cornell University developed a photo-curable hydrogel to bioprint 3D structures with the use of support material consisting of very viscous alginate/gelatine solution. The bio-ink used was 20% Poly (ethylene glycol)-diacrylate (PEG-DA), 12.5% alginate with 1% photoinitiator. The bio-ink was printed by Fab@Home using a 0.85 mm diameter

nozzle. Once a layer of bio-ink is printed the support material is printed correspondingly (Figure 1.15). This is then exposed to Ultraviolet (UV) light for 30-60 seconds to cross-link the bio-ink. The process is repeated as many times as desired until the 3D structure is formed. The technique is capable of bioprinting 3D structures with great complexity; however the exposure of cells to potentially harmful UV radiation could damage the cells. Furthermore, the bio-ink used is very concentrated, which would lead to low permeability within the structure, affecting cell proliferation. Another disadvantage of this method is the use of a nozzle with a large diameter, which limits the X-Y resolution. The use of a smaller nozzle would cause higher shear stress, eventually damaging the cells during the bioprinting process. Similar technologies have been used to generate a human ear structure using biodegradable PCL structure, printing a removable sacrificial layer [90]. Due to the high temperature needed to deposit PCL, the technique could potentially be harmful to many delicate cell types.

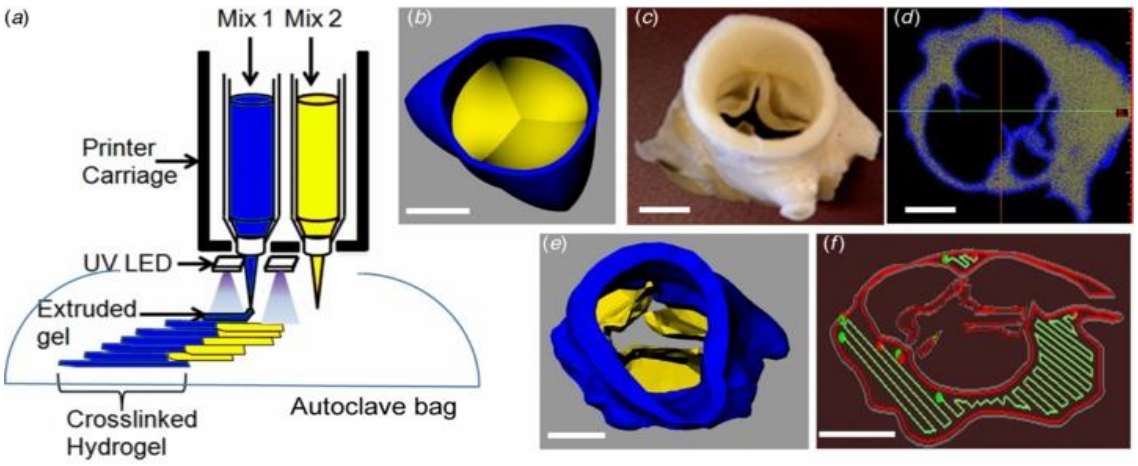

Figure 1.15— *3D bioprinting of human heart valve structure using a novel approach by incorporating photocurable bio-inks with support materials [89].*

1.6 Hydrogels

Hydrogels are the basis of 3D bioprinting in tissue engineering due to their many unique features, such as the creation of a hydrated and mechanically supportive extracellular matrix (ECM) to ensure cell encapsulation. Biocompatibility of each hydrogel is mainly determined by its hydrophilicity [3]. Due to their high biocompatibility hydrogels are commonly used in the bioprinting field [91]. Hydrogels can generally mimic the 3D environment similar to the physiological condition.

Hydrogels are divided into two categories. One is naturally-derived hydrogels such as fibrin, chitosan, collagen and alginate [92-94]. The other category is synthetically-derived hydrogels such as polyethylene glycol and pluronics [95-97]. Naturally-derived hydrogels are favoured over the synthetically-derived hydrogels in the tissue engineering and bioprinting field due to their higher biocompatibility, as synthetic hydrogels are not as biofunctional as natural hydrogels.

For bioprinting, hydrogels are used as bio-ink to encapsulate cells and provide the initial cell delivery platform. Several cell types, especially stem cells, can be encapsulated within these hydrogels and subsequently printed [98].

Although many hydrogels have been used for bioprinting, alginate hydrogel is chosen in this present study to be used for the bioprinting process due to its high biocompatibility and wide range tunability of the hydrogel especially when used with stem cells [98]. Mechanically this hydrogel can be enhanced by increasing its concentration or through ionic cross-linking with $CaCl_2$ or $BaCl_2$, which makes it suitable for printing 3D structures with better mechanical properties and integrity. Another advantage of this hydrogel is the controllability over its degradation, which provides cells encapsulated within the hydrogel with enough time to grow and proliferate. Another reason for choosing alginate hydrogel over other hydrogels and biomaterials is its fast gelation, which makes it one of the most printable hydrogels.

1.7 Conclusion

Of the main four 3D bioprinting techniques, Inkjet-based and valve-based bioprinting techniques have a high throughput and high cell viability. They are limited to printing simple 2D and 3D structures with a limited aspect ratio, however, which will certainly lack mechanical stiffness due to the limitation in printing concentrated bio-inks. Extrusion- and laser-based technologies are capable of printing bio-inks using medium to high viscosity materials, which creates a suitable bioprinting platform for printing 3D structures with better mechanical properties as previously demonstrated. The use of bio-inks with higher viscosity could damage the cells during the printing process due to high shear stress, however. Alterations in either the bio-inks or the 3D printing process are therefore essential. In this thesis, extrusion-based printing was chosen over laser-based printing. This was due to the ability to print medium to high viscosity biomaterials using this method.

Research carried out so far involved the creation of simple structures using extrusion-based bioprinting. This study investigates the feasibility of enhancing the biomechanical properties before, during and after bioprinting, with a view to enabling the creation of a complex cell-laden 3D structure. Manual approaches for fabricating cell-laden tubular structures and, potentially, complex 3D structures are also considered. The availability of an effective manual approach would allow more widespread fabrication of 3D structures without the need for complex and expensive machinery and the associated operational resources.

Following the introduction and literature review on 3D printing, 3D bioprinting and hydrogels in this chapter, the remaining chapters are as follows:

Chapter 2 describes the experimental techniques and methods used in the thesis.

Chapter 3 explains the development of the novel 3D bioprinting platform to bioprint complex 3D structures through a three step cross-linking process using a tuneable alginate hydrogel.

Chapter 4 further investigates the novel 3D bioprinting platform by focusing on cell viability for short-term cell culture (immediately after bioprinting) using different viscous alginate hydrogel. The most suitable hydrogel concentration is used to assess the long-term cell viability within the alginate hydrogel.

Chapter 5 presents a simple approach for the 3D fabrication of single and multi-layered alginate hydrogel tubular structures.

Chapter 6 reports on the feasibility of a dip coating approach, considering factors such as cell viability, cell function, cell attachment and incorporation of other biomaterials into alginate hydrogel tubular structures.

Chapter 7 summarises the work output from the thesis and possible recommendations for future studies.

Chapter 1 References

[1] Langer R, Vacanti JP. Tissue engineering Science (1993);260:920}???6.

[2] Groll J, Boland T, Blunk T, Burdick JA, Cho DW, Dalton PD, Derby B, Forgacs G, Li Q, Mironov VA, Moroni L, Nakamura M, Shu W, Takeuchi S, Vozzi G,Woodfield TB, Xu T, Yoo JJ, Malda J. (2016). "Biofabrication: reappraising the definition of an evolving field." Biofabrication 8(1): 013001.

[3] Dababneh, A. B. and I. T. Ozbolat (2014). "Bioprinting Technology: A Current State-of-the-Art Review." Journal of Manufacturing Science and Engineering 136(6): 061016-061016.

[4] Wilson, H.V. (1907) On some phenomena of coalescence and regeneration in sponges. J. Exp. Zool. 5, 245–258.

[5] Just, E.E. (1939) The Biology of Cell Surface. Blakiston.

[6] Townes, P.L. and Holtfreter, J. (1955) Directed movements and Selective adhesion of embryonic amphibian cells. J. Exp. Zool. 128, 53–120.

[7] Steinberg, M.S. (1996) Adhesion in development: an historical Overview. Dev. Biol. 180, 377–388

[8] U. Kneser, P. M. Kaufmann, H. C. Fiegel, J. M. Pollok, D. Kluth, H. Herbst, X. Rogiers, J. Biomed. Mater. Res. (1999),47, 494

[9] J. F. Hansbrough,J. L. Morgan, G. E. Greenleaf, R. Bartel, J. Burn Care Rehabil. 1993, 14, 485.

[10] T. Hadlock, C. Sundback, D. Hunter, M. Cheney, J. P.Vacanti, Tissue Eng. (2000), 6, 119.

[11] Forgacs, G. et al. (1998) Viscoelastic properties of living embryonic tissues: a quantitative study. Biophys. J. 74, 2227–2234

[12] Beysens, D. et al. (2000) Cell sorting is analogous to phase separation in fluids. Proc. Natl. Acad. Sci. U. S. A. 97, 9467–9471

[13] OPTN. Donation and transplantation. Online. Available from URL: http://optn.transplant.hrsa.gov/about/; 2012.

[14] NHS Blood and Transplant, Organ and transplantation activity report (2011/2012)

[15] X.H. Liu, P.X. Ma Phase separation, pore structure, and properties of nanofibrous gelatin scaffolds, Biomaterials, 30 (2009), pp. 4094–4103

[16] M.D. Nichols, E.A. Scott, D.L. Elbert (2009) actors affecting size and swelling of poly (ethylene glycol) microspheres formed in aqueous sodium sulfate solutions without surfactants, Biomaterials, 30 (2009), pp. 5283–5291

[17] S. Lee, S.C. Seong, J.H. Lee, I.K. Han, S.H. Oh, K.J. Cho (2007) prosthesis for meniscal regeneration, Key Eng Mat, 342–343, pp. 33–36

[18] Y.Y. Wang, L. Liu, S.R. Guo (2010) Characterization of biodegradable and cytocompatible nano-hydroxyapatite/polycaprolactone porous scaffolds in degradation in vitro, Polym Degrad Stabil, 95, pp. 207–213

[19] M.E. Gomes, H.S. Azevedo, A.R. Moreira, V. Ella, M. Kellomaki, R.L. Reis (2008) Starch-poly (epsilon-caprolactone) and starch-poly (lactic acid) fibre-mesh scaffolds for bone tissue engineering applications: structure, mechanical properties and degradation behaviour, J Tissue Eng Regen M, 2, pp. 243–252

[20] D.T. Mooney, C.L. Mazzoni, C. Breuer, K. McNamara, D. Hern, J.P. Vacanti (1996) Stabilized polyglycolic acid fibre based tubes for tissue engineering, Biomaterials, 17 (1996), pp. 115–124

[21] L. Martin, M. Alonso, A. Girotti, F.J. Arias, J.C. Rodriguez-Cabello (2009) Synthesis and characterization of macroporous thermosensitive hydrogels from recombinant elastin-like polymers, Biomacromolecules, 10, pp. 3015–3022

[22] S.P. Pathi, C. Kowalczewski, R. Tadipatri, C. Fischbach (2010) ,A novel 3-d mineralized tumor model to study breast cancer bone metastasis, PloS One, 5 , p. e8849

[23] X.H. Zhu, D.Y. Arifin, B.H. Khoo, J.S. Hua, C.H. Wang (2010) Study of cell seeding on porous poly(d, l-lactic-co-glycolic acid) sponge and growth in a couette-taylor bioreactor, Chem Eng Sci, 65 , pp. 2108–2117

[24] A. Salerno, P.A. Netti, E. Di Maio, S. Iannace (2009) Engineering of foamed structures for biomedical application, J Cell Plast, 45, pp. 103–117

[25] T.W. Wang, M. Spector (2009), Development of hyaluronic acid-based scaffolds for brain tissue engineering, Acta Biomater, 5 (2009), pp. 2371–2384[26] J.M. Estelles, A. Vidaurre, J.M.M. Duenas, I.C. Cortazar (2008) ,Physical characterization of polycaprolactone scaffolds, J Mater Sci Mater M, 19 , pp. 189–195

[27] C. Tsioptsias, I. Tsivintzelis, L. Papadopoulou, C. Pallayiotou (2009), A novel method for producing tissue engineering scaffolds from chitin, chitin-hydroxyapatite, and cellulose Mat Sci Eng C-Bio S, 29 , pp. 159–164

[28] L. Martin, M. Alonso, A. Girotti, F.J. Arias, J.C. Rodriguez-Cabello (2009), Synthesis and characterization of macroporous thermosensitive hydrogels from recombinant elastin-like polymers, Biomacromolecules, 10 , pp. 3015–3022

[29] S.P. Pathi, C. Kowalczewski, R. Tadipatri, C. Fischbach (2010), A novel 3-d mineralized tumor model to study breast cancer bone metastasis, PloS One, 5 , p. e8849

[30] Kelly, Jan Seaman (2006) Scientific Examination of Questioned Documents. CRC Press, P.204

[31] Ken Kataokaa, Kanji Tsuru (2004) An organic–inorganic hybrid scaffold for the culture of HepG2 cells in a bioreactor

[321] Sachs E, Cima M, Cornie J. Three-dimensional printing: rapid tooling and prototypes directly from a cad model. CIRP Ann Manufacturing Technol 1990;39:201e4.

[33] Wilson WC, and Boland T, (2003). “Cell and organ printing 1: Protein and cell printers,” *The Anatomical Record*, **272A**(2), pp. 491–496.

[34] MicroFab technote 99-01: Background on ink-jet technology. http://www.microfab.com/ equipment/technotes/technote99-01.pdf. Accessed 19 March 2006

[35] Xiaofeng Cui, Thomas Boland, (2009), Human microvasculature fabrication using thermal inkjet printing technology

[36] Janmey PA. Kinetics of formation of fibrin oligomers. 1. Theory. Biopolymers

1982;21:2253–64.

[37] Fussenegger M, Meinhart J, Hobling W, Kullich W, Funk S, Bernatzky G. Stabilized autologous fibrin-chondrocyte constructs for cartilage repair in vivo. Annals of Plastic Surgery 2003;51:493–8.

[38] Perka C, Spitzer RS, Lindenhayn K, Sittinger M, Schultz O. Matrix-mixed culture: New methodology for chondrocyte culture and preparation of cartilage transplants. Journal of Biomedical Materials Research 2000;49:305–11.

[39] Huang YC, Dennis RG, Larkin L, Baar K. Rapid formation of functional muscle in vitro using fibrin gels. Journal of Applied Physiology 2005;98:706–13

[40] Hecker L, Khait L, Welsh MJ, Birla R. Bioengineering functional human aortic vascular smooth-muscle strips in vitro. Biotechnology and Applied Biochemistry 2008;50:155–63.

[41] Tao Xu, Weixin Zhao, Jian-Ming Zhu (2012) Complex heterogeneous tissue constructs containing multiple cell types Prepared by inkjet printing technology

[42] Nakamura M, Nishiyama Y, and Henmi C, (2008). "3D Micro-fabrication by inkjet 3D biofabrication for 3D tissue engineering," Micro-NanoMechatronics and Human Science, 2008. MHS 2008. International Symposium on, IEEE, pp. 451–456.

[43] Dababneh AB, Ozbolat IT. Bioprinting Technology: A Current State-of-the-Art Review. ASME. *J. Manuf. Sci. Eng.* 2014;136(6):061016-061016-11. doi:10.1115/1.4028512.

[44] Norman J J and Desai T A 2006 Methods for fabrication of nanoscale topography for tissue engineering scaffolds Ann. Biomed. Eng. **34** 89–101

[45] Herran L C and Huang Y 2012 Alginate microsphere fabrication using bipolar wave-based drop-on-demand jetting J. Manuf. Process. **14** 98–106

[46] Herran L C, Huang Y and Chai W 2012 Performance evaluation of bipolar and tripolar excitations during nozzle-jetting-based alginate microsphere fabrication J. Micromech. Microeng. **22** 085025

[47] William E. Kasdorf (January 2003). The Columbia Guide to Digital Publishing. Columbia University Press. pp. 383–. ISBN 978-0-231-12499-7.

[48] Odde, D., and Renn, M., 1999, “Laser-Guided Direct Writing for Applications in Biotechnology,” Trends Biotechnol., 17(10), pp. 385–389.

[49] Barron JA, Ringeisen BR, Kim H, Spargo BJ, and Chrisey DB, (2004). “Application of laser printing to mammalian cells,” *Thin Solid Films*, **453-454**, pp. 383–387.

[50] Barron JA, Spargo BJ, and Ringeisen BR, (2004). “Biological laser printing of three dimensional cellular structures,” Applied Physics A, 79, pp. 1027–1030.

[51] Duocastella M, Colina M, Fernández-Pradas JM, Serra P, and Morenza JL, (2007). “Study of the laser-induced forward transfer of liquids for laser bioprinting,” *Applied Surface Science*, **253**(19), pp. 7855–7859.

[52] Barron, J., Ringeisen, B., Kim, H., Spargo, B., and Chrisey, D., 2004, “Application of Laser Printing to Mammalian Cells,” Thin Solid Films, 453(383), pp. 383–387.

[53] Gudapati H, Yan J, Huang Y and Chrisey D B 2014 Alginate gelation-induced cell death during laser-assisted cell printing *Biofabrication* **6** 035022

[54] Wang W, Li G and Huang Y 2009 Modeling of bubble expansion-induced cell mechanical profile in laser-assisted cell direct writing Trans. ASME, J. Manuf. Sci. Eng. 131051013

[55] Wang W, Huang Y, Grujicic M and Chrisey D B 2008 Studyof impact-induced mechanical effects in cell direct writing using smooth particle hydrodynamic method Trans. ASME, J. Manuf. Sci. Eng. 130 021012

[56] Wang W, Huang Y and Chrisey D B 2007 Numerical study of cell droplet and hydrogel coating impact process in cell direct writing Trans. NAMRI/SME 35 217–24

[57] Nathan, R. S., T. C. David, H. Yong, R. Nurazhani Abdul, X. Yubing and B. C. Douglas (2010). "Laser-based direct-write techniques for cell printing." Biofabrication 2(3): 032001.

[58] Huang X, Zhang X, Wang X, Wang C and Tang B 2012 Microenvironment of alginate-based microcapsules for cell culture and tissue engineering J. Biosci. Bioeng. 114 1–8

[59] Loh Q L, Wong Y Y and Choong C 2012 Combinatorial effect of different alginate compositions, polycations, and gelling ions on microcapsule properties Colloid Polym. Sci. 290 619–29

[60] Kingsley, D., Dias, A., Chrisey, D., & Corr, D. (2013). Single-step laser-based fabrication and patterning of cell-encapsulated alginate microbeads. Biofabrication, 5(4), 045006.

[61] Yan J, Huang Y, Chrisey D B 2013 Laser-assisted printing of alginate long tubes and annular constructs *Biofabrication* **5** 015002

[62] Kong H J, Smith M K and Mooney D J 2003 Designing alginate hydrogels to maintain viability of immobilized cells *Biomaterials* **24** 4023–9

[63] (38) Xiong, R.; Zhang, Z.; Chai, W.; Huang, Y.; Chrisey, D. B. Freeform drop-on-demand laser printing of 3d alginate and cellular constructs. Biofabrication 2015, 7 (4), 045011.

[64] Moon S, Lin P-A, Keles HO, Yoo S-S, and Demirci U, (2007). "Cell Encapsulation by Droplets," J Vis Exp, 8.

[65] Demirci U, and Montesano G, (2007). "Cell encapsulating droplet vitrification," Lab on a Chip, 7(11), p. 14281433.

[66] Xu F, Emre AE, Turali ES, Hasan SK, Moon S, Nagatomi J, Khademhosseini A, and Demirci U, (2009). "Cell proliferation in bioprinted cell-laden collagen droplets," Bioengineering Conference, 2009 IEEE 35th Annual Northeast, IEEE, pp. 1–2.

[67] aulkner-Jones A, Greenhough S, King J A, Gardner J, Courtney A and Shu W 2013 Development of a valve-based cell printer for the formation of human embryonic stem cell spheroid aggregates *Biofabrication* **5** 015013

[68] Li C, Faulkner-Jones, A, Dun A R, Jin J, Chen P, Xing Y, Yang Z, Li Z, Shu W, Liu D, Duncan R R 2015 Rapid Formation of a Supramolecular Polypeptide–DNA Hydrogel for In Situ Three-Dimensional Multilayer Bioprinting *Angew. Chem. Int. Ed* 54: 3957–3961.

[69] Faulkner-Jones A, Fyfe C, Cornelissen D J, Gardner J, King J, Courtney A and Shu W 2015 Bioprinting of human pluripotent stem cells and their directed differentiation

into hepatocyte-like cells for the generation of mini-livers in 3D *Biofabrication* **7** 044102

[70] Chee Kai Chua; Kah Fai Leong, Chu Sing Lim (2003). *Rapid Prototyping*. World Scientific. p. 124.

[71] Vozzi G, Flaim C, Ahluwalia A and Bhatia S 2003 Fabrication of PLGA scaffolds using soft lithography and microsyringe deposition Biomaterials 24 2533–40

[72] am C X F, Mo X F, Teoh S H and Hutmacher D W 2002 Scaffold development using 3D printing with a starch-based polymer Mater. Sci. Eng. C 20 49–56

[73] Xiong Z, Yan Y N, Zhang R J and Sun L 2001 Fabrication of porous poly(L-lactic acid) scaffolds for bone tissue engineering via precise extrusion Scr. Mater. 45 773–9

[74] Chen X B, Schoenau G and Zhang W J 2002 On the flow rate dynamics in time-pressure dispensing processes Trans. ASME, J. Dyn. Syst. Meas. Control 124 693–8

[75] Ringeisen B.R., Othon C.M., Barron J.A., Young D., Spargo B.J. Jet-based methods to print living cells.Biotechnol. J. 2006;1:930–948

[76] E.A. Roth, T. Xu, M. Das, C. Gregory, J.J. Hickman, T. Boland ,Inkjet printing for high-throughput cell patterning, Biomaterials, 25 (2004), pp. 3707–3715

[77] F. Guillemot, A. Souquet, S. Catros, B. Guillotin, Laser-assisted cell printing: principle, physical parameters versus cell fate and perspectives in tissue engineering, Nanomedicine, 5 (2010), pp. 507–515

[78] C. Born, Z. Zhang, M. Al-Rubeai, C. Thomas ,Estimation of disruption of animal cells by laminar shear stress ,Biotechnol. Bioeng., 40 (1992), pp. 1004–1010

[79]] Chang R and Sun W 2008 Effects of dispensing pressure and nozzle diameter on cell survival from solid freeform fabrication-based direct cell writing Tissue Eng. A 14 41–8

[80] L. Koch, A. Deiwick, B. Chichkov Laser-based 3D cell printing for tissue engineering BioNanoMaterials, 15 (2014), pp. 71–78

[81] X. Cui, D. Dean, Z.M. Ruggeri, T. Boland Cell damage evaluation of thermal inkjet printed Chinese hamster ovary cells Biotechnol. Bioeng., 106 (2010), pp. 963–969

[82] Benjamin, H., B. Kartik, P. Michael and Z. Lijie Grace (2016). "A synergistic approach to the design, fabrication and evaluation of 3D printed micro and nano featured scaffolds for vascularized bone tissue repair." Nanotechnology 27(6): 064001.

[83] Hollister S J 2005 Porous scaffold design for tissue engineering *Nat. Mater.* **4** 518–524

[84] Wang C, Tang Z, Zhao Y, Yao R, Li L and Sun W 2014 Three-dimensional in vitro cancer models: a short review *Biofabrication* **6** 022001

[85] Zhao Y, Yao R, Ouyang L, Ding H, Zhang T, Zhang K, Cheng S and Sun W 2014 Three-dimensional printing of Hela cells for cervical tumor model in vitro Biofabrication 6 035001

[86] Liliang O, Rui Y, Shuangshuang M, Xi C, Jie N and Wei S 2015 Three-dimensional bioprinting of embryonic stem cells directs highly uniform embryoid body formation *Biofabrication* **7** 044101

[87] Wu, Z., X. Su, Y. Xu, B. Kong, W. Sun and S. Mi (2016). "Bioprinting three-dimensional cell-laden tissue constructs with controllable degradation." Scientific Reports 6: 24474.

[88] Campos D F D, Blaeser A, Weber M, Jäkel J, Neuss S, Jahnen-Dechent W and Fischer H 2013 Three-dimensional printing of stem cell-laden hydrogels submerged in a hydrophobic high-density fluid*Biofabrication* **5** 015003

[89] Hockaday, L. A., K. H. Kang, N. W. Colangelo, P. Y. C. Cheung, B. Duan, E. Malone, J. Wu, L. N. Girardi, L. J. Bonassar, H. Lipson, C. C. Chu and J. T. Butcher (2012). "Rapid 3D printing of anatomically accurate and mechanically heterogeneous aortic valve hydrogel scaffolds." Biofabrication 4(3): 035005.

[90] Lee J-S, Hong J M, Jung J W, Shim J-H, Oh J-H and Cho D-W 2014 3D printing of composite tissue with complex shape applied to ear regeneration *Biofabrication* **6** 024103

[91] Patterson, J., Martino, M., and Hubbell, A., 2010, “Biomimetic Materials in Tissue Engineering,” Mater. Today, 13(1–2), pp. 14–22.

[92] Hunt, N., and Grover, L., 2010, “Cell Encapsulation Using Biopolymer Gels for Regenerative Medicine,” Biotechnol. Lett., 32(6), pp. 733–742.

[93] Spiller, K., Maher, S., and Lowman, A., 2011, “Hydrogels for the Repair of Articular Cartilage Defects,” Tissue Eng., Part B, 17(4), pp. 281–299.

[94] Dash, M., Chiellini, F., Ottenbrite, R., and Chiellini, E., 2011, “Chitosan—A Versatile Semi-Synthetic Polymer in Biomedical Applications,” Prog. Polym. Sci., 36(8), pp. 981–1014

[95] Censi, R. S. W., Malda, J., di Dato, G., Burgisser, P., Dhert, W., van Nostrum, C., di Martino, P., Vermonden, T., and Hennink, W., 2011, “A Printable Photopolymerizable Thermosensitive p(HPMAm-Lactate)-PEG Hydrogel for Tissue Engineering,” Adv. Funct. Mater., 21(10), pp. 1833–1842.

[96] Fedorovich, E., De Wijn, R., Verbout, J., Alblas, J., and Dhert, J., 2008, “Three-Dimensional Fibre Deposition of Cell-Laden, Viable, Patterned Constructs for Bone Tissue Printing,” Tissue Eng., Part A, 14(1), pp. 127–133.

[97] Fedorovich, N., Swennen, I., Girones, J., Moroni, V., Blitterswijk, C., Schacht, E., Alblas, J., and Dhert, W., 2009, “Evaluation of Photocrosslinked Lutrol Hydrogel for Tissue Printing Applications,” Biomacromolecules, 10(7), pp. 1689–1696.

[98] Lutolf, M., Gilbert, P., and Blau, H., 2009, “Designing Materials to Direct Stem-Cell Fate,” Nature, 462(7272), pp. 433–441

Chapter 2 - Experimental techniques

2.1 Introduction

This chapter summarises experimental techniques and other methodologies to assist the research towards the completion of the thesis. The methods and experiments used to assemble and modify a specialised bioprinter are presented. This is a novel technique to bio-print complex cell-laden alginate hydrogel structures. The main bioprinting technique used to print complex hydrogel structures is discussed in detail in chapter 3. Other experimental techniques in order to measure hydrogel viscosity and mechanical properties are discussed in this chapter. Different imaging instruments used for 2D and 3D live cell imaging are described along with other imaging tools. CAD, image processing and printing programs that were used to assist the project are discussed. The chapter is completed with a review of other techniques such as plasma treatment, cell culture, and nanofibre fabrication.

2.2 Solid Edge V20 and CorelDRAW

Solid Edge V20, a piece of design software, played a crucial role throughout the research carried out within this thesis. It was primarily used to create models for the 3D bioprinting of alginate and cell-laden alginate hydrogel structures. Designs for the creation of complex 3D alginate hydrogel structures through dip-coating approach were created using Solid Edge V20. CorelDRAW, compatible with the CO_2 laser, was used to create X-Y cutting patterns for the laser cutter. The 2D parts were initially designed through Solid Edge and converted to xdf files, which are compatible with CorelDRAW. Solid Edge was an effective tool for creating designs of any broken bioprinter parts. These were then fabricated for bioprinter maintenance purposes.

2.3 Fab@Home 3 printing procedure

A Fab@Home 3 3D printer was purchased from Seraph Robotics for 3D bioprinting of hydrogels and assembled in accordance with the manufacturer's protocol. The Fab@Home consists of 3 main components: the transmission, chassis and the electronics. The chassis, which contains the electronics and transmission is made of 6 mm cast acrylic or PMMA. The transmission was used to guide the printhead in the X-Y-Z plane. The electronics consist of a Snap hub that controls five servo motors. Three

of the servo motors control the X-Y-Z motion of the print head and two are used for the dual extrusion print head for material extrusion purposes. This model of printer is widely used in the bioprinting field. The printing procedure is simple and straightforward as shown in Figure 2.1.

Solid Edge V20 CAD software was used to create designs that were converted to Stereolithography (STL) files. These are compatible with the Fab@Home 3 software called Seraph Studio. Seraph Studio software enabled the positioning of the design on the printing platform as desired. The design was loaded with the desired material and then Seraph Studio generated an xdfl file which would create the printing path, printing speed, path width, path height, and extrusion rate. These parameters were initially calibrated for printing alginate hydrogel at certain concentrations. Once the xdfl file was created, it was opened by the Seraph Print software, which was connected to the 3D printer through a personal computer (PC). The Seraph Print software can adjust the print head to the desired position and start, run and end the printing process.

The 3D printer has a dual extrusion print head with a 10 mL reservoir volume. The positioning accuracy was approximately 100 μm along the XYZ plane with the maximum travel speed of 80 mm/s. The typical travel speed for printing the majority of the materials for this printer was 10 mm/s, however. The printer build platform was 230 mm × 128 mm × 200 mm in the XYZ plane. This printer model could be modified in different ways; for example a heated build tray and a UV light tool could be added to provide the possibility of 3D printing a wider range of materials.

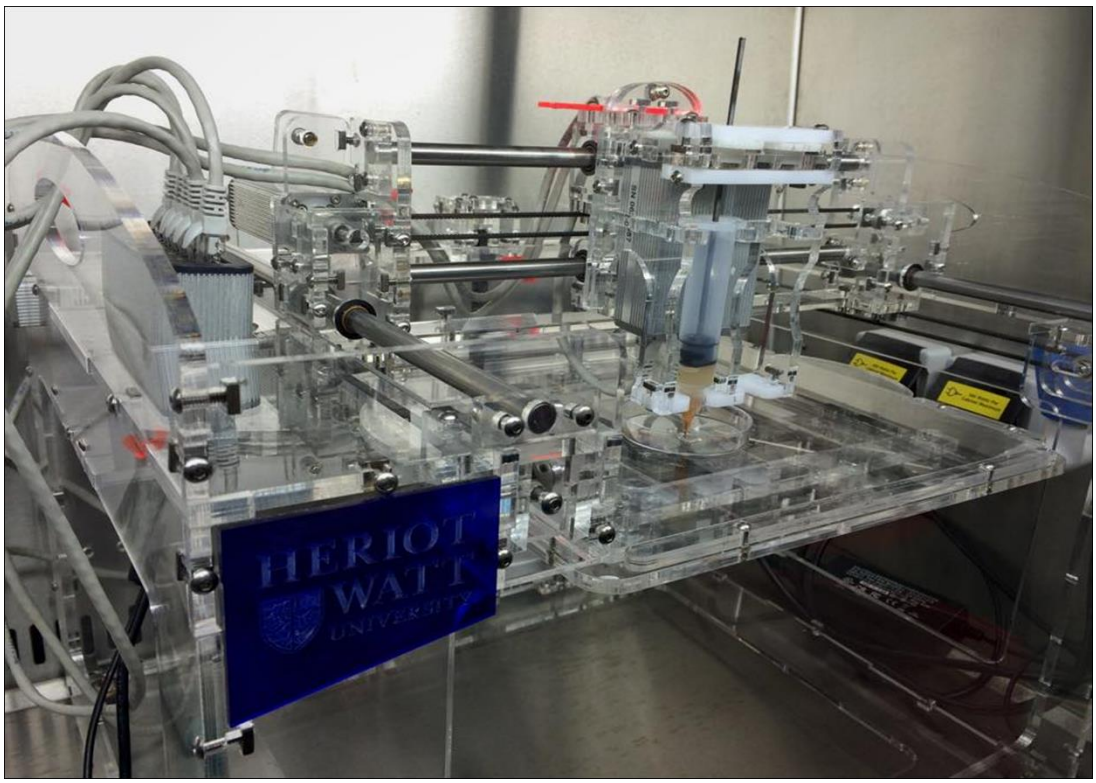

Figure 2.1 *– assembled Fab@Home 3 3D printer*

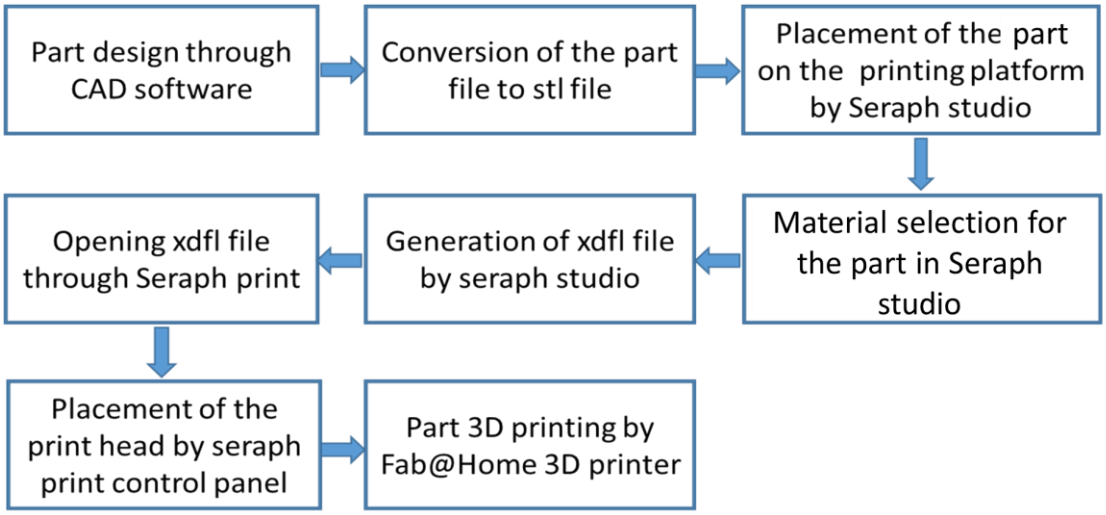

Figure 2.2 *– Fab@Home 3D printing procedure*

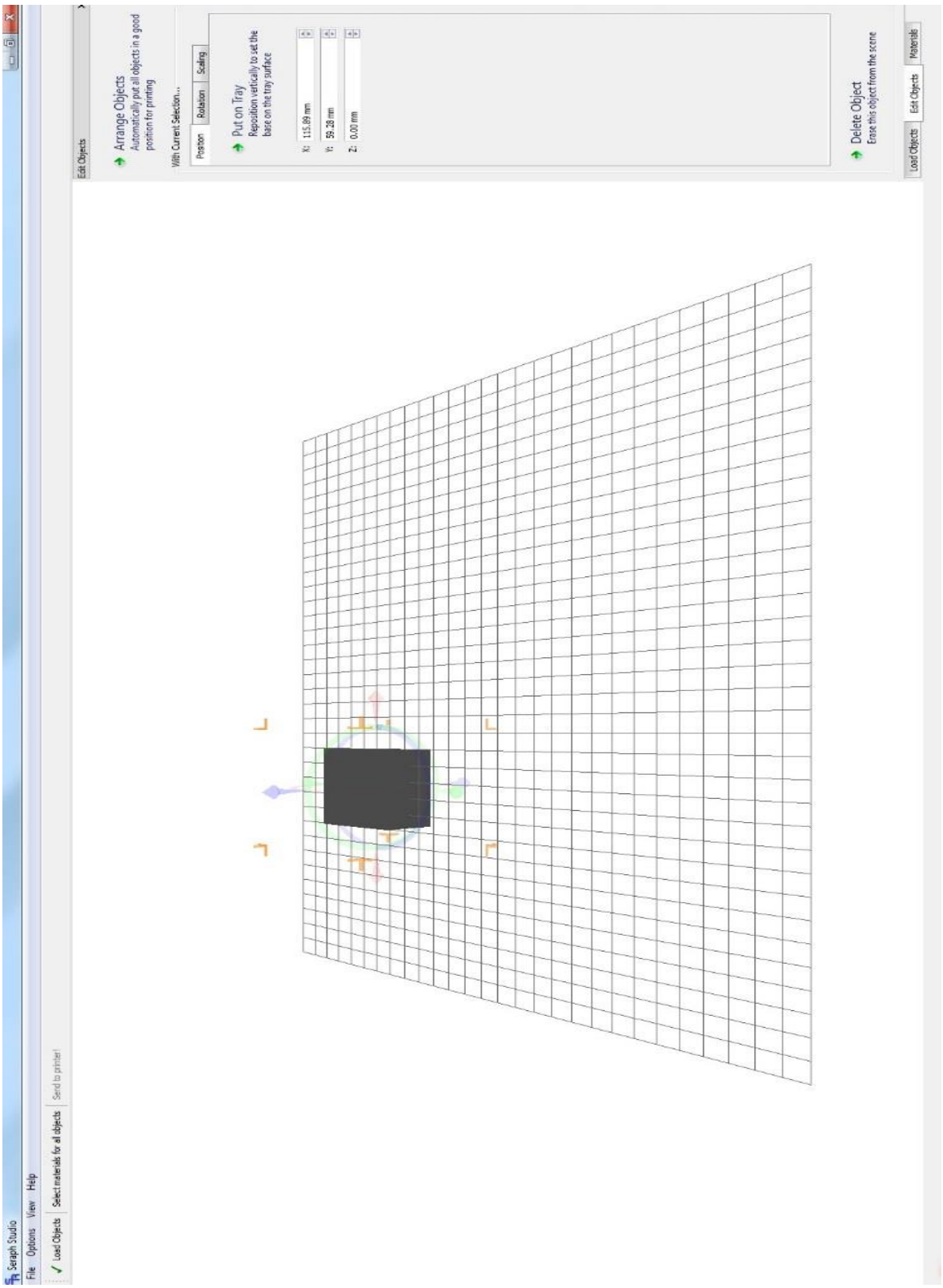

Figure 2.3 *– Seraph studio loaded with STL file to generate xdfl file for print path generation for3D printing of alginate or cell-laden alginate hydrogel structures.*

2.4 CO_2 laser system

The Trotec Speedy 300 CO_2 laser system is an engraving machine with a working area of 726 mm × 432 mm. It was used to laser cut PMMA into parts to modify the Fab@home 3 3D printer or used in order to fabricate parts that needed to be replaced in the 3D printer for maintenance purposes. It was also used to laser cut paper substrates and hollow out PMMA substrates for 3D bioprinting of hydrogel. The laser power ranges from 10-50 Watts.

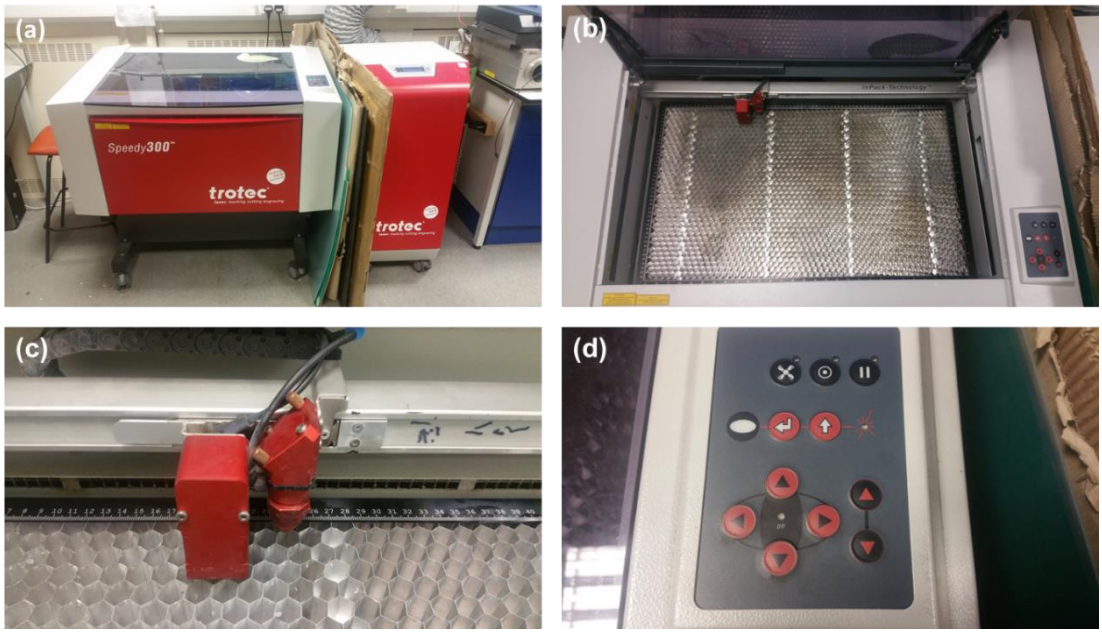

Figure 2.4 *– (a) Trotec Speedy 300 CO_2 laser system setup. (b) The working area of the laser and (c) the laser cutter head. (d) Control panel of the Laser system to adjust the platform Z level and the laser cutter head position in X-Y.*

2.5 Ultrasonic bath

An ultrasonic bath (RK 102 H, BANDELIN SONOREX, Germany) was used to prepare alginate hydrogel, alginate-collagen and alginate-gelatine solution to ease the mixing process. Any nozzles blocked during 3D printing or 3D bioprinting were unblocked by the ultrasonic bath by breaking down the particles causing the blockage inside the printing nozzles.

2.6 Plasma treatment

A plasma Machine (diener electronic, Zepto version B, Germany) was used to make PMMA surfaces hydrophilic to ensure the attachment of alginate hydrogels on PMMA

surfaces for printing simple 2D alginate hydrogel structures. Glass slides or Petri dishes were also treated by the plasma machine to make their surfaces more hydrophilic, ensuring the attachment of bioprinted cell-laden alginate hydrogels. The treated petri dishes were also used for spin-coating of the alginate.

2.7 MakerBot 3D printer for part fabrications

MakerBot Replicator 2X is capable of printing ABS and PLA and was used to 3D print parts needed to modify the Fab@Home 3 for bioprinting alginate and cell-laden alginate hydrogel structures. This 3D printer was used to 3D print solid plastic organ-like structures such as solid stomach and solid branched structures. These were used to to fabricate the silicon moulds needed for the creation of complex 3D hydrogel structures. Fabrication of complex alginate hydrogel structures by the dip-coating approach is further discussed in Chapter 5, section 5.9.

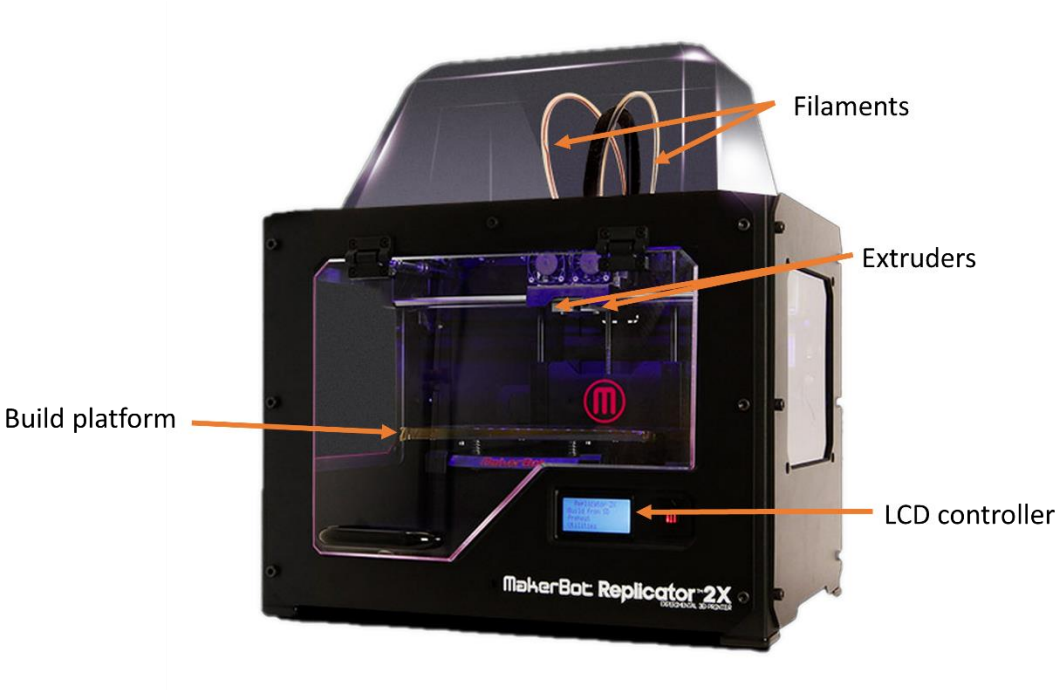

Figure 2.5 *– MakerBot Replicator 2X 3D printer used to fabricate solid plastic human body parts and parts for modification of Fab@Home 3D printer.*

2.8 Mechanical testing

A Mach-1™ mechanical indenter (Biomomentum, Canada) was used to measure the mechanical properties of the bioprinted alginate hydrogel structures treated by different

cross-linking conditions. The settings and configurations used for testing the alginate hydrogel mechanical properties are covered in chapter 4, section 4.11.

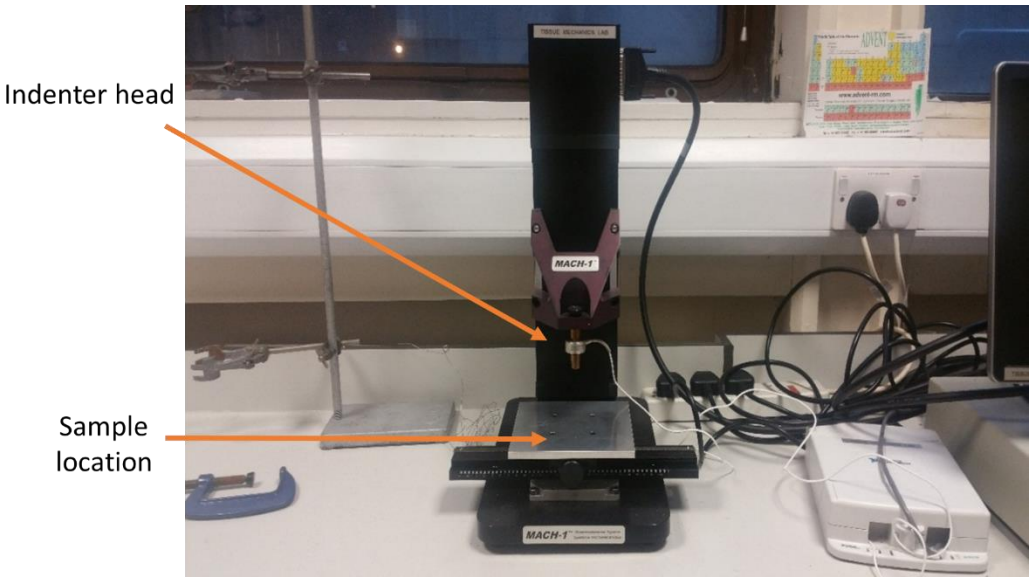

Figure 2.6 *– Mach-1™ mechanical indenter used for hydrogel mechanical properties measurement*

2.9 Viscosity measurements

A Bohlin Gemini rheometer was used to measure zero shear viscosity and dynamic viscosity of various concentrations of partially cross-linked alginate hydrogels in order to find the optimum viscosity conditions for 3D bioprinting cell-laden alginate hydrogel structures. Viscosity measurements were taken at room temperature as the bioprinting of the cell-laden alginate hydrogel was carried out at room temperature. CP4/40, a 40mm diameter cone with an angle of 4°, was used to take the viscosity measurements. The hydrogel viscosity results are further discussed in chapter 3, section 3.6.

Figure 2.7 *– The rheometer used to measure zero shear viscosity and dynamic viscosity of partially cross-linked alginate hydrogels*

2.10 Gelatine nanofibre fabrication to enhance cell attachment

Nanofibres were fabricated in this research for enhancing the attachment of cells to the biomaterial. 10 g of gelatine powder (Gelatine from porcine skin, product code 10011968154, Sigma-Aldrich UK) was mixed with 20 mL of de-ionised water. 40 mL of acetic acid was added to the water-gelatine solution and was gently stirred for 5 minutes. 32 mL of ethyl acetate was added to the solution and stirred gently for 5 another minutes. The final solution was then incubated for 12 hrs at 37°C as shown in Figure 2.8.

Figure 2.8 *– The water-acid based gelatine solution incubation at 37 °C for 12 hrs.*

Once incubated for 12 hours, 3 mL of the water-acid based gelatine solution was loaded into a 5 mL syringe and electrospun for 24 hrs at 0.06 ml/hr by 12.5 KV/8cm with a 500 µm tip.

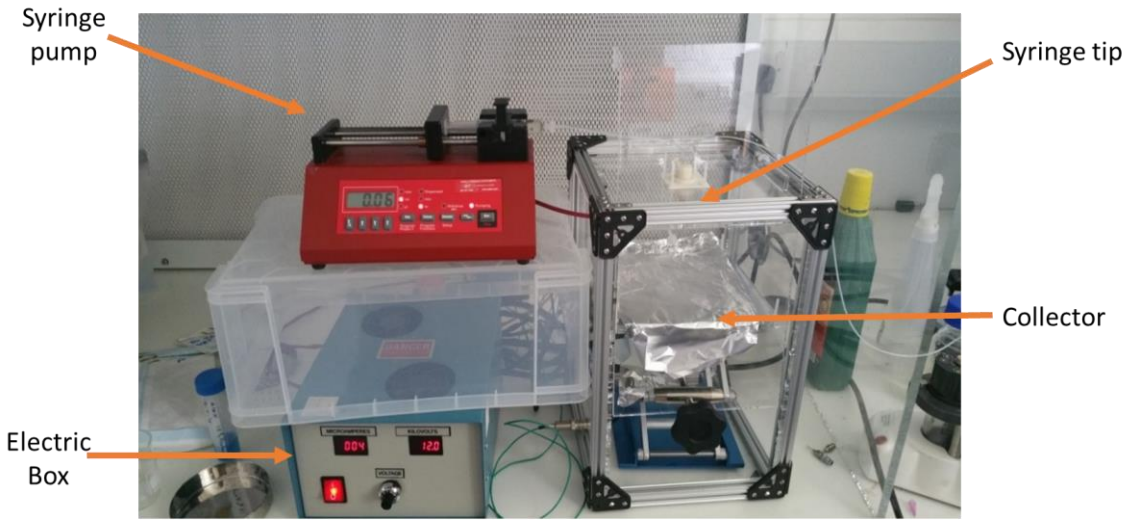

Figure 2.9 *– Electrospinning of water-based gelatine solution setup*

The fabricated nanofibrees then were removed from the aluminium foil tray and were ground using an electric grinder. The fabricated fibrenanofibres had diameters ranging from 50 nm to 250 nm .Once the nanofibres were ground, a 100- micrometre sieve was used to separate the beads that are smaller than 100 µm.

2.11 Scanning electron microscope

A scanning electron microscope (SEM), a powerful imaging device capable of imaging structures at the nanoscale was used to capture images of the electrospun gelatine nanofibre to confirm the existence of nanofibres. Samples were first taken from electrospun gelatine nanofibres and gold sputter coated before SEM examination to make sure the electrons were directed at the sample for imaging. Samples were transferred to the sputter coating chamber and vacuumed. Once vacuumed, sputter coating was performed at 2.5 KV and 20 mA for 45 seconds, resulting in a few nanometre-thick gold layers on the samples. Sputter coated samples then were taken to SEM for imaging. Images were taken at 5 KV with magnifications of 3000, 5000, 20000 and 50000.

Figure 2.10 *– Sputter coating chamber used to coat nano layers of gold on gelatine nanofibre samples.*

Figure 2.11– *Scanning electron microscope setup used for imaging gelatine nanofibre samples at different magnifications.*

2.12 2D cell imaging

2.11.1 Nikon eclipse Ts100 2D imaging microscope

One of the imaging instruments used in this research was the Nikon eclipse TS100. It was mainly used to count the number of U87-MG cells to estimate the overall number of cells used for bioprinting cell-laden alginate hydrogel structures as described in chapter 4. It was also used to image U87-MG and fibroblast cell attachment throughout the 4 days of culture of alginate-gelatine tubular structures fabricated by the dip-coating approach described in chapter 6. Images of U87-MG cell-laden alginate hydrogel extruded manually through altered-diameter tips were captured by this 2D imaging device throughout the 4 days of culture as described in chapter 4.

Figure 2.12 *– Nikon eclipse Ts100 2D imaging microscope.*

2.11.2 Zeiss Axiovert Immunofluorescence

A Zeiss Axiovert Immunofluorescence 2D imaging microscope was used to capture images of induced and non-induced tHEK cells within the tubular structures fabricated by the dip-coating approach through 6 days of culture as described in chapter 6. The instrument was also used to capture images of MDCK cell attachment on monolayer sheets of different biomaterial compositions, as well as capturing images of the tubular structures over 6 days of culture as described in chapter 6. Images of fibroblast cell attachment on different 2D monolayer biomaterial compositions were captured by this microscope as described in chapter 6.

Figure 2.13 *– Zeiss Axiovert Immunofluorescence 2D imaging microscope*

2.13 3D cell imaging

2.12.1 Leica SP5 SMD

Leica SP5 SMD confocal microscopy was used to capture confocal images of bioprinted U87-MG cell-laden alginate hydrogel structures throughout 11 days of culture to quantify the cell viability immediately after bioprinting and throughout the 11 days. Confocal images of encapsulated U87-MG cells in different tubular structures and fabricated by various alginate compositions via the dip-coating approach were captured by this confocal imaging instrument to identify the attachment of U87-MG cells to the alginate compositions.

Figure 2.14 *– Leica SP5 SMD confocal imaging microscope setup*

2.12.2 Nikon A1R FLIM confocal microscope

A Nikon A1R FLIM confocal microscope was used to capture confocal images of mouse dermal fibroblast cells encapsulated within tubular structures fabricated by the dip-coating approach. The images were captured throughout 6 days of culture within the tubular structures to identify the cell viability.

Figure 2.15 *– Nikon A1R FLIM confocal microscope*

Chapter 2 references

[1] Hooper, R. C., D. Bin, A. Harper, A. Jacoby, A. Laibangyang, J. T. Butcher and J. A. Spector (2014). "Abstract P1: Bioprinted Vascularized Tissue-Engineered Constructs for In Vivo Perfusion." Plastic and Reconstructive Surgery 133(3S): 186.

[2] Wüst, S., M. E. Godla, R. Müller and S. Hofmann (2014). "Tunable hydrogel composite with two-step processing in combination with innovative hardware upgrade for cell-based three-dimensional bioprinting." Acta Biomaterialia 10(2): 630-640.

[3] Duan, B., E. Kapetanovic, L. A. Hockaday and J. T. Butcher (2014). "Three-dimensional printed trileaflet valve conduits using biological hydrogels and human valve interstitial cells." Acta Biomaterialia 10(5): 1836-1846.

[4] Diogo, G. S., V. M. Gaspar, I. R. Serra, R. Fradique and I. J. Correia (2014). "Manufacture of β-TCP/alginate scaffolds through a Fab@home model for application in bone tissue engineering." Biofabrication 6(2): 025001.

Chapter 3 - 3D bioprinting of complex alginate hydrogel structures

3.1 Introduction

In the past decade, three-dimensional (3D) bioprinting as an emerging new technology for tissue engineering has made significant progress towards the regeneration of transplantable tissues [1-3] and even organs such as human ear, bones, skins, and nose [4-7] for restoring or repairing damaged body tissues. Various biofabrication techniques including inkjet printing [8-12], bioextrusion [13-15], valvejet printing [16-19], laser based printing [20-24] and photopolymerization [25-26] have been developed for the 3D printing of live cells and bioscaffold. Although the fabrication of clinically scaled hard tissues such as bones has already been successfully demonstrated [6], the bioprinted scaffolds for soft tissues has to date been limited to clinically small-scale structures with limited complexity.

The key challenge has been the difficulty of striking a good balance between the conditions for printing highly viable cells and producing sufficiently a strong scaffold to support clinical scale cell-laden structures at the same time. Take bioextrusion of hydrogels, for example, where small-diameter nozzles and highly viscous hydrogel materials were desirable for achieving a good printing resolution with sufficient mechanical rigidity for building 3D hydrogel structures. But the higher extrusion forces needed to print these highly viscous materials from a small nozzle would lead to higher shear stresses and hence reduced cell viability during the printing process. To overcome this key challenge, different bioprinting approaches have been developed. Butcher and his co-workers [27] developed a novel ultraviolet (UV) bioextrusion printing technique for complex 3D structures. Living cells in a UV curable, low-viscosity PEG hydrogel solution were printed with in-situ UV radiation to solidify the printed hydrogel constructs layer by layer. As the hydrogel was cross-linked after the cells were extruded from the printing nozzle, this technique was able to significantly reduce the shear stress associated with printing high-viscosity hydrogels and produce sufficiently strong UV cross-linked structures for the regeneration of a clinical-scale human heart valve. The limitation of this approach, though, was the need for photosensitive hydrogel materials and the exposure of live cells to potentially harmful UV radiation and toxic photo-initiators.

On the other hand, more rigid poly (ε-caprolactone) PCL as a biodegradable scaffold [28] or high dense fluid oil [29] was used to support soft cell-laden hydrogels. The use of such hybrid plastic and hydrogel scaffolds enables bioprinting of organ-size structures like a human ear. However, the need for high temperature printing and acid, producing degradation of PCL, might limit their application for tissue regeneration. Alternatively, lowering the temperature of hydrogels in printing enhanced mechanical rigidity before the gel was cross-linked, resulting in pure alginate constructs that have shown the ability to support tumour growth in 3D [30, 31].

In this chapter, a new bioprinting technique using modified Fab@Home 3D printer for complex 3D alginate hydrogel structures is presented. The technique uses a three step cross-linking process to ensure the printability, rigidity, and stability of the gel that could be gentle to cells during the bioprinting process. Alginate hydrogels were chosen because of their biocompatibility and ability to form highly porous structures for cell regeneration. The degradation time of the alginate hydrogel is also investigated. Cell studies on live cell printing are described in the subsequent chapter.

3.2 Hair gel 3D printing

Hairgel (Sainsbury's Hair Gel Pot, Item Code: 6303600, Sainsbury's, UK) was first used to mimic 3D printing of alginate hydrogel. The gel was selected due to its similar viscosity and low cost in large quantities. 2D and 3D structures were printed by Fab@Home 3 model. Path speed was set 6 mm/s and extrusion rate was set at 0.45 mL/min. A nozzle with 514 µm tip diameter (OK International) was used to print the hairgel structures. Simple 2D rectangular and triangular shapes (Figure 3.1a and Figure 3.1c), hollow square structure (Figure 3.1c), star shape (Figure 3.1d) and 2D lines (Figure 3.1e) were successfully printed. The best possible repeatable resolution, achieved with the 514 µm tip, was roughly 625 µm.

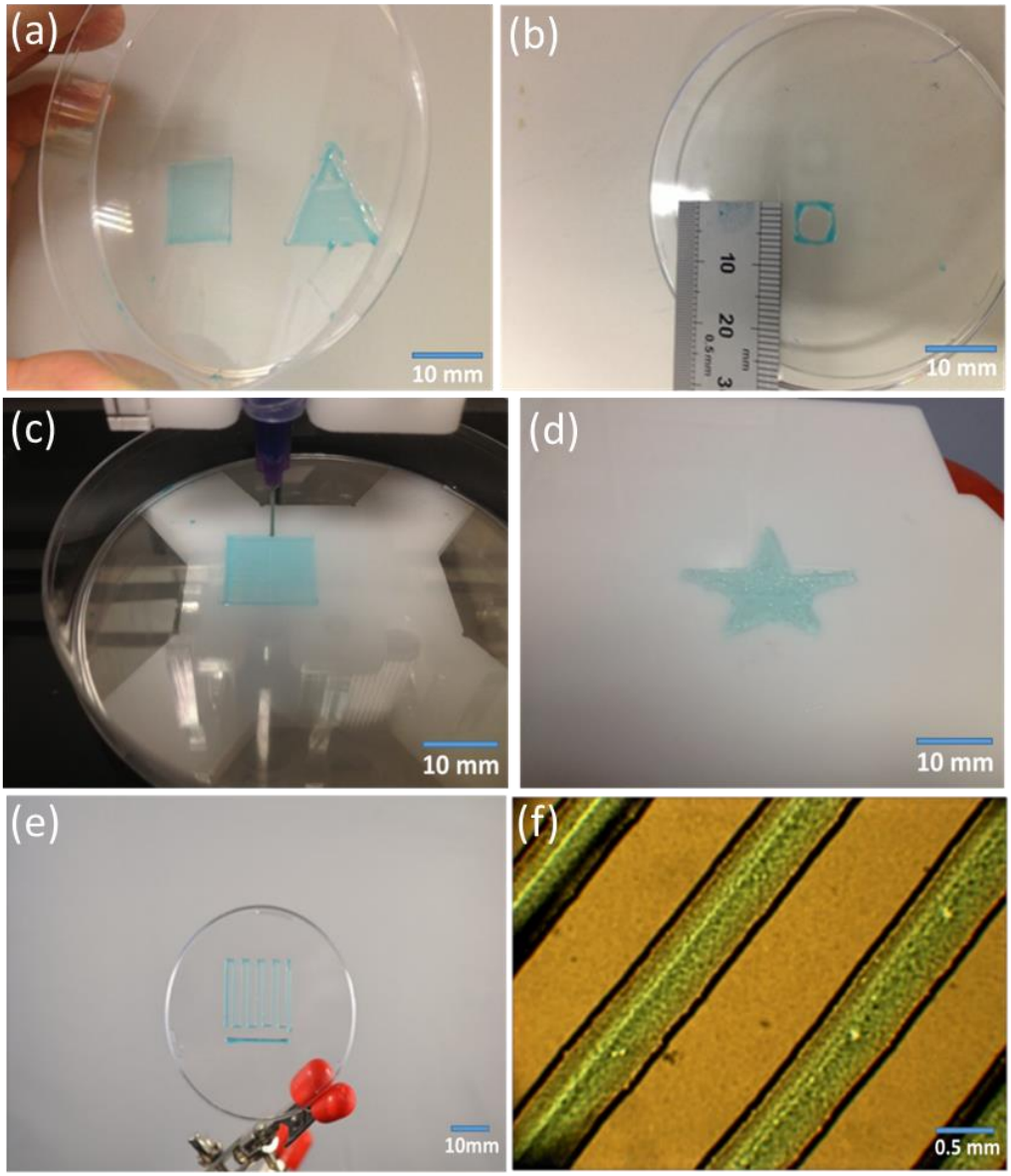

***Figure** 3.1 — Simple hairgel 2D structures printed by Fab@Home 3D printer. (a, c) Simple 2D rectangular and triangular shapes (b) hollow square structure (d) star shape (e) and 2D lines. (f) Best achievable resolution by 514 µm tip.*

3.2.1 3D printing of 3D hair gel structures

Once 2D hairgel structures were successfully printed as shown in Figure 3.1, 3D structures were designed and printed via Fab@home model 3 3D printer to investigate the possibility of printing 3D structures by hairgel.

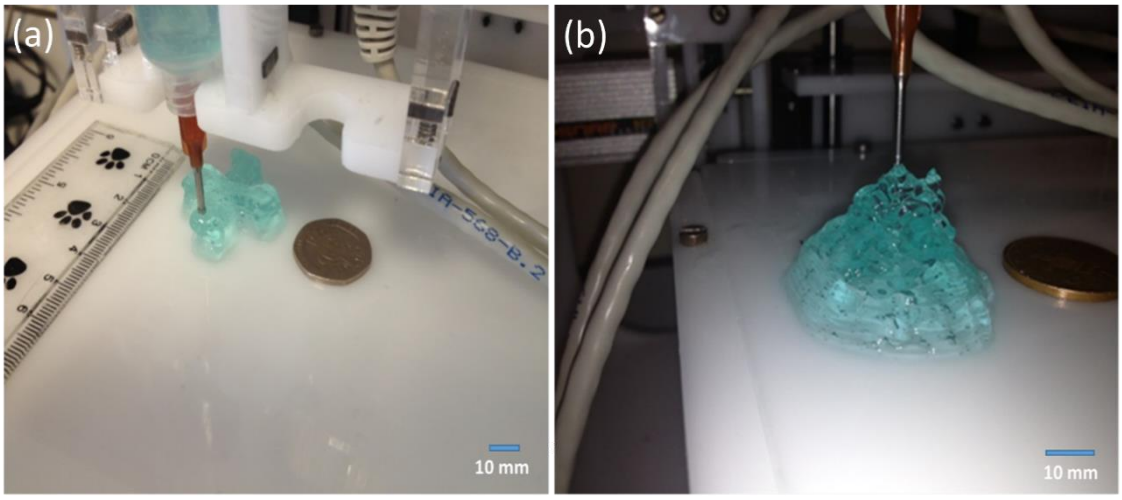

Figure 3.2 *– 3D printed hairgel structures (a) plus sign and (b) cone structure by Fab@Home 3.*

Simple 3D hair structures with limited aspect ratio were successfully printed as shown in Figure 3.2a. However 3D structures with a higher aspect ratio as shown in Figure 3.2b could not be successfully printed. The first few layers were printed successfully but due to the lack of suitable rigidity of the hairgel, the structure started to fall apart as the printing progressed. At this stage, the investigation with 3D printing of complex hairgel structures was therefore not feasible. The results generated using hairgel printing provided an improved understanding of printing alginate hydrogel.

3.3 Preparation of partially crosslinked homogeneous alginate hydrogel to increase alginate hydrogel rigidity

Non-cross-linked alginate hydrogels in general do not exhibit the required rigidity for printing complex 3D structures regardless of their concentrations and viscosity. Therefore only 2D alginate hydrogel structures could be printed. Results similar to hairgel 3D printing would be obtained if alginate structures with high aspect ratio were printed. $CaCl_2$ solutions are used to enhance the mechanical rigidity by cross-linking the alginate hydrogel [32, 33]. To enhance the mechanical rigidity of alginate hydrogel, various alginate hydrogel and $CaCl_2$ concentrations were used in order to form a homogenous partially cross-linked alginate hydrogel that might have similar mechanical properties to the hair gel. Alginate solutions (Product number W201502, Sodium Alginate, Sigma-Aldrich, Gillingham, UK) and $CaCl_2$ solutions (Product number 223506 $CaCl_2$ dehydrate, Sigma-Aldrich, Gillingham, UK) at different concentrations

and dilutions were mixed. Sodium alginate at concentrations of 1%, 2% and 3% weight to volume ratio (w/v) were mixed respectively with $CaCl_2$ solutions at concentrations of 100 mM, 200 mM and 300 mM at dilutions of 2:1, 4:1 and 10:1. The two solutions were mixed and kept at room temperature overnight allowing $CaCl_2$ to diffuse throughout the sodium alginate.

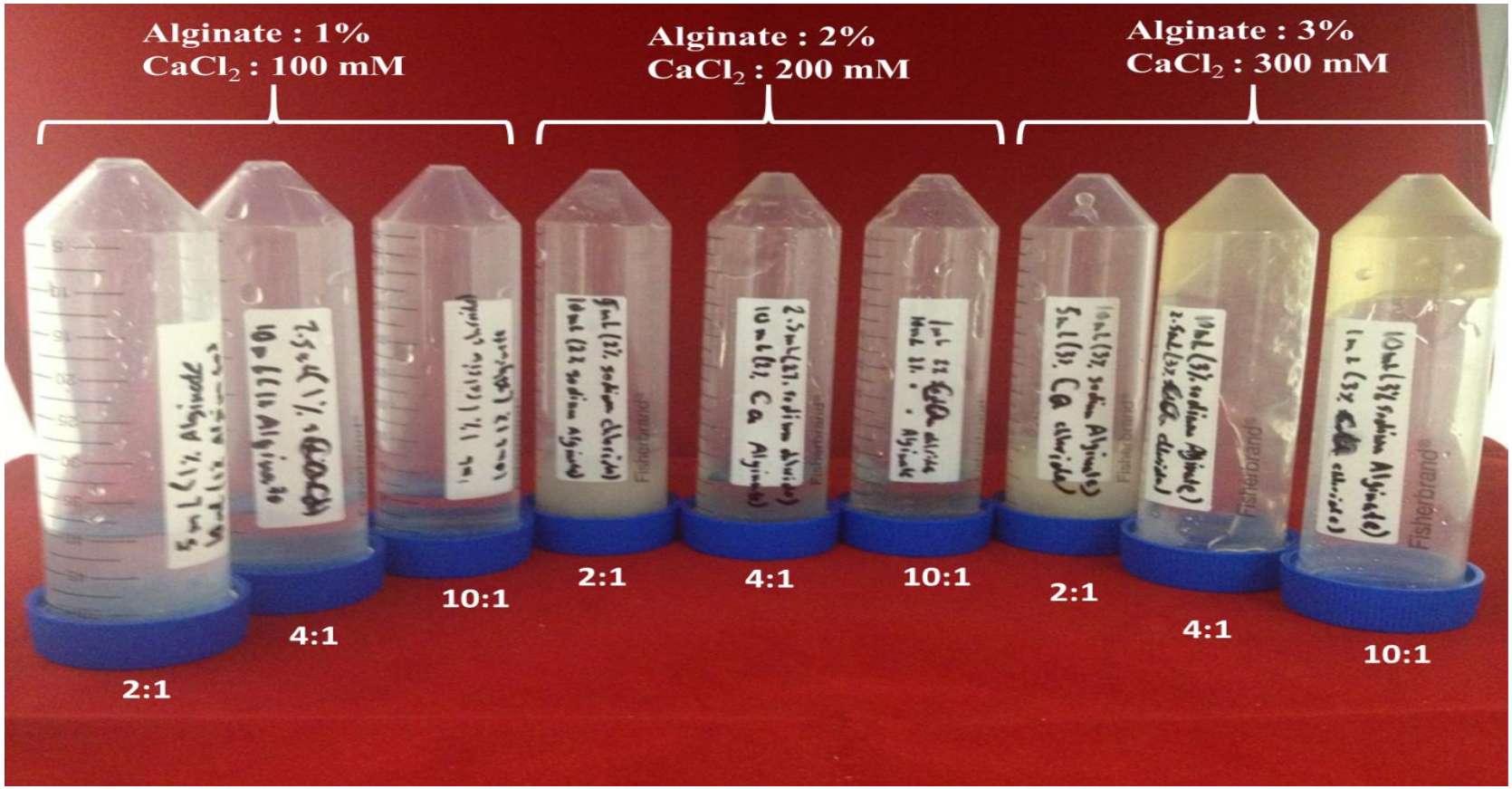

Figure 3.3 *– 1%, 2% and 3 % w/v alginate hydrogel mixed with 100 mM, 200 mM and 300 mM $CaCl_2$ respectively at 1:1, 2:1 and 4:1 dilutions.*

As shown in Figure 3.3, sodium alginate and $CaCl_2$ with the same concentrations mixed at a 2:1 dilution ratio resulted in a fully cross-linked alginate hydrogel. At a dilution of 4:1 sodium alginate appeared to be less rigid due to decreased dilution but the final gel at all concentrations was not homogenous. A 10:1 dilution resulted in a more homogenous gel at all three concentrations, however. 3% alginate mixed with 300 mM $CaCl_2$ and diluted by 10:1 featured a much more rigid property compared to 1% and 2% sodium alginate respectively mixed with 100 mM and 200 mM $CaCl_2$ at 10:1 dilution. Therefore 3% alginate with 300 mM $CaCl_2$ mixture at 10:1 dilution was chosen for 3D printing.

3.4 3D printing of 3% partially cross-linked alginate hydrogel structures

To identify the possibility of 3D printing the 3% partially cross-linked alginate hydrogel, it was printed by Fab@Home with the path speed set at 6 mm/s and the extrusion rate set at 0.45 mL/min. As shown in Figure 3.4, the partially cross-linked alginate hydrogel does not have sufficient rigidity. Therefore only simple 2D structures could be printed. To achieve a simple 2D structure with a higher aspect ratio similar to the hair gel printing, a higher concentration of sodium alginate and $CaCl_2$ were needed.

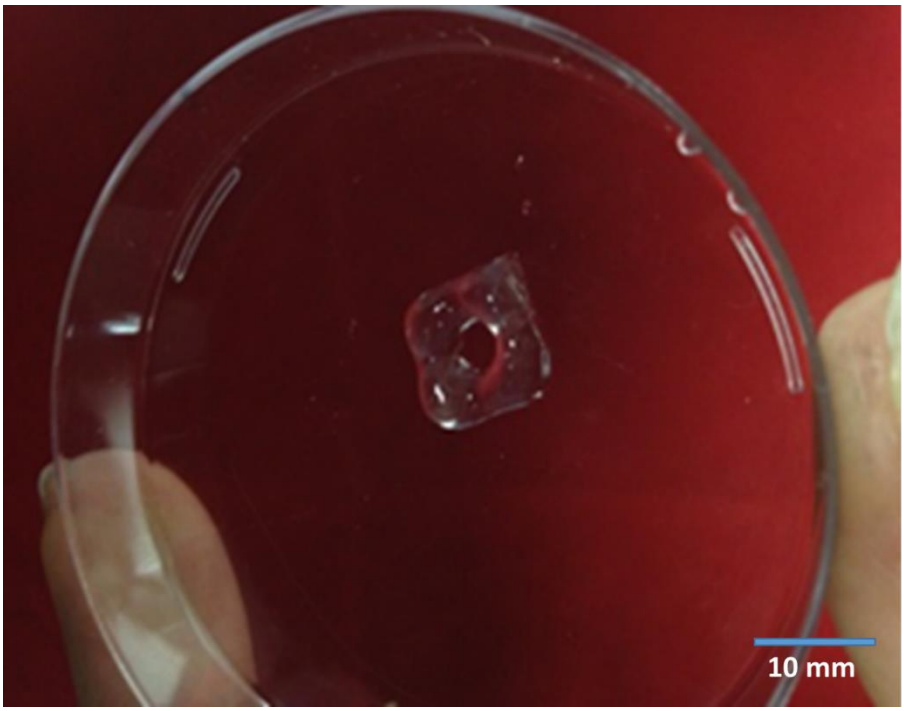

Figure 3.4 *– 3D printed 3% partially cross-linked alginate hydrogel by Fab@Home 3.*

3.5 Rapid generation of partially cross-linked alginate hydrogel

To enhance the rigidity of the gel, a higher concentration of 4% w/v sodium alginate and 400 mM $CaCl_2$ were mixed at a dilution of 10:1 and then kept overnight to partially cross-link the gel. However, this approach for producing partially cross-linked alginate hydrogel was not suitable due to the time needed for the alginate to be partially cross-linked. If cell studies are going to be carried out using bioprinting, the long wait for the gel would most probably affect the cell survival rate. For this reason, 8% alginate (w/v) and 80 mM $CaCl_2$ were mixed at 1:1 dilution. This approach resulted in partially cross-linked alginate hydrogel with the gel forming instantly. The gel was rigid and homogenous similar to the 4 % sodium alginate mixed with 400 mM $CaCl_2$ at 10:1 dilution that initially had a longer preparation time.

3.6 3D printing and viscosity measurement of different range of partially cross-linked alginate hydrogel

Sodium alginate at concentrations of 1%, 2%, 3%, 4%, 5%, 6%, 7%, 8%, 9%, 10%, 11 % and 12 % (w/v) were mixed with $CaCl_2$ Solutions at concentrations of 10 mM, 20 mM, 30 mM, 40 mM, 50 mM, 60 mM, 70 mM, 80 mM, 90 mM, 100 mM, 110 mM and 120 mM respectively at a volume ratio of 1:1 to partially cross-link the sodium alginate as shown in Figure 3.5. Various ranges of partially cross-linked alginate hydrogels were printed into 20 mm × 20mm × 2 mm structures to find the optimum hydrogel concentration with the ability to self-support. The zero shear viscosity profile measurement of each partially cross-linked alginate hydrogel was measured by Bohlin Gemini rheometer (Malvern Instruments). Dynamic viscosities of the partially cross-linked alginate hydrogels were also measured by Gemini rheometer for 6 minutes at a shear rate of 1/s.

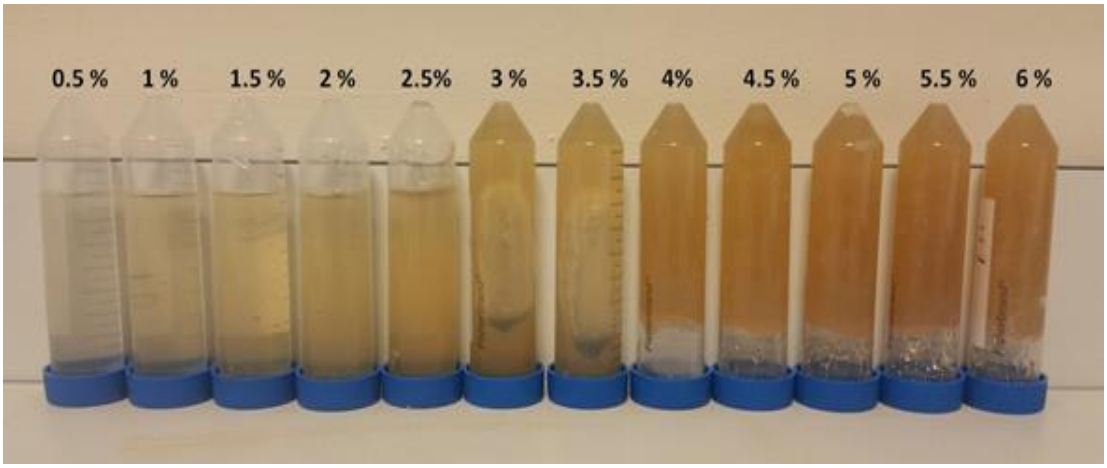

Figure 3.5 *– Prepared partially cross-linked alginate hydrogels with their relevant cross-linking reagents in ascending order from left to right.*

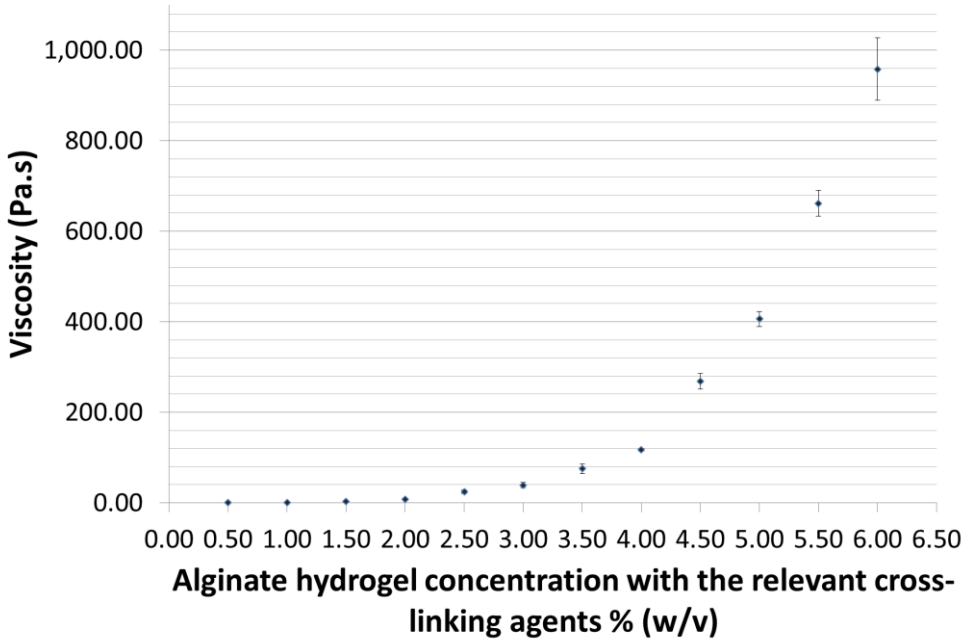

Figure 3.6 *– partially cross-linked alginate hydrogel zero shear viscosity measurements.*

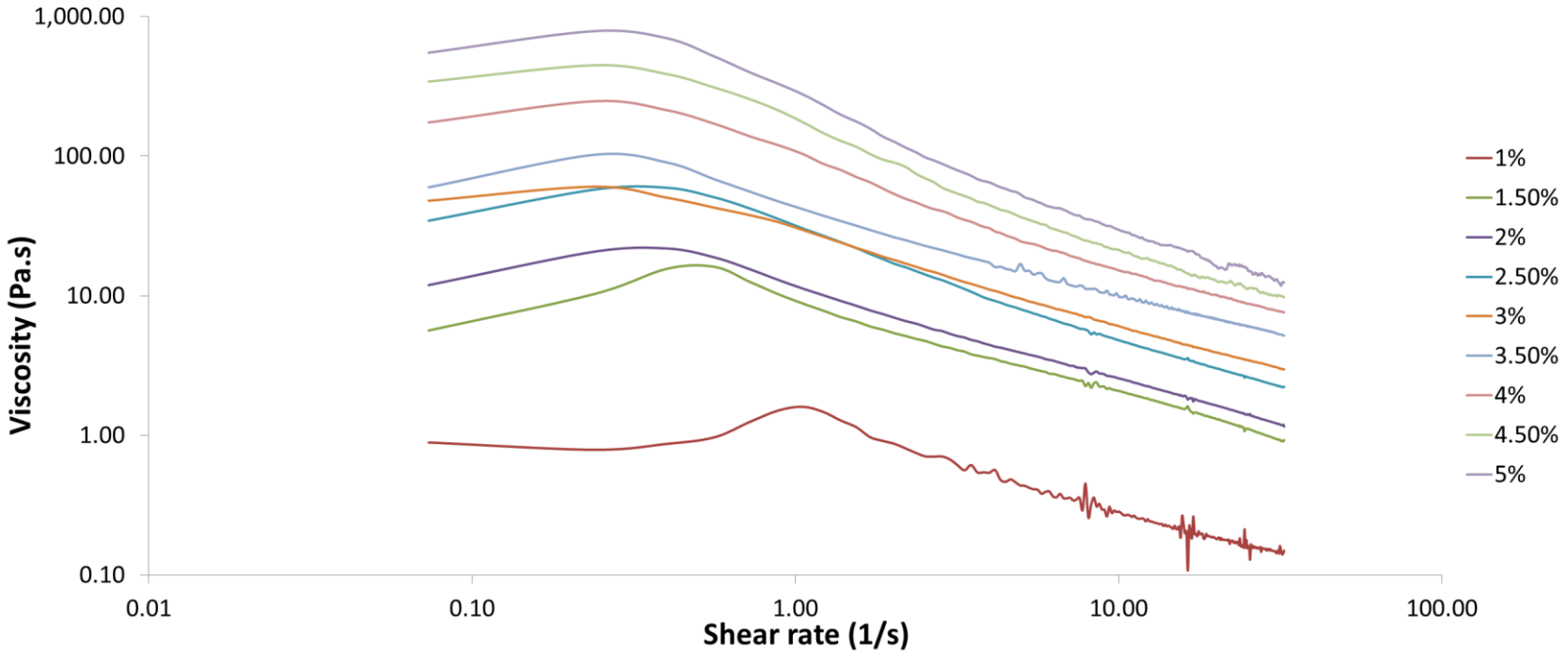

Figure 3.7 *— Dynamic viscosity measurement of partially cross-linked alginate hydrogels*

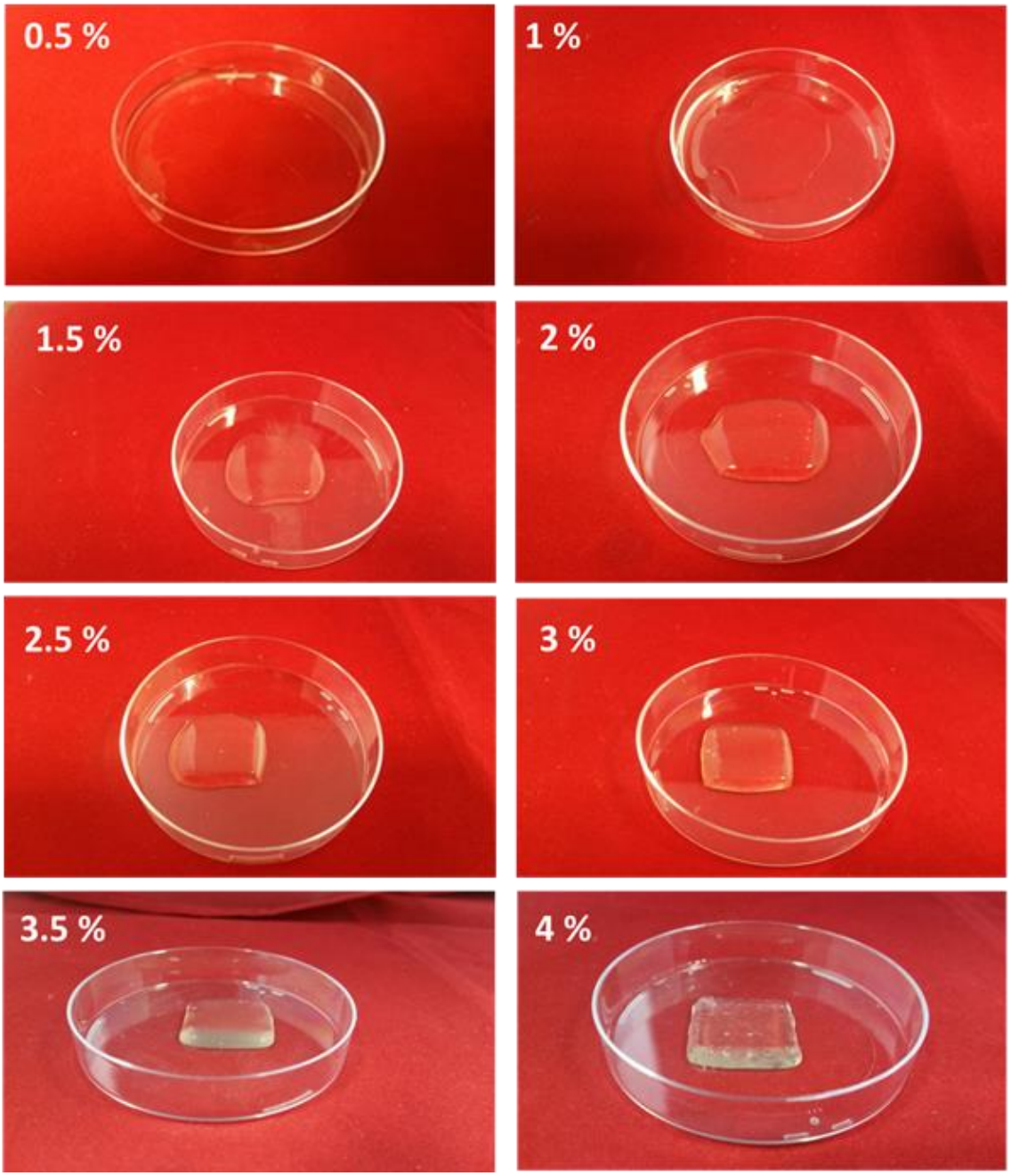

Figure 3.8 *– 3D printed structures (20 mm × 20 mm × 2 mm) with different concentrations of partially cross-linked alginate hydrogel with their relevant pre cross-linking reagents*

In order to fine-tune the optimal conditions for 3D printing partially cross-linked alginate hydrogel, a wide range of alginate hydrogels with relevant cross-linking conditions were prepared and printed as shown in Figure 3.8. Partially cross-linked alginate concentrations from 0.5% up to 2.5 % did not exhibit sufficient mechanical strength to self-support the printed structures shown in Figure 3.8. Higher concentrations of alginate at 3% and 3.5% could preserve the structure's shape, however

the printed structures were too soft to maintain good structural integrity. The minimum alginate concentration that could self-support its structure with good structural integrity was found to be 4% (w/v) with final $CaCl_2$ concentration of 40 mM. The prepared partially cross-linked alginate hydrogels had viscosities ranging from 0.13 ± 0.12 Pa.s at 0.5% to 958 ± 69 Pa.s at 6%. The viscosity increased exponentially with alginate hydrogel concentration as shown in Figure 3.6. The hydrogel with the minimum rigidity needed to withstand its shape had a final alginate concentration of 4% (w/v) and $CaCl_2$ concentration of 40 mM, and had a viscosity of 117 ± 2.5 Pa.s. There appeared to be a turning point in the viscosity change at around 4%. Additionally, visual inspection of alginate in centrifuge tubes shows 4% was also the transitional point of alginate concentration where more solid hydrogel was formed.

3.7 3D printing of 4% partially cross-linked alginate hydrogel structures with higher aspect ratio

20 mm × 20 mm × 5 mm cubic structures with were printed to investigate whether the 4% partially cross-linked alginate hydrogel is able to support itself.

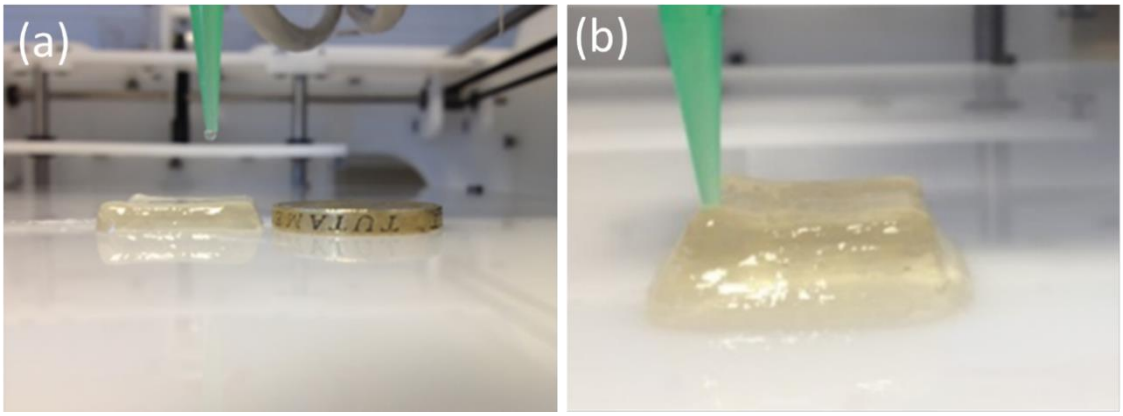

Figure 3.9 *– (a) 3D printed 20 mm × 20 mm × 2 mm (b) and 20 mm× 20 mm × 5 mm by 4% partially cross-linked alginate hydrogel.*

As seen in Figure 3.9a, the 4% partially cross-linked hydrogel could be easily printed up to a height of approximately 2 mm. However, the gel started to collapse once the structure was furthermore printed above this height as shown in Figure 9b. This was similar to the behaviour of hairgel as described earlier. Therefore the 4 % partially

cross-linked hydrogel was suitable for printing 3D structures with a limited aspect ratio similar to the hairgel.

3.8 Development of a novel 3D printing technique to print complex 3D alginate hydrogel structures

At this point, use of higher concentration of partially cross-linked alginate hydrogel would not be recommended as the viscosity would increase and shear stress applied to the cells during bioprinting would significantly increase and eventually damage the cells. A modified version of an open source Fab@Home model dual syringe extrusion-based 3D printer was used as the main printing platform for the alginate hydrogel. It consisted of an automated X-Y-Z stage where the positioning precision is 100 µm. With its dual switchable dispensing system, it was capable of printing with a precision down to 100 µm in the X-Y plane as well as printing with a precision of 100 µm in the Z plane. Fab@Home models have previously been used to print alginate hydrogel and other biomaterials such as gelatine [34, 35]. A modified new Z axis carriage, shown in Figure 3.10, was designed and put in place to enable immersion of the Z platform into a 100 mM $CaCl_2$ solution bath as the secondary cross-linking reagent to further cross-link the printed partially cross-linked alginate hydrogel. Initially the first few layers of partially cross-linked alginate hydrogel are printed above the $CaCl_2$ solution on a porous nitrocellulose membrane. The membrane ensures adhesion of the partially cross-linked hydrogel to the surface for better support while allowing $CaCl_2$ solution diffusing into the structure for cross-linking. The diffusion occurs due to the higher mass concentration of the $CaCl_2$ bath compared with the $CaCl_2$ concentration in the printed layers outside the interface layer. The porous membrane is connected to a thin PMMA (Poly methyl methacrylate) sheet with pore sizes of 0.8 mm to allow $CaCl_2$ to enter the inner sections of the printed structures. The z-axis is lowered, submerging the first printed layers in the $CaCl_2$ solution for further cross-linking as shown in Figure 11. The subsequent printing of the alginate hydrogel was supported by the partially cross-linked hydrogel structures above the solution. Diffusion would also enable $CaCl_2$ solution to penetrate inside the hollow sections of the printed layers as well as the layers that are being printed above the $CaCl_2$ solution, forming an interface layer where rigidity of the hydrogel layers was sufficient to support a few layers of printed hydrogel structures. By repeating this sequential printing process, a complete 3D structure was generated.

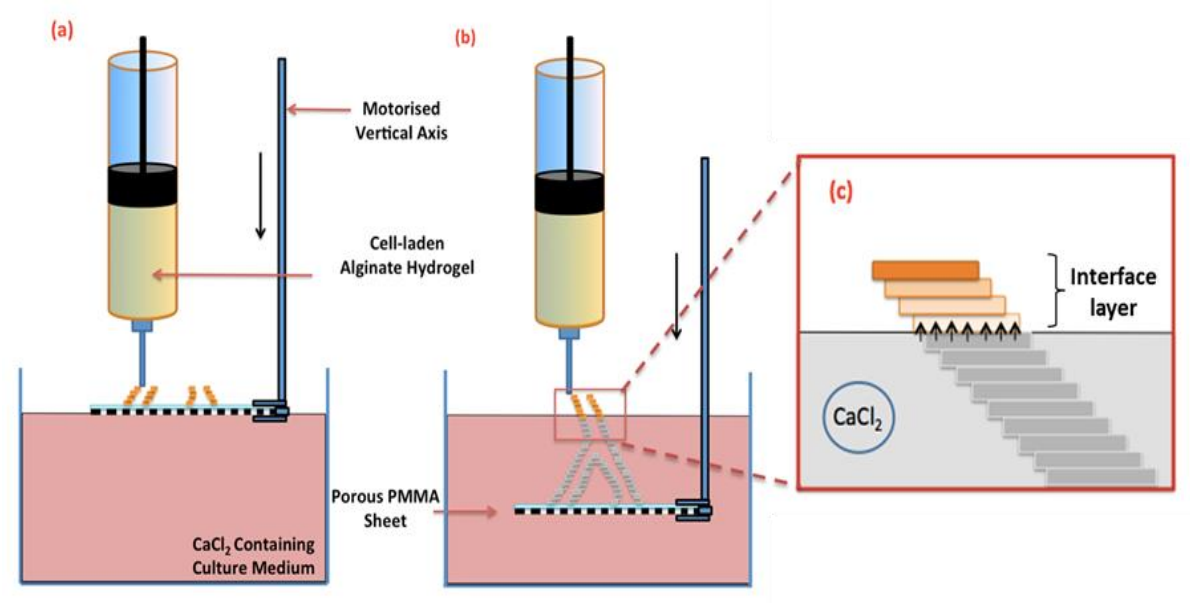

Figure 3.10 *– Schematic drawing of the alginate hydrogel 3D printing setup. (a) First a few layers of partially cross-linked alginate hydrogel were printed on the porous membrane. At this stage the structure was able to support its own shape. (b) Further crosslinking of the hydrogel once the Z axis was lowered down and the printed partially cross-linked alginate hydrogel were submerged into the $CaCl_2$ bath, which creates a better support for the upcoming layers. (c) The interface layers: upward diffusion of Ca^{+2} ions into the interface layers which are partially cross-linked above the $CaCl_2$ solution.*

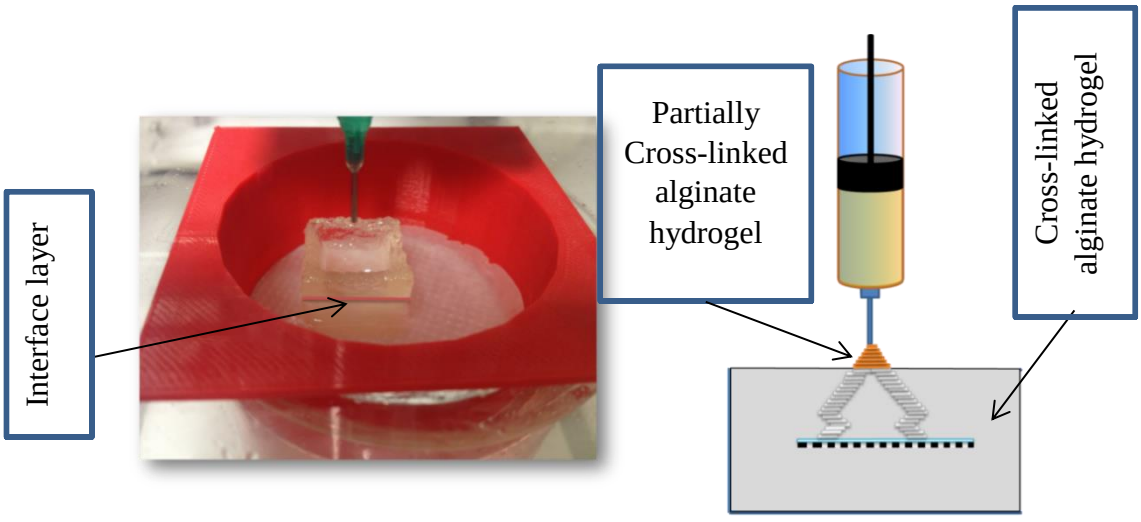

Figure 3.11 *– 3D printing of alginate hydrogel structures showing the interface layer where partially cross-linked alginate hydrogel is being printed above the interface layer*

3.9 Shear stress and viscosity

Shear stress and viscosity play a major role in bioextrusion. The higher the viscosity (the resistance to flow), the higher the shear stress when the cell-laden hydrogels are extruded through the syringe tip. Shear stress in a pipe is defined by:

$$\tau = \mu.\gamma$$

Where τ is the shear stress, μ is the viscosity and γ is the shear rate. In a simple geometry with a single flow direction it is defined by

$$\gamma = \frac{dy}{dx}$$

This is measured in s^{-1}. Based on the shear stress equation, increasing the viscosity and shear rate would increase the shear stress on the cells, causing damage to the cells. However, as shown in Figure 3.7 the partially cross-linked alginate hydrogel behaves like a shear thinning fluid, meaning an increasing the shear rate reduces the viscosity, making is easier for the fluid to flow. Shear thinning fluids do act like Newtonian fluids when subject to extreme low or high shear rates. However the power-Law region is where the fluid exhibits shear thinning behaviour. The shear stress in a shear thinning fluid in the Power-Law region can be written as:

$\tau = a(\dot{\gamma})^n$Where a is a constant that describes the flow consistency of the substance and n is the value of power law index which usually lies in between 0.3 to 0.7 depending upon the concentration and molecular weight of the hydrogel. The viscosity can be now written as:

$$\mu = a(\dot{\gamma})^{n-1}$$

In general, an increase in viscosity enhances the rigidity of the printed structure however this would increase the shear stress, causing cell damage. Another important factor is the time that cells undergo shear stress. The longer cells are exposed to shear stress the greater the chance of cell damage. The effect of viscosities on cell viability is discussed in the next chapter.

3.10 3D printing resolution

To identify the best possible printing resolution, tips with different diameters were used to print grid structures. The grid structure dimensions were set at 3 cm × 3 cm × 2 mm. The tips used for 3D printing had diameters of 838 µm, 514 µm, 337 µm and 210 µm.

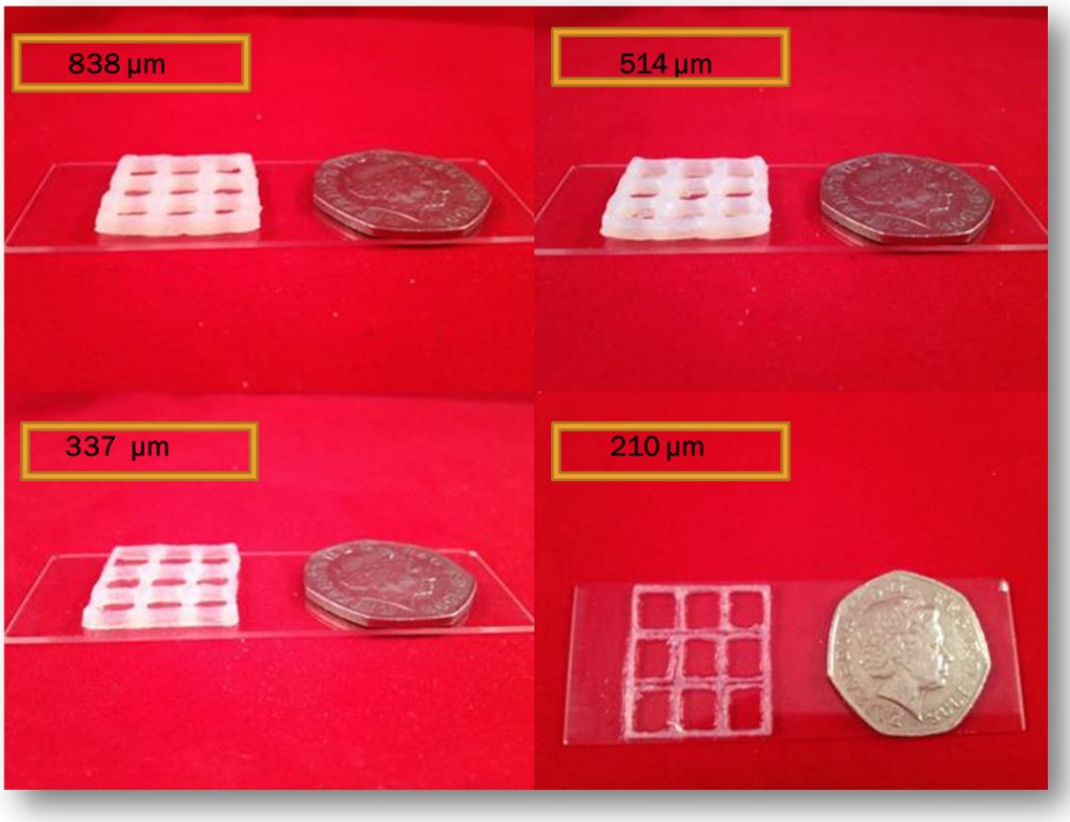

Figure 3.12 *– 3D printed grid structures with 4 % partially cross-linked alginate hydrogel using the proposed technique by 838 µm, 514 µm, 337 µm and 210 µm tip. Scale bar: 50p coin.*

The grid structures created are shown in Figure 3.12. The thickness of the grid structures printed by the 800 µm and 500 µm tips were similar, however the thickness of the grid structure printed by the 300 µm tip was much finer. Grid structures printed by 200 µm tip could not be completed as the structure was not able to hold its shape due to the thin nature of the printed walls. Therefore at this stage the minimum nozzle tip used for 3D printing was set at 337 µm diameter.

3.11 3D printing alginate structures

Figure 3.13a shows the simple 3D printed alginate hydrogel tubular structures with descending diameters of 20 mm, 15 mm, 10 mm, and 7.50 mm. The tubular structures were printed using a 0.33 mm ID nozzle. They were made of 8 printed layers each 2.5 mm in height. All tubes had a wall thickness of 1.25 ± 0.05 mm as measured by a calliper. Figure 3.13b shows 10 mm diameter 3D printed alginate hydrogel tubular structures with 32, 24, 16 and 8 printed layers. The heights of these printed structures were 10.20 mm, 7.40 mm, 5.30 mm and 2.65 mm respectively. This indicated that the

average printing height was 322 ± 11 µm/ layer. Furthermore, complex 3D structures such as branched vascular structures shown in Figure 3.13d and Figure 3.13e were printed successfully by 0.51 mm and 0.33 mm ID tips. The height of the interface layers can be adjusted to ensure the best printing quality depending upon the complexity of the printed structures. For example, for simple 3D structures such as hollow tubes in which the same printing pattern was repeated, the maximum allowable distance of the interface layer from the nozzle tip to the $CaCl_2$ bath was found to be 2 mm i.e. 4 layers for 0.51 mm ID tip and 7 layers for 0.33 mm ID tip. For complex 3D angular structures it was 0.5mm i.e. 1 layer for 0.51 mm ID tip and 2 layers for 0.33 mm ID tip. The reason for having a shorter distance between the nozzle tip and $CaCl_2$ solution interface for bioprinting complex 3D structures was that with a large distance the partially cross-linked alginate hydrogel was unable to support itself when printed at an angle. It was noticed, however, that when the nozzle tip was too close to the $CaCl_2$ solution, boundaries were formed between the printed layers because the Ca^{2+} ions could easily diffuse into the printed layers above the $CaCl_2$ bath. If the nozzle tip is far enough from the $CaCl_2$ bath interface, the printed layers above the $CaCl_2$ solution can merge together more effectively and form a more uniform and continuous construct. This new feature provides improved mechanical properties of the alginate hydrogel structures as well as the possibility to bioprint complex structures. This is consistent with recent findings on continuous 3D printing using the Continuous Liquid Interface Production (CLIP) technique [36]. This is mainly due to printing the partially crosslinked hydrogel outside the interface rather than inside the bath. The partially cross-linked hydrogel has adhesive properties, helping the printed layers to merge into each other outside the interface.

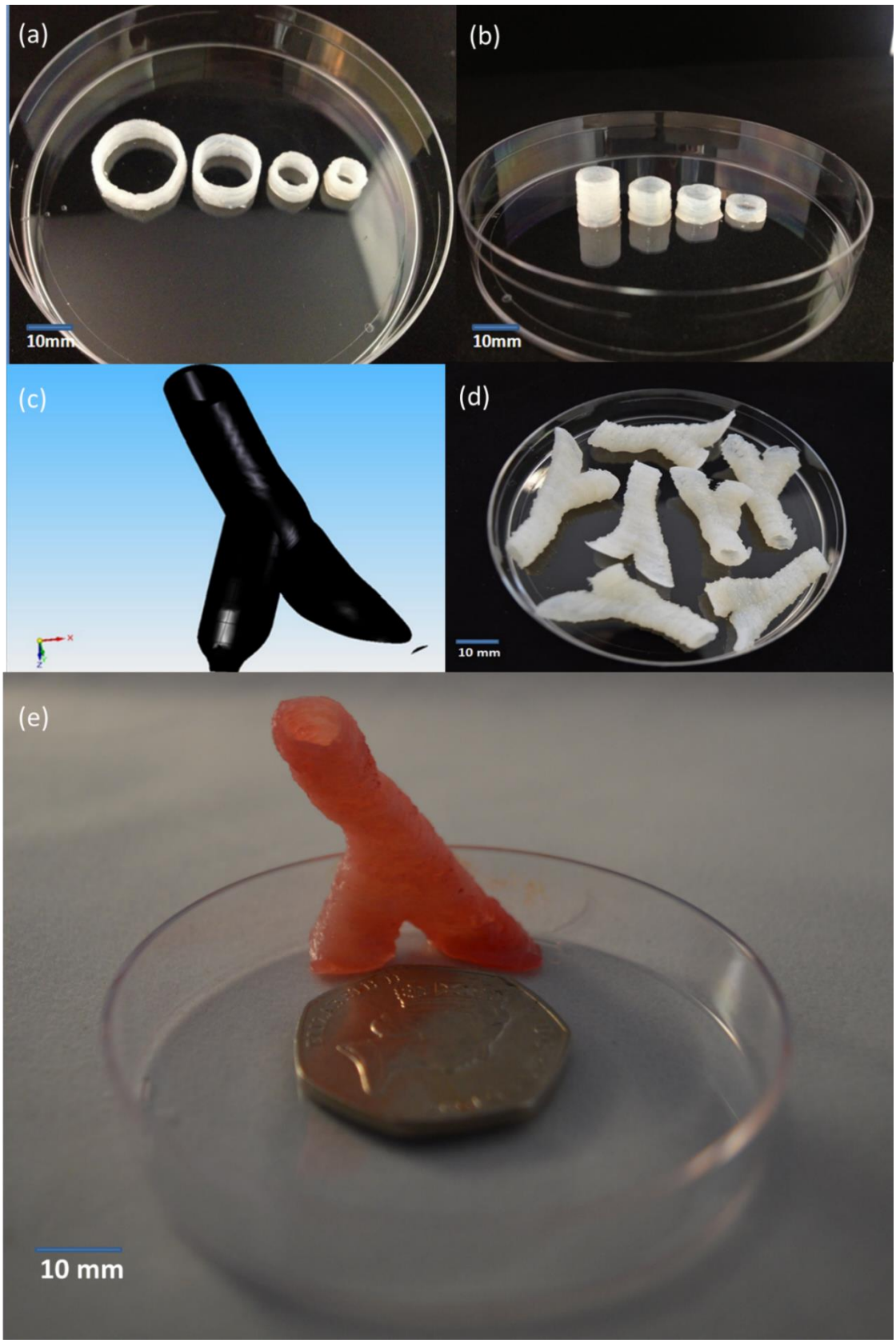

Figure 3.13 *– (a) Printed tube structures with reducing diameters (b) and reducing height .(c) CAD file of the vascular structure in Solid Edge version V20 (d) vascular structures printed by 0.51mm diameter tip (e) vascular structure printed by 0.33 mm diameter tip.*

3.12 Degradation of hydrogel and the optimisation of cross-linking conditions

This study was carried out to control and enhance the degradation time of the alginate hydrogel by further cross-linking it with other reagents [37]. $BaCl_2$ solutions at different concentrations were used in order to achieve a suitable degradation time of the alginate hydrogel. The printed grid structures were exposed to 100 mM of $CaCl_2$ for 10 minutes and were kept in a culture medium (DMEM, 1.8mM $CaCl_2$) for 7 days as shown in Figure 3.14a. The alginate structure started to break down by the second day and slowly degraded completely after 7 days as expected. By exposing the alginate hydrogel to 10 mM, 20 mM and 40 mM of $BaCl_2$ for 2 minutes after initially being exposed to 100 mM of $CaCl_2$ for 10 minutes, structural degradation was reduced in proportion to the $BaCl_2$ concentration. Exposure to 10 mM of $BaCl_2$ as shown in Figure 3.14b was not enough to keep the printed structure in place over 7 days, as the printed grid structure broke down day by day although it was not completely dissolved by day 7. Exposure to 20 mM of $BaCl_2$ as shown in Figure 3.14c improved the degradation time of the alginate hydrogel. Once again, however, the structure started to crack slowly and any external forces could easily break the grid structure, which can cause the cells to escape the alginate structures. 40 mM $BaCl_2$ as shown in Figure 3.14d was able to keep the structure in place over 7 days without the appearance of visible cracks within the grid structure. Based on the alginate hydrogel degradation results, at this stage, 40 mM $BaCl_2$ was the minimum concentration needed to be used as the tertiary cross-linking reagent. The cell viability needed to be examined, however, to investigate whether the secondary and tertiary cross-linking process had any negative effects.

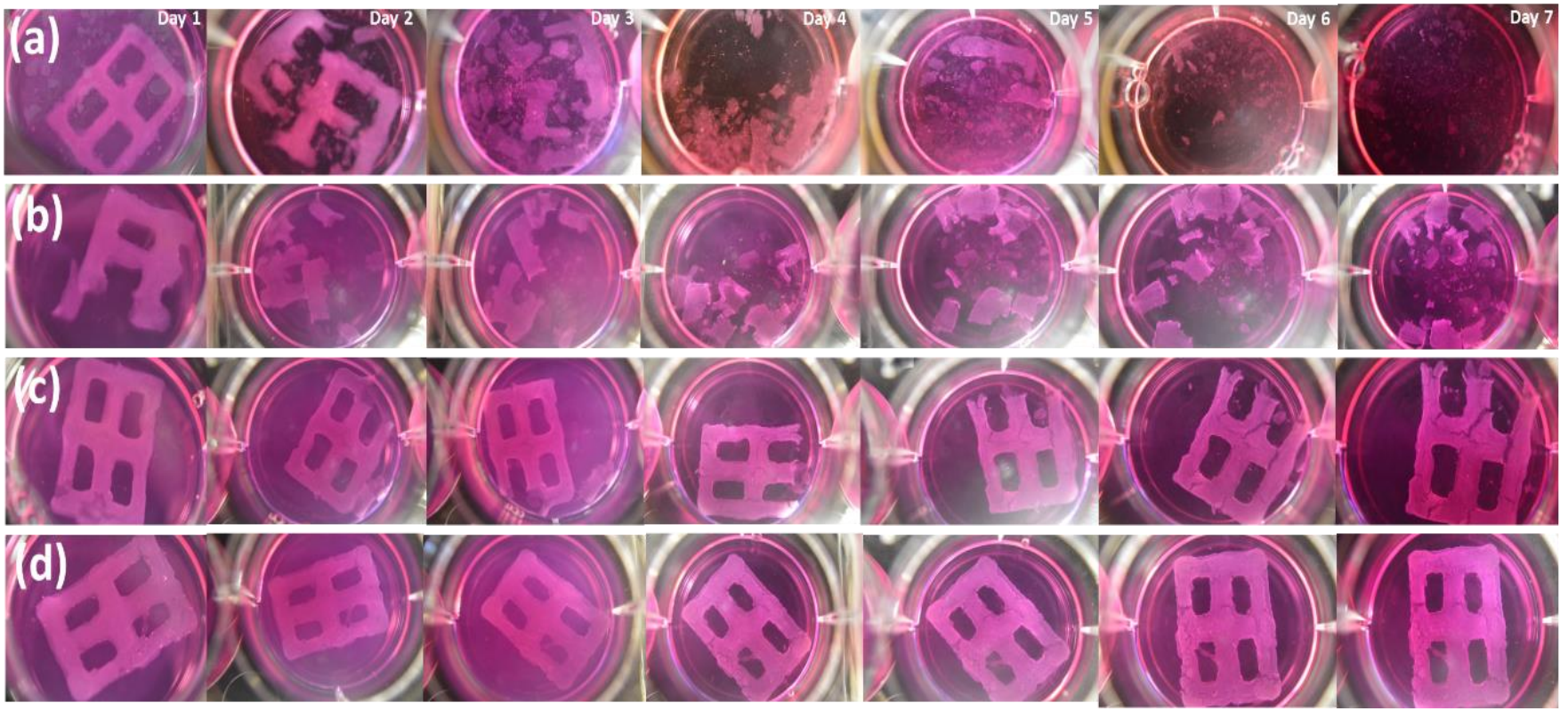

Figure 3.14 *– (a) Bioprinted 4% partially cross-linked alginate hydrogel grid structure exposed to 100 mM $CaCl_2$ for 10 minutes and (b) 10 mM (c) 20 mM (d) 40 mM $BaCl_2$ for 2 minutes. The structures were then kept in culture medium over 7 days. (All grid structures were cultured in 6 well plates with each well having 50 mM diameter)*

3.12.1 Gel degradation based on constant exposure of the gel to $CaCl_2$

Another set of experiments was carried out to investigate the degradation time of the gel when it is constantly exposed to 10 mM, 20 mM, 30 mM, 40 mM and 50 mM of $CaCl_2$ within the culture medium. As shown in Figure 15b, the printed gel stayed stable until day 5 and then started to break down on day 6. However, by the constant exposure of the gel to 20 mM, 30 mM, 40 mM, and 50 mM of $CaCl_2$ the grid structures stayed stable over 7 days as shown in Figure 15c, Figure 15d, Figure 15e and Figure 15f respectively. Although the gel is kept stable, this condition might be harmful to cells. Cell studies therefore need to be carried out to identify the effect of constant exposure of the cells to $CaCl_2$.

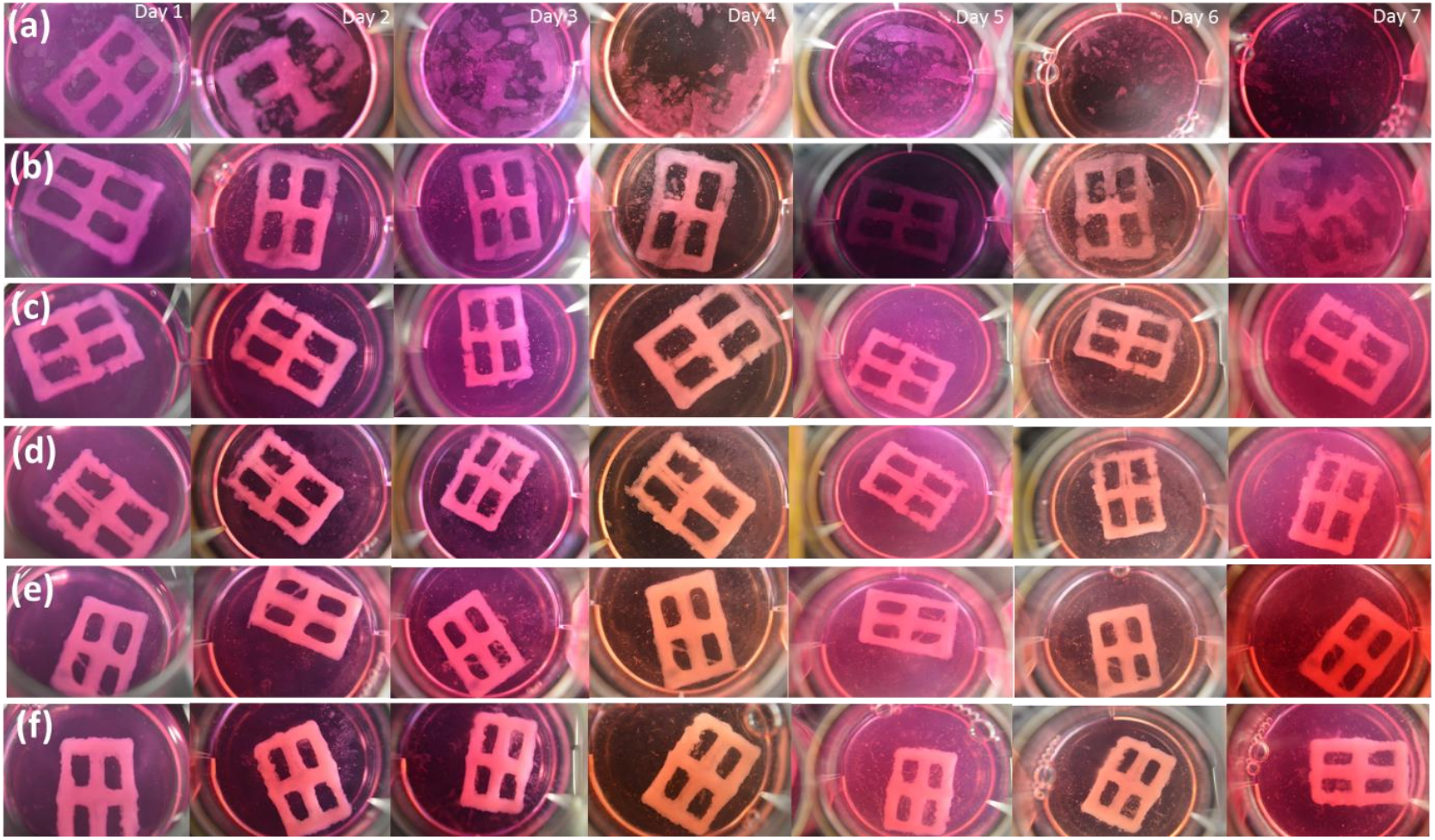

Figure 3.15 *— (a) Bioprinted 4 % partially cross-linked alginate hydrogel grid structure exposed to 100 mM $CaCl_2$ for 10 minutes. Grid structures exposed to constant exposure to (b) 10 mM (c) 20 mM (d) 30 mM (e) 40 mM (f) 50 mM in culture medium. The structures were then kept in culture medium over 7 days. (All grid structures were cultured in 6 well plates with each well having 50 mM diameter)*

3.13 Conclusions

In this chapter, a new printing technique for 3D printing of alginate-based hydrogel structures was developed. Using this new free-form fabrication technique, partially cross-linked alginate hydrogels were formulated with tuneable mechanical properties to create tubular and more complex, continuous 3D hydrogel structures. The degradation time of alginate hydrogel in cell culture media was investigated and the stability of the alginate hydrogel can be enhanced by post-printing treatment of $BaCl_2$. This is a promising bioprinting technique that can be applied to fabricate clinically sized soft tissues with more complex and multi-cellular structures.

The key working principle of the new bioprinting method is the ability to print alginate hydrogels with sufficiently high viscosity so that the printed structure can self-support and form an interface layer. In this way, new layers of fresh partially crosslinked alginate hydrogel can be printed onto a relatively solid substrate or the interface layer above the crosslinking reagent bath to build the structure layer-by-layer. However, the fully cross-linked hydrogel for extrusion would not be suitable because it would require a higher shear stress for printing. This could have an adverse effect on cell viability, in addition to the poor adhesion between the printed layers. In order to achieve this balance, concentrations of alginate and $CaCl_2$ solutions were developed to form partially cross-linked alginate hydrogel. This was designed to achieve sufficient mechanical rigidity with sufficiently low viscosity to avoid high printing shear stresses. A range of alginate concentrations (i.e. 1% w/v to 8% w/v) and $CaCl_2$ concentrations (i.e. 10 mM to 800 mM) combinations were made to produce the partially crosslinked hydrogel mixture for testing the best printing quality. The composition of 4% alginate and 40 mM $CaCl_2$ was found to be the minimum concentration needed to create the interface layers.

The next chapter investigates the cell survival rate based on this new 3D printing concept.

Chapter 6 References

[1] Mironov, V., Trusk, T., Kasyanov, V., Little, S., Swaja, R., & Markwald, R. (2009). Biofabrication: a 21st century manufacturing paradigm. Biofabrication, 1(2), 022001.

[2] Wang, C., Tang, Z., Zhao, Y., Yao, R., Li, L., & Sun, W. (2014). Three-dimensional in vitro cancer models: a short review. Biofabrication, 6(2), 022001.

[3] Huang, G., L. Wang, S. Wang, Y. Han, J. Wu, Q. Zhang, F. Xu and T. J. Lu (2012). "Engineering three-dimensional cell mechanical microenvironment with hydrogels." Biofabrication 4(4): 042001.

[4] Reiffel AJ, Kafka C, Hernandez KA, Popa S, Perez JL, Zhou S, Pramanik S, Brown BN, Ryu WS, Bonassar LJ, Spector JA (2013) High-Fidelity Tissue Engineering of Patient-Specific Auricles for Reconstruction of Pediatric Microtia and Other Auricular Deformities. PLoS ONE 8(2): e56506.

[5] Boland, T., X. Tao, B. J. Damon, B. Manley, P. Kesari, S. Jalota and S. Bhaduri (2007). "Drop-on-demand printing of cells and materials for designer tissue constructs." Materials Science and Engineering: C 27(3): 372-376.

[6] Hollister, S. J. (2005). "Porous scaffold design for tissue engineering." Nat Mater 4(7): 518-524.

[7] Koch, L., A. Deiwick, S. Schlie, S. Michael, M. Gruene, V. Coger, D. Zychlinski, A. Schambach, K. Reimers, P. M. Vogt and B. Chichkov (2012). "Skin tissue generation by laser cell printing." Biotechnology and Bioengineering 109(7): 1855-1863.

[8] Xu, T., K. W. Binder, M. Z. Albanna, D. Dice, W. Zhao, J. J. Yoo and A. Atala (2013). "Hybrid printing of mechanically and biologically improved constructs for cartilage tissue engineering applications." Biofabrication 5(1): 015001.

[9] Arai, K., S. Iwanaga, H. Toda, C. Genci, Y. Nishiyama and M. Nakamura (2011). "Three-dimensional inkjet biofabrication based on designed images." Biofabrication 3(3): 034113.

[10] Yamaguchi, S., A. Ueno, Y. Akiyama and K. Morishima (2012). "Cell patterning through inkjet printing of one cell per droplet." Biofabrication 4(4): 045005.

[11] Nishiyama, Y., M. Nakamura, C. Henmi, K. Yamaguchi, S. Mochizuki, H. Nakagawa and K. Takiura (2008). "Development of a Three-Dimensional Bioprinter: Construction of Cell Supporting Structures Using Hydrogel and State-Of-The-Art Inkjet Technology." Journal of Biomechanical Engineering 131(3): 035001-035001.

[12] Kang, K.H., L.A. Hockaday, and J.T. Butcher (2013) Quantitative optimization of solid freeform deposition of aqueous hydrogels. Biofabrication, 5(3): p. 035001.

[13] Cui, X. and T. Boland (2009). "Human microvasculature fabrication using thermal inkjet printing technology." Biomaterials 30(31): 6221-6227.

[14] Shim, J.-H., J. Y. Kim, M. Park, J. Park and D.-W. Cho (2011). "Development of a hybrid scaffold with synthetic biomaterials and hydrogel using solid freeform fabrication technology." Biofabrication 3(3): 034102.

[15] Shim, J.-H., J.-S. Lee, J. Y. Kim and D.-W. Cho (2012). "Bioprinting of a mechanically enhanced three-dimensional dual cell-laden construct for osteochondral tissue engineering using a multi-head tissue/organ building system." Journal of Micromechanics and Microengineering 22(8): 085014.

[16] Faulkner-Jones, A., S. Greenhough, J. A. King, J. Gardner, A. Courtney and W. Shu (2013). "Development of a valve-based cell printer for the formation of human embryonic stem cell spheroid aggregates." Biofabrication 5(1): 015013.

[17] Li, C., A. Faulkner-Jones, A. R. Dun, J. Jin, P. Chen, Y. Xing, Z. Yang, Z. Li, W. Shu, D. Liu and R. R. Duncan (2015). "Rapid Formation of a Supramolecular

Polypeptide–DNA Hydrogel for In Situ Three-Dimensional Multilayer Bioprinting." Angewandte Chemie International Edition 54(13): 3957-3961.[18] Khalil, S. and Sun, W. (2009). Bioprinting Endothelial Cells With Alginate for 3D Tissue Constructs. Journal of Biomechanical Engineering,. 131(11): p. 111002-111002.

[19] Faulkner-Jones, A., Fyfe, C., Cornelissen, DJ., Gardner, J., King, J., Courtney, A., and Shu, W. (2015). "Bioprinting of Human Pluripotent Stem Cells and Their Directed Differentiation into Hepatocyte-Like Cells for the Generation of Mini-Livers in 3D." Biofabrication 7(4): 044102.

[20] Ali, M., E. Pages, A. Ducom, A. Fontaine and F. Guillemot (2014). "Controlling laser-induced jet formation for bioprinting mesenchymal stem cells with high viability and high resolution." Biofabrication 6(4): 045001

[21] Gudapati, H., J. Yan, Y. Huang and D. B. Chrisey (2014). "Alginate gelation-induced cell death during laser-assisted cell printing." Biofabrication 6(3): 035022.

[22] Gruene, M., M. Pflaum, A. Deiwick, L. Koch, S. Schlie, C. Unger, M. Wilhelmi, A. Haverich and B. N. Chichkov (2011). "Adipogenic differentiation of laser-printed 3D tissue grafts consisting of human adipose-derived stem cells." Biofabrication 3(1): 015005.

[23] Ovsianikov, A., M. Gruene, M. Pflaum, L. Koch, F. Maiorana, M. Wilhelmi, A. Haverich and B. Chichkov (2010). "Laser printing of cells into 3D scaffolds." Biofabrication 2(1): 014104.

[24] Guillotin, B., A. Souquet, S. Catros, M. Duocastella, B. Pippenger, S. Bellance, R. Bareille, M. Rémy, L. Bordenave, J. Amédée and F. Guillemot (2010). "Laser assisted bioprinting of engineered tissue with high cell density and microscale organization." Biomaterials 31(28): 7250-7256. .

[25] Arcaute, K., B. Mann, and R. Wicker (2006). Stereolithography of Three-Dimensional Bioactive Poly(Ethylene Glycol) Constructs with Encapsulated Cells. Annals of Biomedical Engineering,. 34(9): p. 1429-1441.

[26] Censi, R., W. Schuurman, J. Malda, G. di Dato, P. E. Burgisser, W. J. A. Dhert, C. F. van Nostrum, P. di Martino, T. Vermonden and W. E. Hennink (2011). "A Printable Photopolymerizable Thermosensitive p(HPMAm-lactate)-PEG Hydrogel for Tissue Engineering." Advanced Functional Materials 21(10): 1833-1842.

[27] Hockaday, L. A., K. H. Kang, N. W. Colangelo, P. Y. C. Cheung, B. Duan, E. Malone, J. Wu, L. N. Girardi, L. J. Bonassar, H. Lipson, C. C. Chu and J. T. Butcher (2012). "Rapid 3D printing of anatomically accurate and mechanically heterogeneous aortic valve hydrogel scaffolds." Biofabrication 4(3): 035005.

[28] Lee, J.-S., J. M. Hong, J. W. Jung, J.-H. Shim, J.-H. Oh and D.-W. Cho (2014). "3D printing of composite tissue with complex shape applied to ear regeneration." Biofabrication 6(2): 024103.

[29] Campos, D. F. D., A. Blaeser, M. Weber, J. Jäkel, S. Neuss, W. Jahnen-Dechent and H. Fischer (2013). "Three-dimensional printing of stem cell-laden hydrogels submerged in a hydrophobic high-density fluid." Biofabrication 5(1): 015003.

[30] Zhao, Y., R. Yao, L. Ouyang, H. Ding, T. Zhang, K. Zhang, S. Cheng and W. Sun (2014). "Three-dimensional printing of Hela cells for cervical tumor model in vitro." Biofabrication 6(3): 035001.

[31] Zhao Y, Yao R, Ouyang L, Ding H, Zhang T, Zhang K, Cheng S and Sun W 2014 Three-dimensional printing of Hela cells for cervical tumor model in vitro *Biofabrication* **6** 035001

[32] Aslani, P. and R. A. Kennedy (1996). "Studies on diffusion in alginate gels. I. Effect of cross-linking with calcium or zinc ions on diffusion of acetaminophen." Journal of Controlled Release 42(1): 75-82.

[33] Lee, K. Y., J. A. Rowley, P. Eiselt, E. M. Moy, K. H. Bouhadir and D. J. Mooney (2000). "Controlling Mechanical and Swelling Properties of Alginate Hydrogels Independently by Cross-Linker Type and Cross-Linking Density." Macromolecules 33(11): 4291-4294.

[34] Daniel L. Cohen, Winifred Lo, Andrew Tsavaris, David Peng, Hod Lipson, and Lawrence J. Bonassar. Tissue Engineering Part C: Methods. February 2011, 17(2): 239-248. doi:10.1089/ten.tec.2010.0093.

[35] Aleksander Skardal, Jianxing Zhang, Lindsi McCoard, Xiaoyu Xu, Siam Oottamasathien, and Glenn D. Prestwich. Tissue Engineering Part A. August 2010, 16(8): 2675-2685. doi:10.1089/ten.tea.2009.0798.

[36] Tumbleston, J. R., Shirvanyants, D., Ermoshkin, N., Janusziewicz, R., Johnson, A. R., Kelly, D., Chen, K., Pinschmidt, R., Rolland, J. P., Ermoshkin, A., Samulski, E. T., DeSimone, J. M. (2015). Continuous liquid interface production of 3D objects. Science, 347(6228), 1349-1352. doi: 10.1126/science.aaa2397

[37] Mørch, Ý. A., I. Donati and B. L. Strand (2006). "Effect of Ca^{2+}, Ba^{2+}, and Sr^{2+} on Alginate Microbeads." Biomacromolecules 7(5): 1471-1480.

Chapter 4 - Live cell investigation for bioprinting

4.1 Introduction

In the previous chapter, 3D printing of simple and complex alginate hydrogel structures through a three step cross-linking process was successfully demonstrated. The chapter was an investigation into a new 3D bioprinting concept for bioprinting cell-laden alginate hydrogel structures. The key challenge of the new bioprinting concept was to achieve high cell viability and gel stability without compromising the cell viability. To optimise the printing cross-linking conditions to keep the gel stable in the long term, MTT assays was carried out to investigate the U87-MG cell behaviour based on various concentrations of cross-linking reagents. Once printing cross-linking conditions were optimised, the viability of the U87-MG cells right after bioprinting was assessed for different alginate hydrogel concentrations. The best condition was used to investigate the U87-MG cell viability within the bioprinted gel over 11 days. For validation of the new 3D bioprinting technology, a U87-MG cell line was chosen; this is an established human brain tumour cell line for cancer disease models with full genetic characterisation [1-4]. The mechanical properties of the gel were examined after printing based on secondary and tertiary cross-linking conditions. The ability to co-print was presented, demonstrating that the new bio-printing concept had the ability to bioprint two types of cells.

4.2 Sterilisation of hydrogel for bioprinting

In this study, sodium alginate 8% (w/v) (Product number W201502, Sodium Alginate, Sigma-Aldrich, Gillingham, UK) [5-8] , $CaCl_2$ solution (Product number 223506 $CaCl_2$ dehydrate, Sigma-Aldrich, Gillingham, UK) and $BaCl_2$ Solution (Product number 1001253915 $BaCl_2$ trace metals basis, Sigma-Aldrich, Gillingham, UK) were prepared in deionised water at room temperature. In addition, an ultra-sonic bath set at 60 ºC was used to reduce the mixing time of sodium alginate in deionised water to produce a homogenous solution overnight. 80 mM $CaCl_2$, 100 mM $CaCl_2$ and 60 mM $BaCl_2$ were used respectively as primary, secondary and tertiary cross-linking reagents for 8 % (w/v) sodium alginate.

4.3 Partially cross-linked alginate hydrogel preparation

Sodium alginate 8% (w/v) was sterilised by Gamma radiation (IBL-637 CIS-BioINternational gamma irradiator, France) with 10 Gy at a rate of 1 Gy/min. 80 mM

$CaCl_2$ stocks were autoclaved at 121 ºC for 15 minutes. The two solutions consisting of 8% (w/v) sodium alginate and 80 mM $CaCl_2$ were mixed with a volume ratio of 1:1 to result in a partially cross-linked hydrogel in a 50 mL conical tube (Centrifuge tube, Fisher Scientific Ltd, Loughborough, UK). The hydrogel solution was further mixed using a vortex mixer at room temperature at 1500 rpm for 30 seconds in order to produce the homogeneous partially cross-linked alginate hydrogel.

4.4 The effect of the $CaCl_2$ and $BaCl_2$ cross-linking baths on the mechanical properties of printed hydrogels

The partially cross-linked alginate hydrogel was printed by exposure to 50 mM, 100 mM, 200 mM and 300 mM $CaCl_2$ solutions to generate cubic structures with dimensions of 20 mm × 20 mm × 8 mm. The structures were kept in the solution for 10 minutes followed by exposure to 60 mM $BaCl_2$ solution for 2 minutes. A Mach-1™ mechanical indenter (Biomomentum, Canada) was used to measure the static stiffness. The partially cross-linked alginate hydrogel was also mechanically tested before printing to understand the role of $CaCl_2$ in enhancing the mechanical properties of the gel.

The mechanical testing suggested that the partially cross-linked alginate hydrogel had elastic behaviour after it was further cross-linked. The elastic moduli were 5.2 ± 0.12 kPa, 20.18 ± 1.62 kPa, 20.87 ± 1.78 kPa and 28.24 ± 0.91 kPa with exposure to 50 mM, 100 mM, 200 mM and 300 mM $CaCl_2$ respectively and followed by exposure to 60 mM $BaCl_2$. The partially cross-linked alginate hydrogel showed elastic behaviour with an elastic modulus of 1.55 ± 0.027 kPa for a strain of 1 ± 0.05 mm. Therefore the secondary cross-linking process ($CaCl_2$) boosted the mechanical properties of the alginate hydrogel to create suitable rigidity and strength for the structure to hold its shape during the bioprinting process. The results shown in Figure 4.1 indicate that 50 mM $CaCl_2$ as the secondary cross-linking agent did not improve the mechanical properties of the alginate hydrogel sufficiently; it had similar mechanical properties to the partially cross-linked alginate hydrogel itself. However, 100 mM of $CaCl_2$ resulted in a noticeable change in partially cross-linked alginate hydrogel mechanical properties, improving its rigidity and strength. The secondary cross-linking agent was kept at 100 mM to prevent exposure of cells to higher concentrations of $CaCl_2$, which could be harmful and affect the cell viability and function. Exposure to 60 mM $BaCl_2$ did not

have a significant effect on the mechanical properties of the hydrogel in general (as shown in Figure 4.1). The change in mechanical stiffness upon $BaCl_2$ treatment appeared less obvious when the hydrogel was cross-linked with higher $CaCl_2$ concentrations.

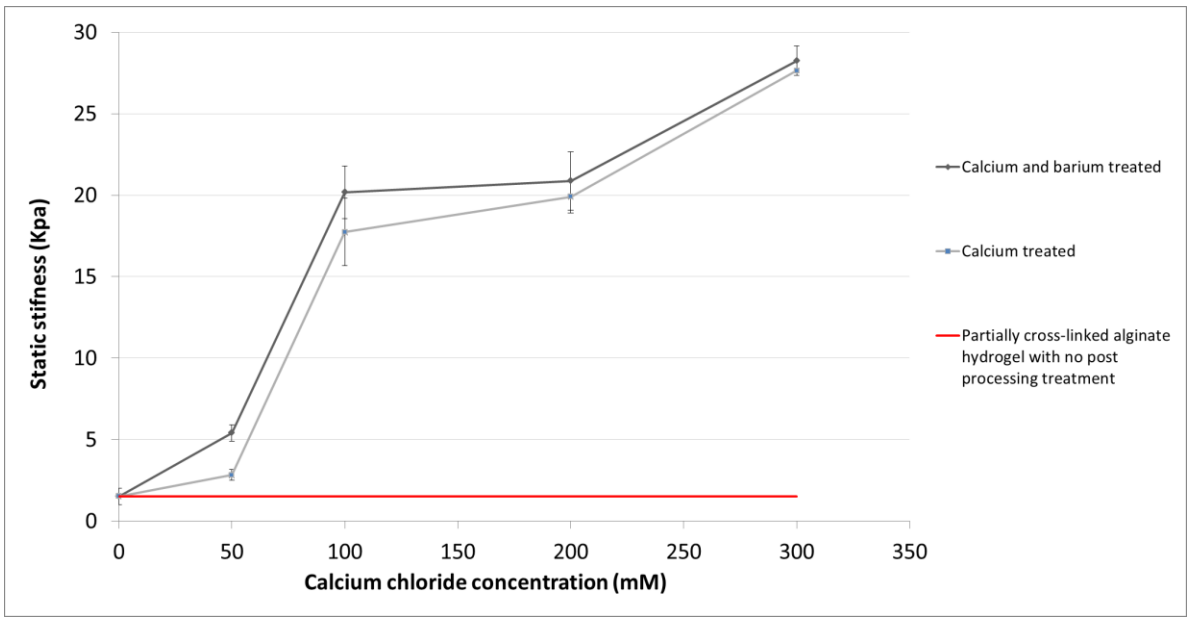

Figure 4.1 *– Elastic modulus of partially cross-linked alginate hydrogel exposed to different $CaCl_2$ concentrations for 10 minutes followed with or without exposure to $BaCl_2$.*

4.5 Cell culture and transduction for 3D bioprinting

Human glioma U87-MG cells, purchased from the European Collection of Cell Cultures (ECACC) (Public Health England, UK), were seeded at a density of 0.5×10^6/mL in 6-well plates and were allowed to attach and acquire normal morphology. The cells were transduced using a lentiviral vector, which expresses enhanced green fluorescent protein (EGFP) under control of the SFFV promoter. After transduction, cells were seeded in 96-well plates at a cell density of 0.7 cells per well, allowing the selection of a single transduced cell population. This was replicated for 2 weeks until a stable clone GFP1-U87-MG line was generated. U87-MG cells were cultured in minimum essential medium (MEM) supplemented with 10 % (v/v) fetal bovine serum (FBS), L-Glutamine, non-essential amino acids (NEAA), and sodium pyruvate. All culture medium components were acquired from Life Technologies. During experimental procedures, the medium was supplemented with penicillin/streptomycin (100 UI/ml and 100 µg/ml).

After printing, cells were maintained at 37 °C and with 5 % CO_2 in 10 cm petri dishes (Fisher Scientific, UK). The culture media were changed every 2 days.

4.6 Manual extrusion of U87-MG cells with partially cross-linked alginate hydrogel

TManual extrusion of U87-MG cells was carried out to understand the feasibility of the new bioprinting concept; whether the cells could stay viable and grow within the alginate hydrogel. Initially, 2 mL of sterile sodium alginate was mixed with 1 mL of cell solution with concentration of 13.5×10^6/mL. Once the cell-laden alginate solution was prepared it was mixed with 1 mL of $CaCl_2$ with a concentration of 120 mM. The final partially cross-linked cell-laden hydrogel consisted of 4% (w/v) alginate, 40 mM $CaCl_2$ and cell a concentration of 3.375×10^6/ mL. The cell-laden hydrogel was loaded into the extrusion syringes and was manually extruded through nozzle tips of 800 µm, 500 µm, 300 µm and 200 µm into 300 mM $CaCl_2$ and was kept in the solution for 2 minutes. The $CaCl_2$ was then removed and replaced with a culture medium. Cells were cultured for four days and images of the encapsulated U87-MG cells were taken at day 1, day 2, day 3 and day 4.

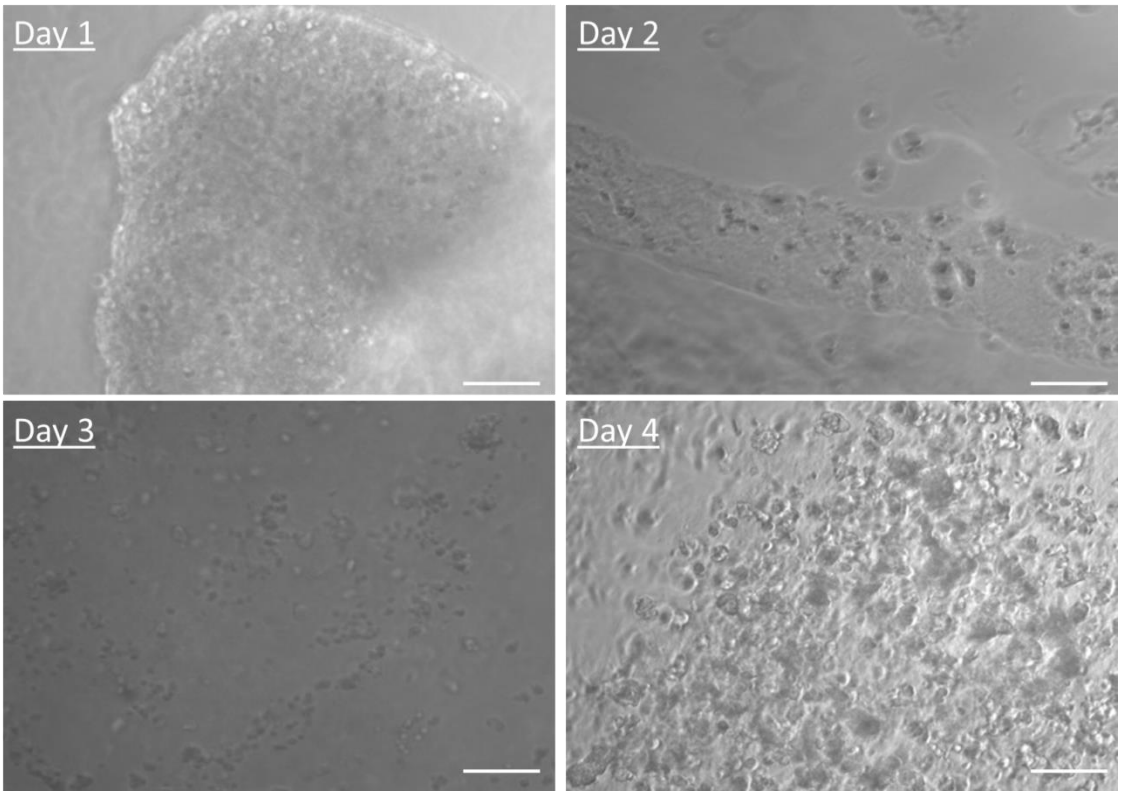

Figure 4.2 *– Manual extrusion of U87-MG cells with partially cross-linked alginate hydrogel by 200 µm, tip. Scale bar: 100 µm.*

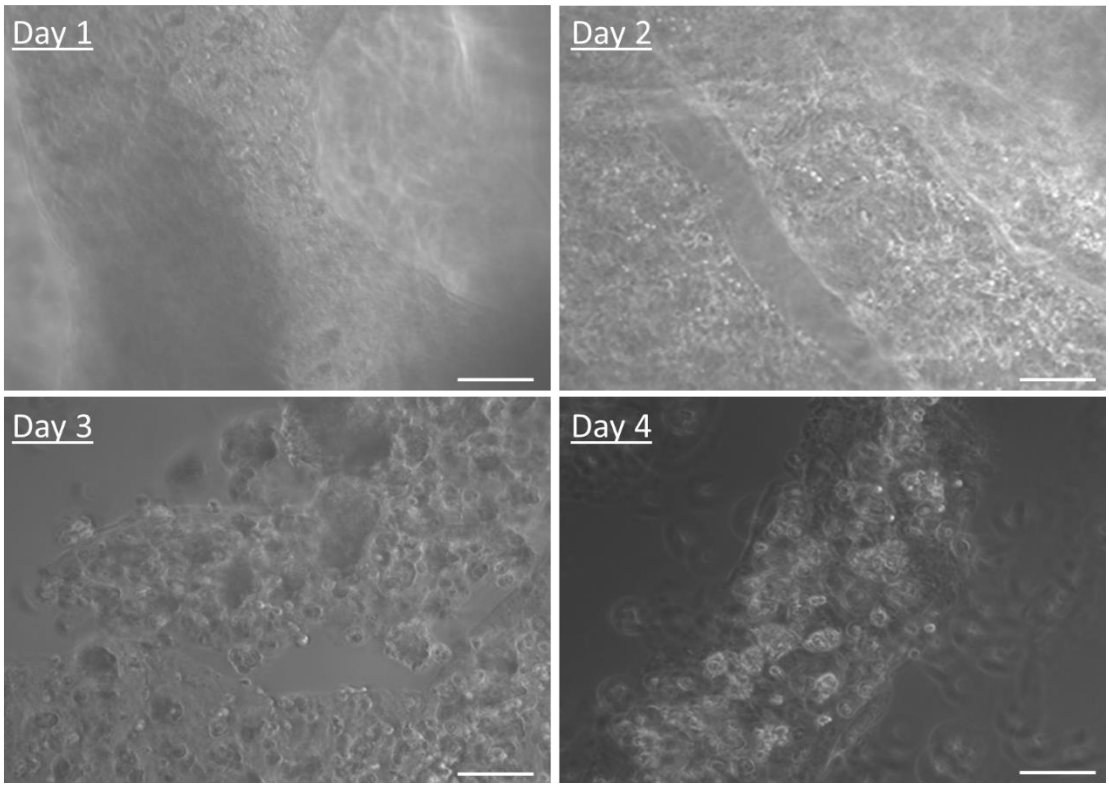

Figure 4.3 *– Manual extrusion of U87-MG cells with partially cross-linked alginate hydrogel by 300 µm, tip. Scale bar: 100 µm.*

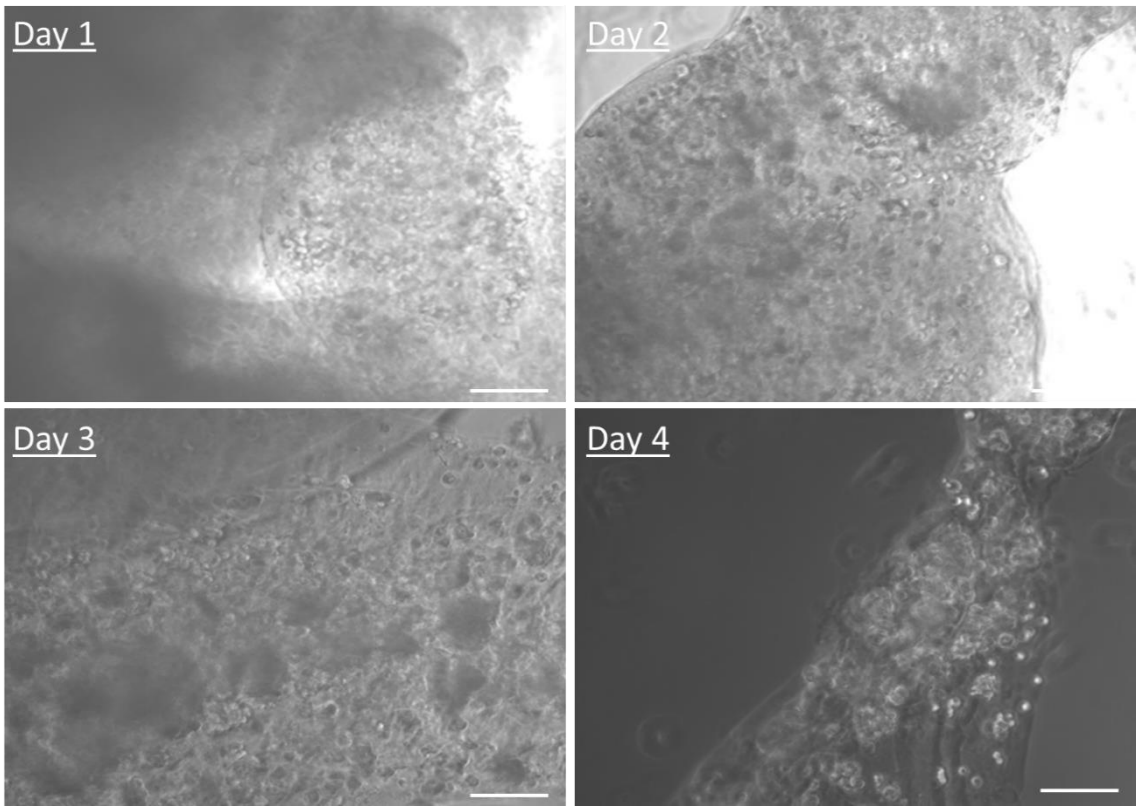

Figure 4.4 *– Manual extrusion of U87-MG cells with partially cross-linked alginate hydrogel by 500 µm, tip. Scale bar: 100 µm.*

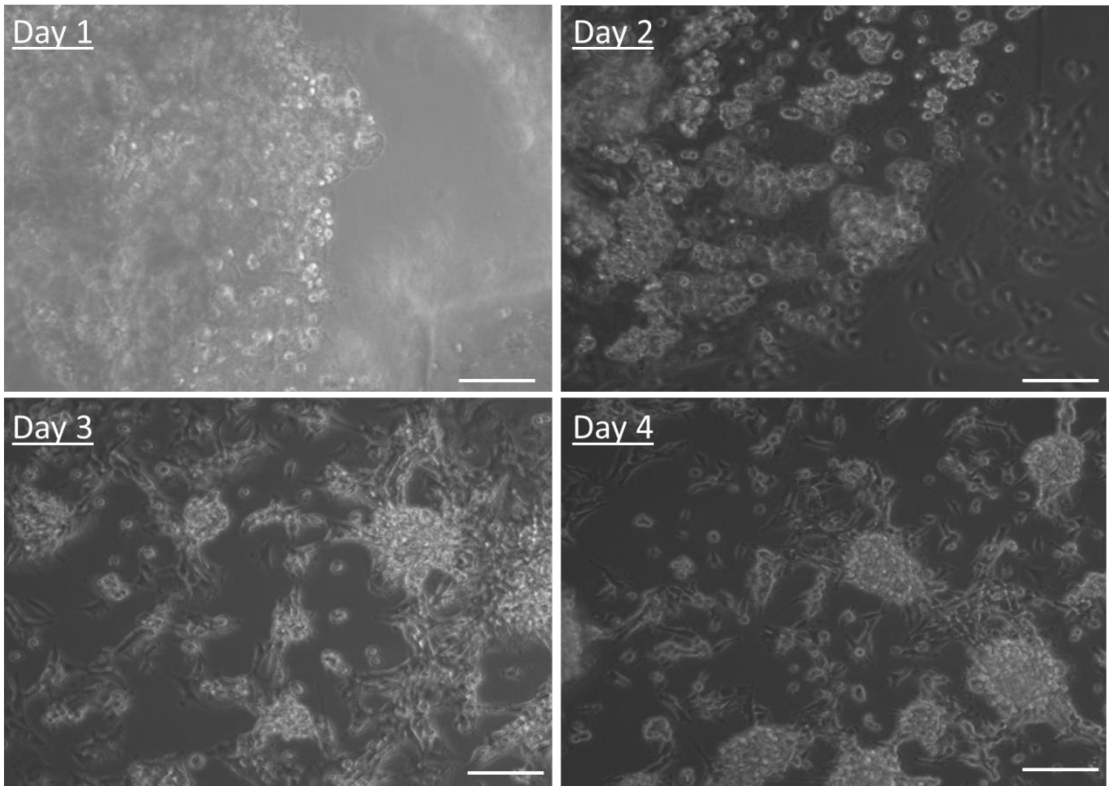

Figure 4.5 *– Manual extrusion of U87-MG cells with partially cross-linked alginate hydrogel by 800 µm tip. Scale bar: 100 µm.*

The results shown in Figure 4.2 indicate that the cell number had increased on day 2 compared to day 1. The gel started to degrade at day 2, however, and cells attached to the bottom of the culture dish. This could be due to the greater thickness of the cell-laden hydrogel extruded into the $CaCl_2$ solution where the cross-linking time was short and $CaCl_2$ diffusion time was insufficient to fully cross-link the alginate. The cell-laden hydrogel extruded with the 200 µm, 300 µm and 500 µm tips did not fully degrade by day 4 as shown in Figure 4.3, Figure 4.4 and Figure 4.5 respectively, as cells proliferated and grew within the gel and formed small cell clusters within the gel. This study showed cells could stay viable and grow within the alginate hydrogel; however, the degradation of the gel needed to be enhanced to keep the gel stable for longer allowing more time for cells to proliferate within the gel.

4.7 MTT assay

MTT assay was used to determine the effect of the cross-linking reagents on U87-MG cells. The cell number was assessed using (3-(4,5-Dimethylthiazol-2-yl)-2,5-diphenyltetrazolium bromide (MTT). U87-MG cells were seeded in a 96 well plate at 7.5×10^4 cells/mL and incubated overnight. Cells were then exposed to different conditions and the number of metabolically active cells was estimated after 24 hrs by measuring absorbance at 570 nm. Each condition was determined using triplicates. It should be noted that $BaCl_2$ could be very toxic to cells if exposed for long-term. In a simple test U87-MG cells were exposed to 1% $BaCl_2$ solution and after 24 hrs in culture, all cells had died. Therefore the exposure time was limited to 2 minutes.

4.7.1 The effect of calcium and barium concentration on U87-MG Cells

Based on the degradation studies from the previous chapter, this study was carried out to examine the effects on U87-MG cells when exposed to 100 mM $CaCl_2$ as a secondary cross-linking reagent and 40 mM $BaCl_2$ as the tertiary cross-linking reagent. U87-MG cells were first treated with 100 mM $CaCl_2$ for 10 minutes, then exposed to 10 mM, 20 mM, 40 mM, 60 mM and 100 mM $BaCl_2$ for 2 minutes (similar to the printing conditions to enhance the gel degradation time [9-12]) and then cultured for 24 hours. The MTT assay data presented in Figure 4.6 show that after 24 hours of culture U87-MG cells were not only unaffected negatively by exposure to $BaCl_2$ but also the cell growth was seen to be reproducibly improved within 24 hours using $BaCl_2$

concentrations of 60 mM and 100 mM. Based on the degradation results in chapter 3 and MTT assay data, 60 mM of $BaCl_2$ was therefore chosen as the tertiary cross-linking reagent rather than 40 mM of $BaCl_2$. This could further enhance the alginate hydrogel stability and support cell growth within the alginate structure for at least 7 days or more as previously discussed. By visual inspection of Figure 4.7, it can be seen that the U87-MG cells exhibited a normal morphology after 24 hrs when initially exposed to 100 mM $CaCl_2$ for 10 minutes and exposed to 10 mM, 20 mM, 40 mM, 60 mM and 100 mM $BaCl_2$ for 2 minutes.

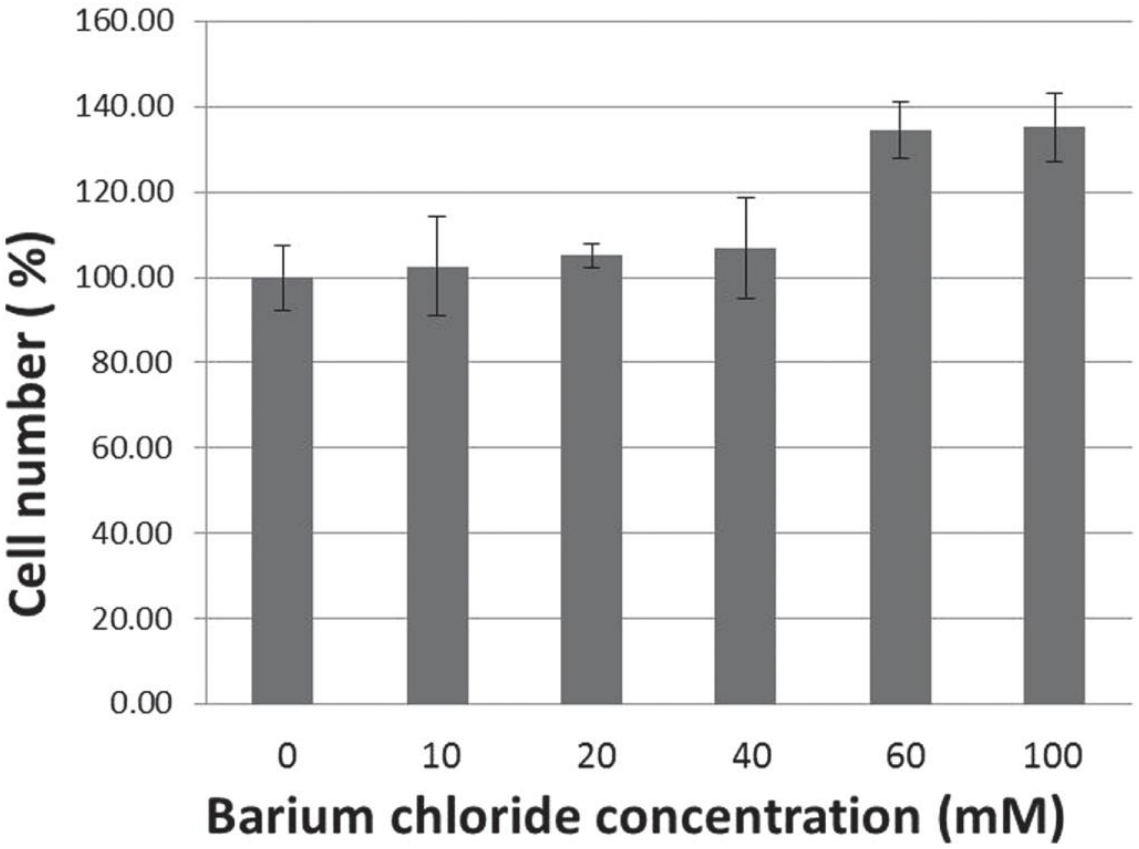

Figure 4.6 *– MTT assay of U87-MG cells after 24 hours of culture after being exposed 100 mM of $CaCl_2$ for 10 minutes and then exposed to different $BaCl_2$ concentrations for 2 minutes.*

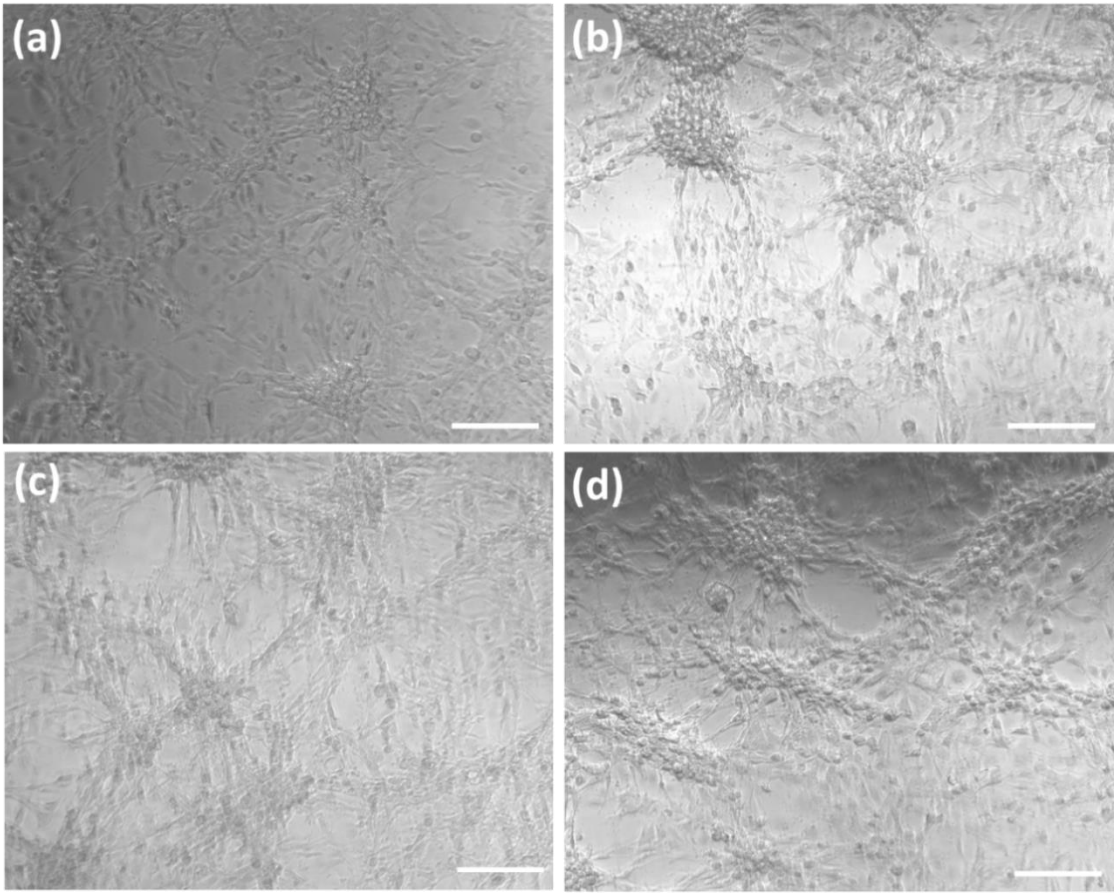

Figure 4.7 *— Images of (a) U87-MG cells in normal culture medium after 24 hours, and U87-MG cells temporary exposed to (b) 10 mM, (c) 20 mM, and (d) 40 mM $BaCl_2$ for 2 minutes and cultured in medium for 24 hours. Scale bar: 100 µm*

4.7.2 Effect of constant exposure of U87-MG cells to Calcium in the culture medium.

This study was carried out to investigate wether constant exposure of the gel to $CaCl_2$ would have a positive or negative effect on cells. Gels with constant exposure to 20 mM and higher concentrations of $CaCl_2$ could keep their integrity over 7 days. U87-MG cells were first treated with 100 mM $CaCl_2$ for 10 minutes and then constantly exposed to 10 mM, 20 mM, 30 mM and 40 mM $CaCl_2$ for 24 hours in the culture medium. Based on MTT assay data shown in Figure 4.8, U87-MG cells constantly exposed to 10 mM $CaCl_2$ exhibited a slightly increased cell growth compared to the control, however it was not able to sustain its integrity and eventually started to break down and degrade after day 2 or day 3 in culture medium. On the other hand, U87-MG cells exhibited a decreased cell viability of around 20% to 25% when exposed constantly to 20 mM, 30mM, and 40 mM $CaCl_2$ in culture medium for 24 hours. The MTT Assay results based on temporary exposure of U87-MG cells to various $BaCl_2$ concentrations and

constant exposure of U87-MG cells to various $CaCl_2$ concentrations indicated that $BaCl_2$ was a more effective tertiary cross-linking reagent than CaCl2, maintaining the gel's integrity over 7 days in the culture medium. On visual inspection of Figure 4.9, cells did not exhibit normal morphology when constantly exposed to $CaCl_2$ present within the culture medium.

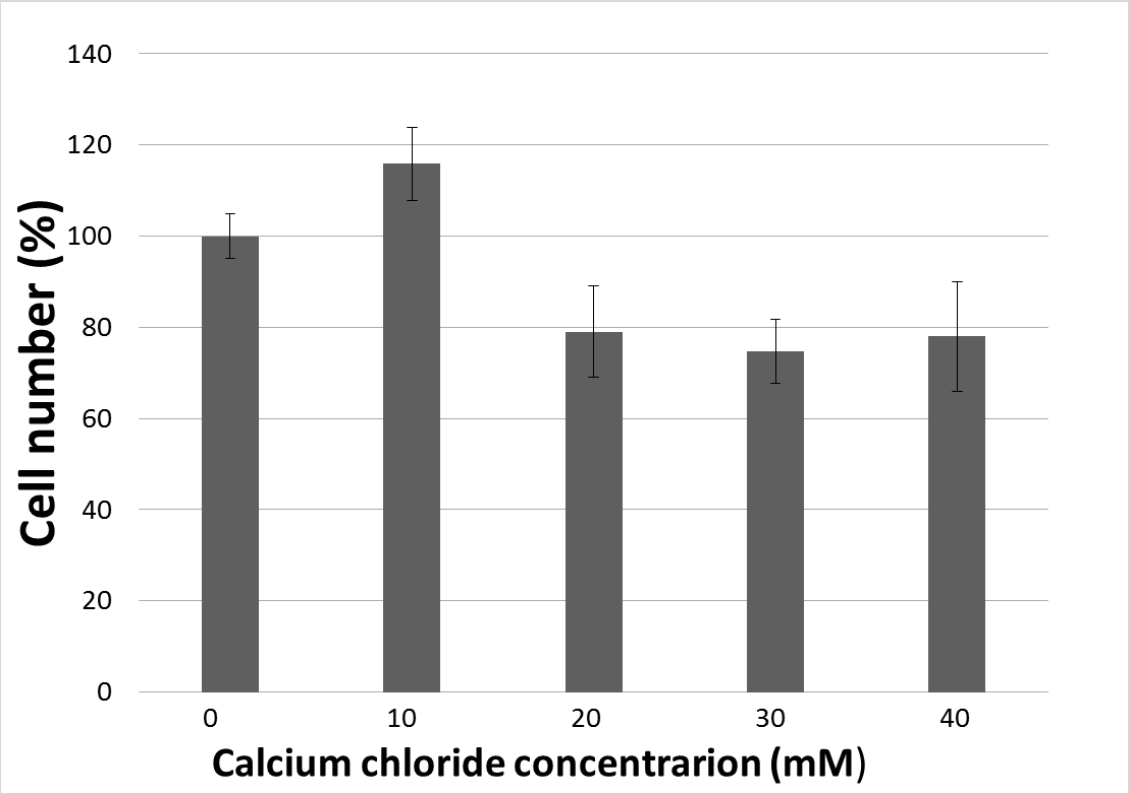

Figure 4.8 *– MTT Assay of U87-MG cells after 24 hours of culture after being constantly exposed to 10 mM, 20mM, 30 mM and 40 mM $CaCl_2$ for 24 hours.*

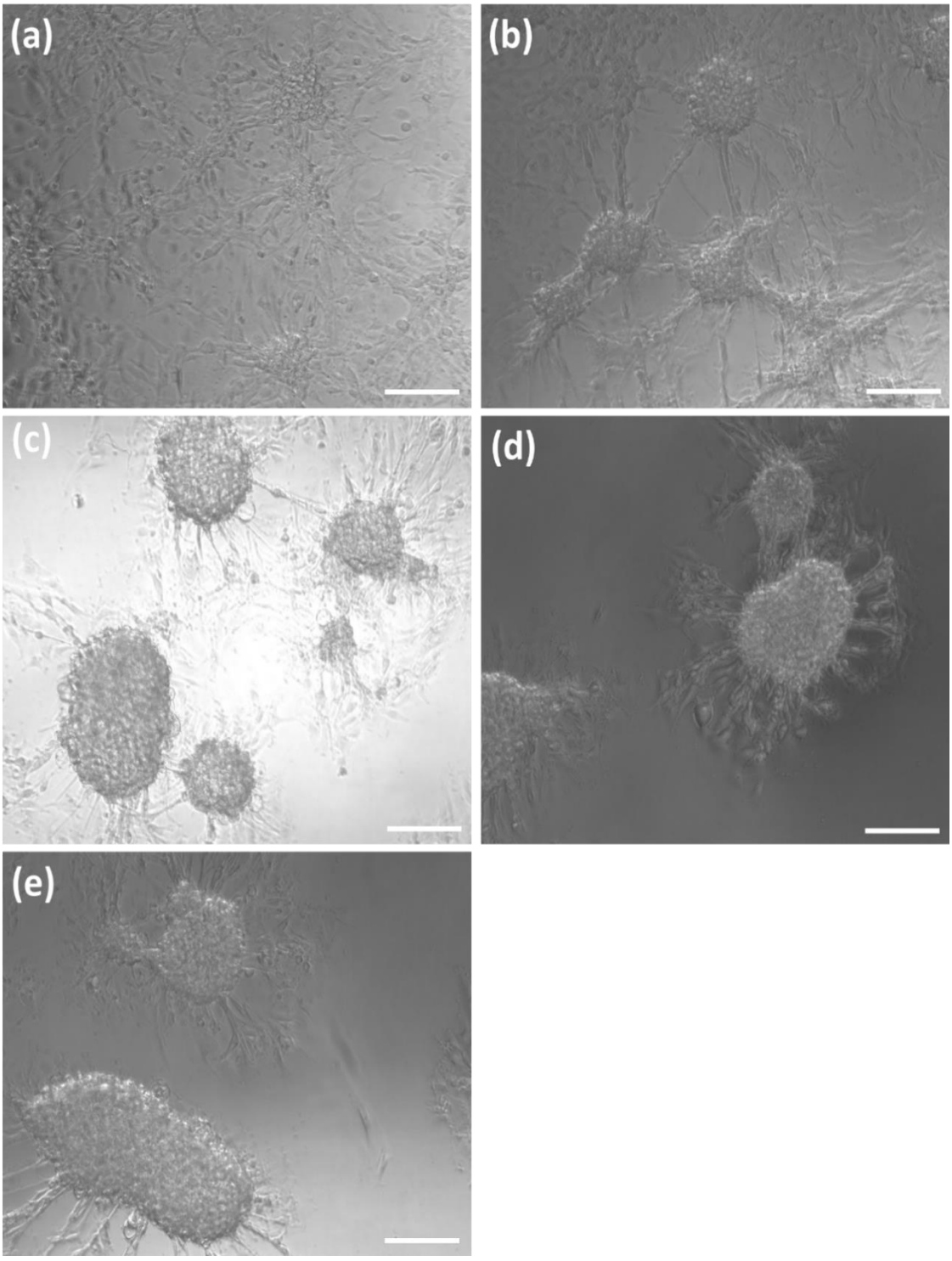

Figure 4.9 *– Images of (a) U87-MG cells in normal culture medium after 24 hours, and U87-MG cells constantly exposed to (b)10 mM, (c) 20 mM, (d) 30 mM and (e) 40 mM* $CaCl_2$ *present within the culture medium for 24 hours. Scale bar: 100 µm*

4.8 Design and 3D printing of alginate hydrogel structures

3D printed structures were designed using the CAD program Solid Edge V20. Vascular structure design was extracted from online open source 3D CAD library GrabCAD. The CAD files were then converted to STL files and transferred to the relative software to generate printing paths. The partially cross-linked alginate hydrogel was loaded into the extrusion syringes and then nozzles with 0.33 mm ID or 0.51 mm ID (TE series Nozzles, OK International, Hampshire, UK) were fitted to the end of syringes. The printing path width was 0.35 mm and 0.55 mm with printing heights of 0.3 mm and 0.475 mm respectively. The printing speed was 6 mm/s, which was the optimum for both sets of nozzles. The extrusion speeds were set to 0.45 mL/min and 0.65 mL/min respectively.

4.9 Cell-laden alginate hydrogel solution for printing

2 mL of 8% (w/v) sodium alginate initially was loaded with 1 mL of U87-MG cell suspension at a concentration of 21×10^6/mL in the extrusion syringe. The solution was then mixed with 1 mL of 160 mM $CaCl_2$ to partially cross-link the hydrogel using a vortex mixer at 1200 rpm for 30 seconds at room temperature. The cell-laden alginate solution had final concentrations of 4% (w/v) alginate and 5.25×10^6/mL cells.

4.10 Live and dead cell assay

For the visualization of dead cells in the hydrogel, propidium iodide (PI, Sigma-Aldrich UK) was added directly to the media in 10 cm Petri dishes (Fisher Scientific, UK) containing the constructs at a final concentration of 2.5 μM. After 30 minutes incubation in the dark at 37°C, the culture medium was removed and the coverslips (Cover Glass, 631-0152, VWR International USA) containing the hydrogel were mounted on microscope slides for imaging.

4.11 3D Cell imaging and viability test

Confocal laser scanning microscopy (Leica SP5 SMD; Leica microsystems) was used for image acquisition. Images were taken using a dry 20X objective. CLSM images were analysed using Imaris software to investigate the viability of the bioprinted cells over 11 days. Cell viability of the bioprinted structures at 2 %, 3 %, 4 %, 5 % and 6 %

of alginate concentrations (w/v) was assessed after bioprinting. Cell viability was quantified as the number of live cells as a proportion of the total number of cells (live and dead cells).

4.12 The influence of the alginate viscosity on cell viability

The higher the alginate concentration, the higher the shear stress needed to extrude cell-laden hydrogels. This reduced the cell viability [13, 14]. This experiment was designed to understand the effect of the alginate hydrogel concentration on cell survival rate based on the extrusion of 2%, 3%, 4%, 5% and 6% partially cross-linked alginate hydrogel with their respective primary cross-linking reagent described in the previous chapter. The partially cross-linked cell-laden alginate hydrogel was printed into a 100 mM $CaCl_2$ bath, where it was kept for 10 minutes, followed by exposure to 60 mM $BaCl_2$. The cell viability of bioprinted U87-MG cells in 2 %, 3 %, and 4 % (w/v) partially cross-linked alginates with their respective cross-linking reagents were maintained above 90 % immediately after bioprinting as shown in Figure 4.11. However, cell viability of U87-MG cells dropped to 83.8 ± 1.2 % when the concentration of partially cross-linked alginate hydrogel was 5% compared to the lower concentrations due to the higher viscosity of the cell-laden hydrogel. The cell viability in 6% partially cross-linked alginate hydrogel was 61.5 ± 9.8 %. This was a dramatic change and was due to the significant increase in viscosity of the hydrogel, being almost 8 times the normal printing condition of 4% partially cross-linked alginate hydrogel. Based on the viability results, the 4% partially cross-linked alginate hydrogel was chosen as final concentration as lower concentrations could not keep their integrity during the bioprinting process as discussed in the previous chapter. Confocal images of U87-MG cells bioprinted in different alginate hydrogel concentrations are shown in Figure 4.10.

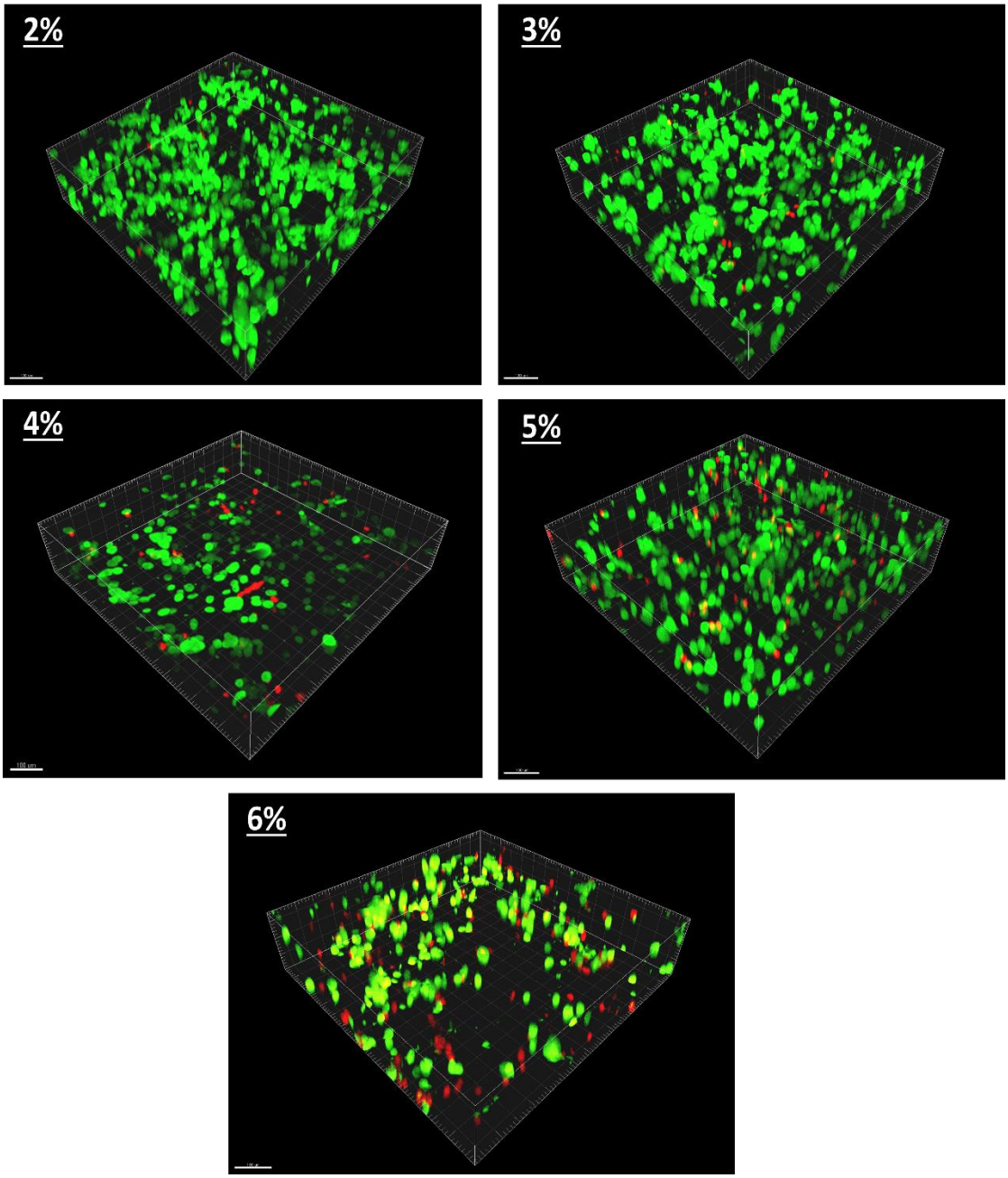

Figure 4.10 *— Confocal images of bioprinted U87-MG cells in different concentrations of alginate hydrogel. The grid boxes are 50 µm.*

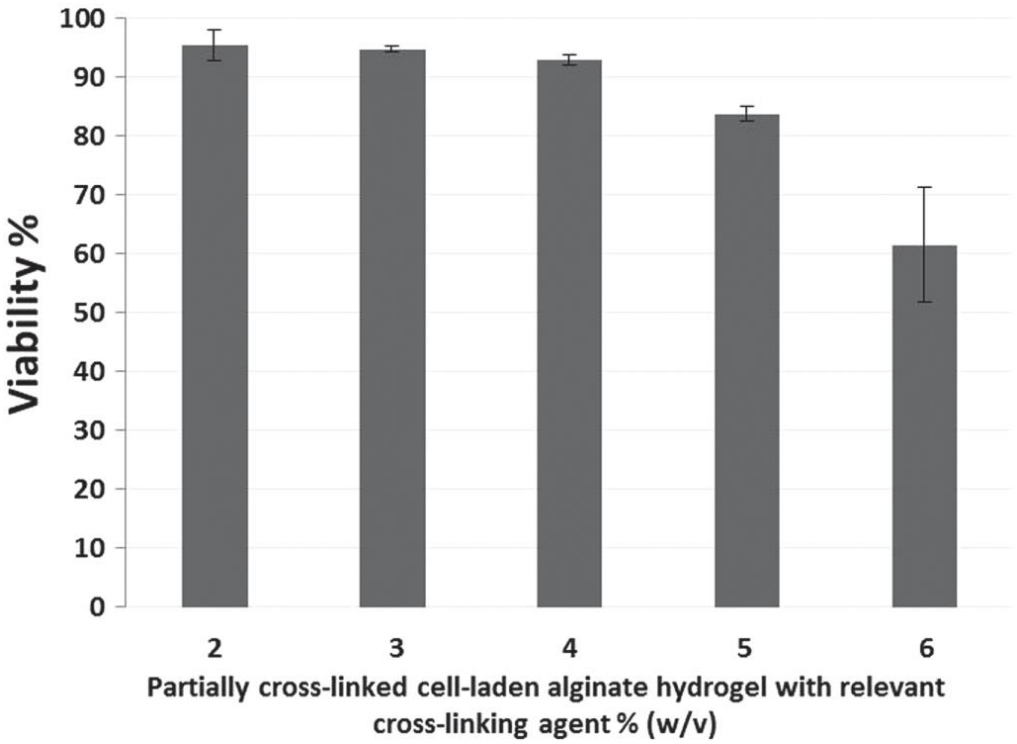

Figure 4.11 *– Cell viability of the bioprinted cell-laden partially cross-linked alginate hydrogel immediately after bioprinting*

4.13 3D printing of U87-MG cells in 4% alginate hydrogel and its effect on long term cell viability

U87-MG cells were bioprinted in partially cross-linked alginate 4% (w/v) hydrogel and then cross-linked with 100 mM $CaCl_2$ for 10 minutes followed by matrix stabilisation with 60 mM $BaCl_2$ for 2 minutes. Cell viability in the 3D constructs was monitored for 11 days post-printing as shown in confocal images in Figure 4.12. Figure 4.14 summarises the 3D cell viability throughout the 11-day period. The bioprinted cells had a viability of 92.9 ± 0.9% immediately after printing at day 0. Viability then remained high, staying over 88% ± 4.3 %. The cross-linked alginate hydrogel maintained its structure over 11 days while keeping the embedded cell viability over 88 ± 4.3 % throughout. This indicated a suitable alginate hydrogel permeability, which allowed efficient diffusion of nutrients, oxygen and waste removal within the alginate hydrogel. Figure 4.12 showed that the U87-MG cells appeared as individual cells immediately after bioprinting, however, within days of culture, proliferation through to the gel allowed intercellular interaction implying good porosity of the alginate hydrogel.

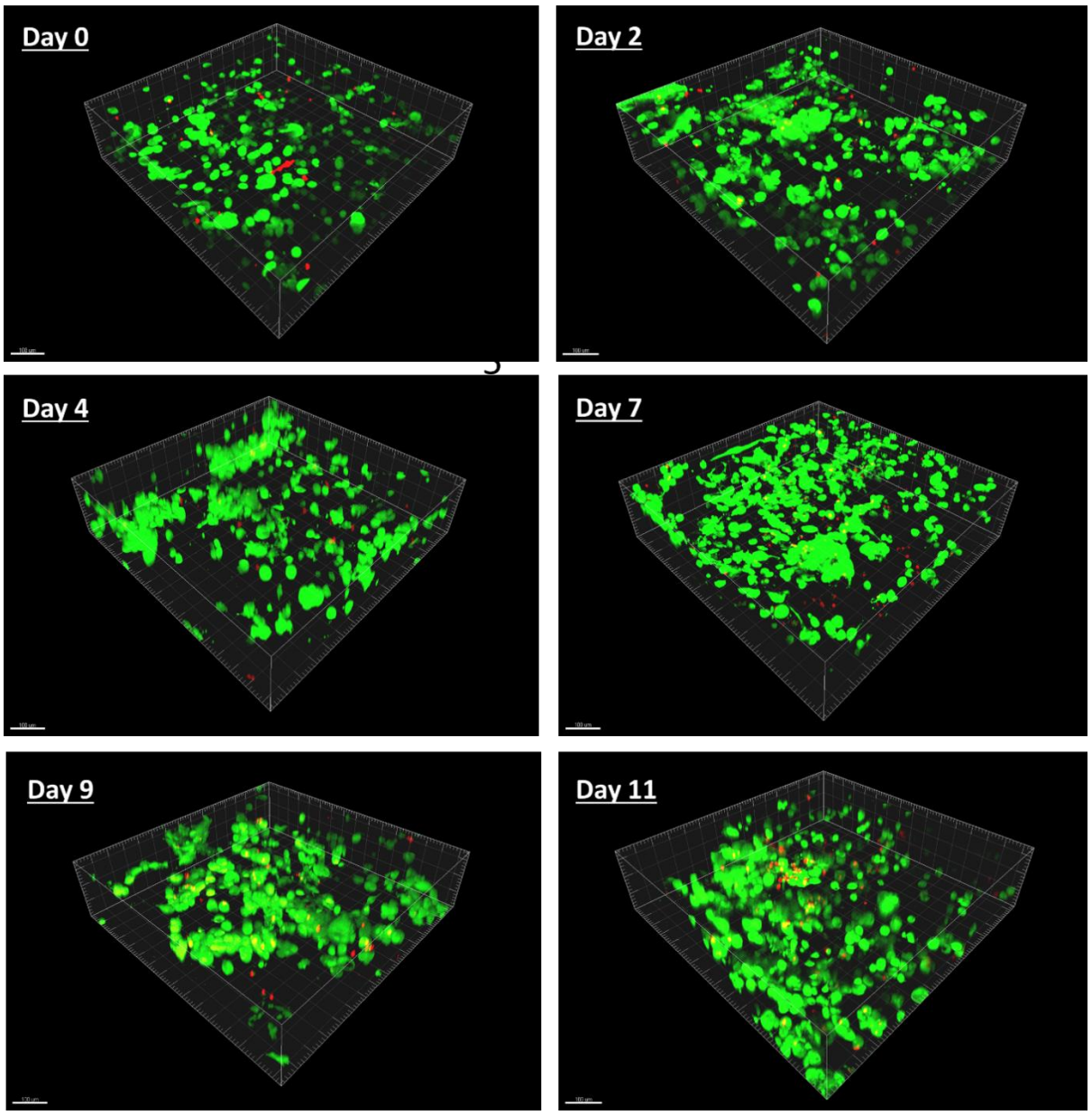

Figure 4.12 *– Confocal images of bioprinted U87-MG cells throughout 11 days. The grid boxes are 50 µm.*

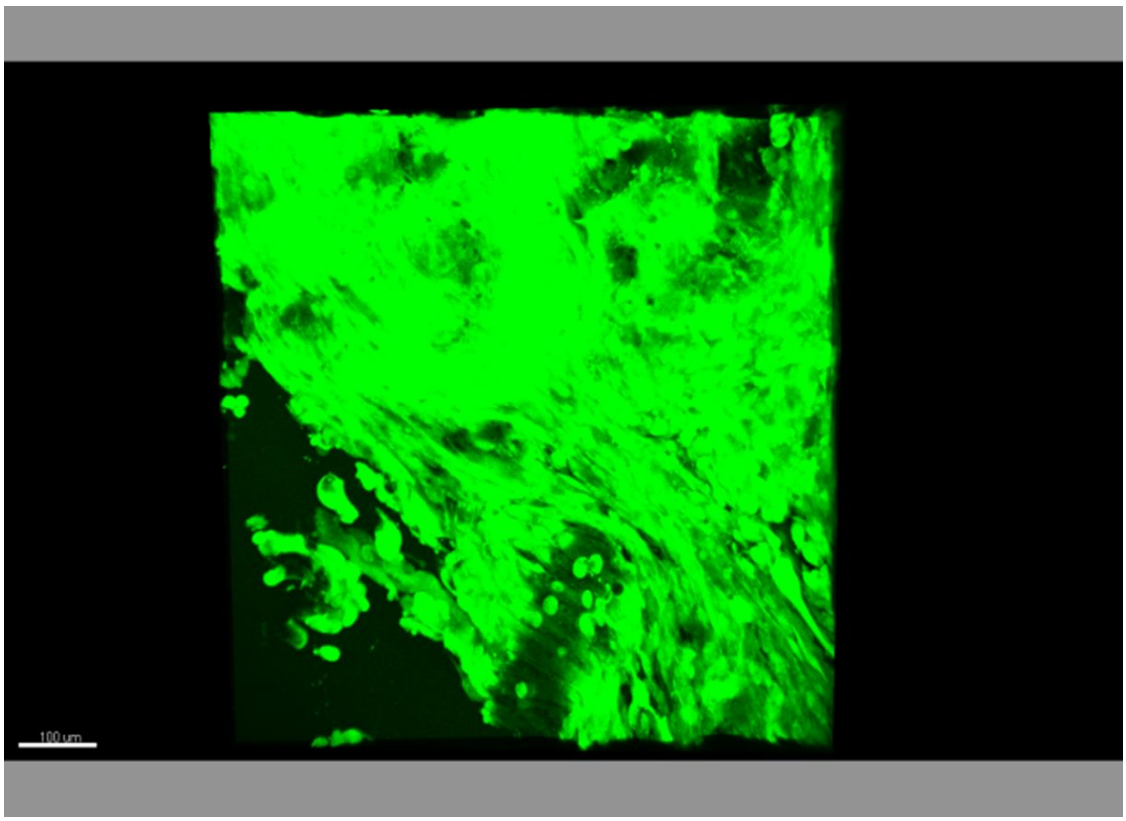

Figure 4.13 — *Formation of tissue-like structures within the alginate hydrogel after day 9 of culture. Scale bar: 100 µm.*

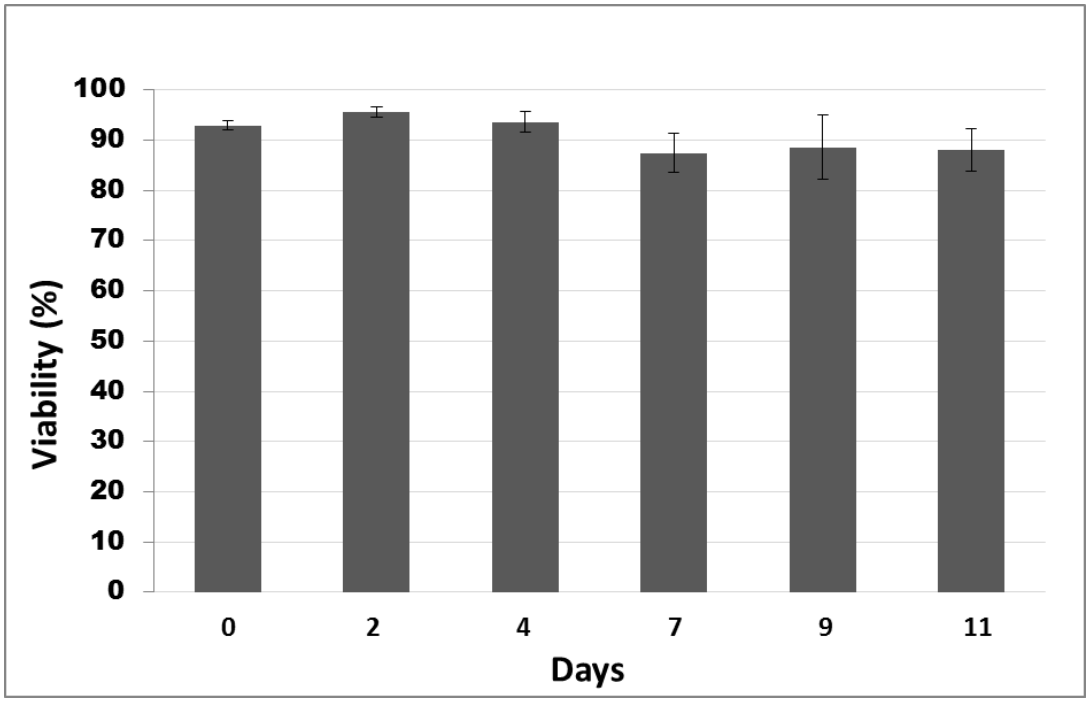

Figure 4.14 — *U87-MG Cell viability within 3D alginate hydrogel structures over the period of 11 days. Viability was assessed by choosing 3 random fields of the same construct.*

4.14 Co-printing of partially-crosslinked alginate hydrogel

Co-printing is a crucial area in bio-printing field due to the need for having two or more type of cells bio-printed in precise locations to simulate the cell placements found in physiological conditions [15-17]. To operate with the Fab@Home dual syringe extrusion system, XDFL codes were written for to extrude a ring containing 6 layers of gel with one print head and 3 layers of another gel with a second print head. The co-printed ring structure is shown in Figure 4.15. The second hydrogel was exposed to red dye for visibility before 3D printing.

Figure 4.15 *– Co-printed ring with partially cross-linked alginate hydrogel followed by the 3D bioprinting protocol containing 6 layers of normal coloured partially cross-linked alginate hydrogel and 3 layers of partially cross-linked alginate hydrogel with red dye. Scale bar: 1 pound coin.*

4.15 Acknowledgments

This chapter was completed in Collaboration with Miguel A. Hermida and Nicholas R. Leslie from the institute of Biological Chemistry, Biophysics and Bioengineering at Heriot Watt University. The culture of U87-MG cells as well as confocal imaging and MTT assay was carried out by Miguel A. Hermida. Gamma sterilisation of the alginate hydrogel was carried out by Christopher G. Mills at the University of Edinburgh.

4.16 Conclusions

In this chapter a new free form fabrication technique was developed for the 3D printing of alginate-based hydrogel structures and evaluated for its applicability to 3D bioprinting of tumour cells. Partially cross-linked alginate hydrogels were formulated with tuneable mechanical properties to create tubular and more complex continuous 3D hydrogel structures. The degradation time of alginate hydrogel in cell culture media was investigated. It was found that the stability of the alginate hydrogel could be enhanced by post-printing treatment with $BaCl_2$. The proposed technique makes it possible to bioprint live human cells with a high cell survival rate after bioprinting. This is a promising bioprinting technique that could be applied to fabricate clinically sized soft tissues with more complex and multi-cellular structures with the potential to co-print two types of cells.

Chapter 4 references

[1] Qian, Y., J. Ma, X. Guo, J. Sun, Y. Yu, B. Cao, L. Zhang, X. Ding, J. Huang and J. F. Shao (2015). "Curcumin Enhances the Radiosensitivity of U87 Cells by Inducing DUSP-2 Up-Regulation." Cellular Physiology and Biochemistry 35(4): 1381-1393.

[2] Kucharzewska, P., H. C. Christianson, J. E. Welch, K. J. Svensson, E. Fredlund, M. Ringnér, M. Mörgelin, E. Bourseau-Guilmain, J. Bengzon and M. Belting (2013). "Exosomes reflect the hypoxic status of glioma cells and mediate hypoxia-dependent activation of vascular cells during tumor development." Proceedings of the National Academy of Sciences 110(18): 7312-7317.

[3] Diaz Miqueli, A., J. Rolff, M. Lemm, I. Fichtner, R. Perez and E. Montero (2009). "Radiosensitisation of U87MG brain tumours by anti-epidermal growth factor receptor monoclonal antibodies." British Journal of Cancer 100(6): 950-958.

[4] Clark MJ, Homer N, O'Connor BD, Chen Z, Eskin A, Lee H, et al. (2010) U87MG Decoded: The Genomic Sequence of a Cytogenetically Aberrant Human Cancer Cell Line. PLoS Genet 6(1): e1000832. doi:10.1371/journal.pgen.1000832

[5] Alves-Sampaio, A., C. García-Rama and J. E. Collazos-Castro (2016). "Biofunctionalized PEDOT-coated microfibres for the treatment of spinal cord injury." Biomaterials 89: 98-113.

[6] Swioklo, S., P. Ding, A. W. Pacek and C. J. Connon "Process parameters for the high-scale production of alginate-encapsulated stem cells for storage and distribution throughout the cell therapy supply chain." Process Biochemistry.

[7] Dalmoro, A., Barba, A. A., Lamberti, G., Grassi, M. and d'Amore, M. (2012), Pharmaceutical applications of biocompatible polymer blends containing sodium alginate. Adv. Polym. Technol., 31: 219–230

[8] Gudapati H, Yan J, Huang Y and Chrisey D B 2014 Alginate gelation-induced cell death during laser-assisted cell printing *Biofabrication* **6** 035022

[9] Bajpai, S. K. and S. Sharma (2004). "Investigation of swelling/degradation behaviour of alginate beads crosslinked with Ca2+ and Ba2+ ions." Reactive and Functional Polymers 59(2): 129-140.

[10] Wong, Y. Y., S. Yuan and C. Choong (2011). "Degradation of PEG and non-PEG alginate–chitosan microcapsules in different pH environments." Polymer Degradation and Stability 96(12): 2189-2197.

[11] Effect of Ca2+, Ba2+, and Sr2+ on Alginate Microbeads Ýrr A. Mørch,*,§, Ivan Donati,‡, Berit L. Strand,§ and, and Gudmund Skjåk-Bræk§ Biomacromolecules 2006 7 (5), 1471-1480

[12] Gaumann, A., M. Laudes, B. Jacob, R. Pommersheim, C. Laue, W. Vogt and J. Schrezenmeir (2000). "Effect of media composition on long-term in vitro stability of barium alginate and polyacrylic acid multilayer microcapsules." Biomaterials 21(18): 1911-1917.

[13] Kong, H. J., M. K. Smith and D. J. Mooney (2003). "Designing alginate hydrogels to maintain viability of immobilized cells." Biomaterials 24(22): 4023-4029.

[14] S.P.M. Bohari, D.W.L. Hukins, L.M. Grover Effect of calcium alginate concentration on viability and proliferation of encapsulated fibroblasts Biomed. Mater. Eng., 21 (2011), pp. 159–170

[11] Ringeisen, B.R., Pirlo, R.K., Wu, P.K., Boland, T., Huang, Y., Sun, W., Hamid, Q. and Chrisey, D.B. (2013) ‘Cell and organ printing turns 15: Diverse research to commercial transitions’, *MRS Bulletin*, 38(10), pp. 834–843.

[12] aebel, R., N. Ma, J. Liu, J. Guan, L. Koch, C. Klopsch, M. Gruene, A. Toelk, W. Wang, P. Mark, F. Wang, B. Chichkov, W. Li and G. Steinhoff (2011). "Patterning human stem cells and endothelial cells with laser printing for cardiac regeneration." Biomaterials 32(35): 9218-9230.

[13] Kolesky, D. B., Truby, R. L., Gladman, A. S., Busbee, T. A., Homan, K. A. and Lewis, J. A. (2014), Bioprinting: 3D Bioprinting of Vascularized, Heterogeneous Cell-Laden Tissue Constructs (Adv. Mater. 19/2014). Adv. Mater., 26: 2966.

Chapter 5 - 3D fabrication of single and multiple layered alginate hydrogel tubular structures

5.1 Introduction

Conventional 2D monolayer cell culture still remains the main approach for the study of cell biology, regenerative medicine and drug discovery [1]. However, the relevance of 2D cell cultures is limited compared with 3D physiological conditions, and 3D cell culture approaches are important in narrowing the gap between *in vitro* and *in vivo* studies [2-6]. Current methods for the fabrication of 3D scaffold materials include self-assembly [7], solvent casting [8], dry freezing [9], electrospinning [10, 11] etc. However, the main barrier in conventional scaffold-based tissue engineering approaches is the inability to position living cells precisely to mimic 3D tissue. Repopulation of decellularised tissues and organs has been reported to regenerate 3D tissue and can be used as a platform for drug discovery and organ transplantation, but this approach relies on the availability of donated organs so cannot be scaled up indefinitely [12-14].

3D biofabrication [15-25] is a very promising emerging field that gives experimenters the ability to position cell-laden bio-inks precisely into a pre-designed 3D structure. Recent studies on 3D bioprinted tumour models using Hela cells [4] shows the cells to be more chemo-resistant than normal 2D monolayer cultures, making the 3D system a potentially better model for the study of real cancer cells from patient biopsies.

There is, however, a significant problem with current 3D biofabrication approaches: although they can generate simple and precise 3D structures, they rely on specialised bio-printing machinery that is not easily accessible to many cell biologists. Therefore a simple, controllable and straight-forward 3D bio-fabrication method that does not involve complicated machinery such as bioprinting platforms would be very valuable for creating biomimetic 3D structures.

In this chapter a new, inexpensive and simple biofabrication technique to generate tubular structures is presented. Alginate hydrogel was used as the main bio-ink for this study for its ease of use, biocompatibility and controllability over its degradation time [15, 26]. Further investigation is carried out to see whether this approach could also be used for the fabrication of complex 3D structures. The chapter mainly focuses on the

fabrication protocol, whereas the next chapter describes the cell studies based on the fabrication method.

5.2 3D Fabrication of alginate hydrogel tubular structures by dip coating approach

Stainless steel metal bars were chosen because of their wettability. Bars with a range of diameters (down to 600 µm) were used as the mould for tubular structure fabrication. The metal bars were kept in ethanol overnight to sterilize them prior to use. As depicted in Figure 5.1a, the mould was first dipped into a 6% w/v sodium alginate solution for approximately 3 seconds and then removed. A thin layer of the cell-laden hydrogel was left coated on the surface of the metal bar. The metal bar was then dipped into filter-sterilized cross-linking reagents (100 mM $CaCl_2$ or 55mM $BaCl_2$) for 2 minutes to cross-link the sodium alginate of the coated layer shown in Figure 5.1b The cross-linked cell-laden alginate hydrogel was then gently pulled off using tweezers from one end of the metal bar mould, leaving a hollow tubular structure of cross-linked cell-laden hydrogel shown in Figure 5.1c. Optimization of cross-linking is discussed later in the chapter.

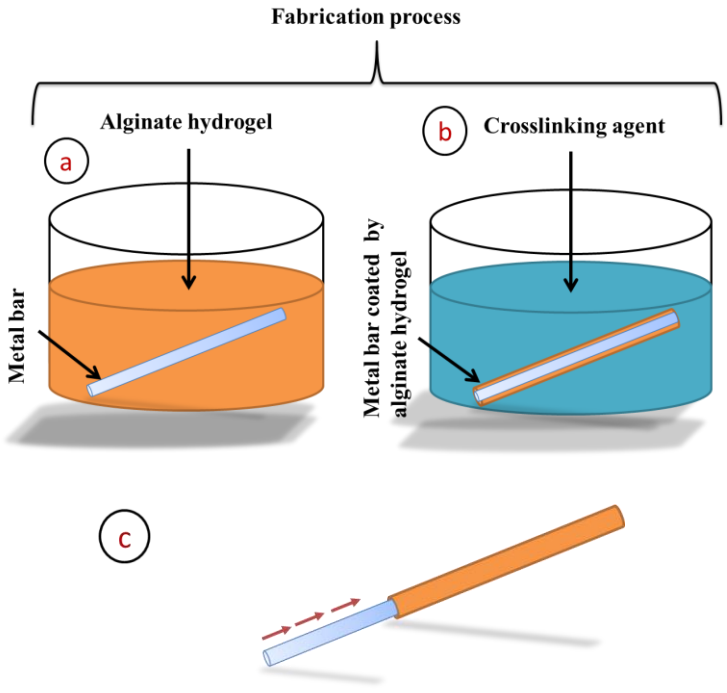

Figure 5.1 *– Schematic drawing of the alginate hydrogel tubular structure fabrication process, (a) a metal bar mould is dipped into 6% w/v sodium alginate to coat the surface by a thin layer of cell-laden alginate hydrogel, followed by (b) the exposure to 55 mM $BaCl_2$ or 100mM $CaCl_2$ to fully cross-link the sodium alginate layer for 2 minutes and then (c) the cross-linked alginate layer is pulled off the mould as a hollow tube.*

5.3 Fabrication methodologies

Based on the fabrication proposal, different experiments were designed to find the optimum conditions such as sodium alginate, $BaCl_2$ and $CaCl_2$ concentrations as well as the cross-linking time of the sodium alginate.

5.3.1 Alginate hydrogel tubular structure fabrication optimisation by $CaCl_2$ cross-linking reagent

5.3.1.1 Alginate hydrogel tubular structure fabrication by short exposure to different CaCl2 concentrations

This experiment was carried out to find the minimum concentration of $CaCl_2$ needed to cross-link the 8 % (w/v) sodium alginate to form a hollow tubular structure within 10 seconds on a 3 mm diameter stainless steel bar mould. The ability to form a tubular structure with the planned conditions is listed in Table 1 along with the ease of removal from the mould.

Constant parameters and variables during the experiments were as follows. The mould bar diameter was 3 mm, the sodium alginate concentration was 8% (w/v) and the cross-linking time was set at 10 seconds.

Table 5.1 *— Optimisation of the $CaCl_2$ concentration needed to cross-link 8% (w/v) sodium alginate on 3 mm mould bar at 10 seconds.*

1000	**Yes**	**Yes**
900	**Yes**	**Yes**
800	**Yes**	**Yes**
700	**Yes**	**Yes**
600	**Yes**	**Yes**
500	**Yes**	**Yes**
400	**Yes**	**Yes**
300	**Yes**	**No**
200	**Yes**	**No**
100	**Yes**	**No**
50	**No**	**No**

Based on the results shown in Table 5.1, 8% (w/v) sodium alginate was cross-linked at 10 seconds and easily removed when cross-linked by 400 mM to 1000 mM $CaCl_2$. When cross-linked with 300 mM $CaCl_2$, the tube structure was formed around the mould, but it was very fragile and without care it would easily collapse. Alginates cross-linked by 100 mM and 200 mM were still able to from the tubular structures, but extremely fragile and needed to be removed with extreme care. At 50 mM the alginate was not cross-linked and no tubular structure was formed.

5.3.1.2 Alginate hydrogel tubular structure fabrication by different cross-linking timings

On the basis of observations of the formation of the tube structure around the mould bar by 8% (w/v) sodium alginate cross-linked by minimum $CaCl_2$ concentration of 100 mM, another experiment was designed to determine the effect of cross-linking time. This was done to optimise the minimum needed time to cross-link 8% (w/v) alginate hydrogel coated on a 3 mm mould by 100 mM $CaCl_2$ cross-linking reagent. The results are listed in Table 5.2 below.

Constant parameters and variables during the experiments were as follows. The tube/mould diameter was 3 mm, sodium alginate was 8 % (w/v) and $CaCl_2$ concentration was set at 100 mM.

Table 5.2 — *Minimum time needed to cross-link 8% (w/v) sodium alginate coated on a 3 mm mould/tube to form rigid hollow tubular structures by 100 mM $CaCl_2$.*

10	**No**
20	**No**
30	**No**
40	**No**
50	**No**
60	**No**
70	**No**
80	**No**
90-120	**Yes**

The results shown in Table-2 indicate that a cross-linking time of 90 seconds or more was suitable for cross-linking alginate hydrogel to form tubular structures that could be easily removed. A cross-linking time of less than 90 seconds resulted in the failure of tubular structure fabrication.

5.3.1.3 Alginate hydrogel tubular structure fabrication by long exposure to different $CaCl_2$ concentrations

This test was carried out to find out the minimum concentration of $CaCl_2$ cross-linking reagent at 25 minutes ne**e**ded to cross-link the alginate to create hollow tubular structures apart with a reasonable uniformity and rigidity that can be removed easily without falling.

Constant Variables for this experiment were as follows. The Sodium alginate concentration was 8 % (w/v), the cross-linking time was 25 minutes and a mould diameter of 3 mm was used.

Figure 5.2 *– Fabricated 8 % alginate hydrogel tubular structures by 3 mm mould bar cross-linked with (a) 20 mM (b) 30 mM and (c) 40 mM of $CaCl_2$ cross-linking agent for 25 minutes. Scale bar: 5p coin.*

At 10 mM $CaCl_{2,}$ alginate was cross-linked and a tubular structure was formed on the mould's surface. Once removed from the mould, however, it was fragile and collapsedmould. At 20 mM and 30 mM $CaCl_{2,}$ shown in Figure 5.2a and Figure 5.2b, tubular structures that could be removed from the mould by extreme care were formed. The tubes did not feature appropriate uniformity and rigidity, however. At 40 mM as shown in Figure 5.2c, the tubular structure was easily removable and featured good uniformity and rigidity.

5.3.1.4 Fabrication of tubular structures by different alginate concentrations with exposure to 40 mM $CaCl_2$

With the first three set of experiments, the minimum $CaCl_2$ concentrations needed to form uniform and rigid tubular structure with 8 % (w/v) sodium alginate solution were 40 mM for long exposure and 100 mM for short exposure. A new test was carried out to find the minimum possible concentration of sodium alginate to form uniform tubular structures when cross-linked with 40 mM $CaCl_2$ at long exposure.

Constant variables for this experiment were as follows. The $CaCl_2$ concentration was 40 mM, the cross-linking time was set to 25 minutes and the mould diameter was 3 mm.

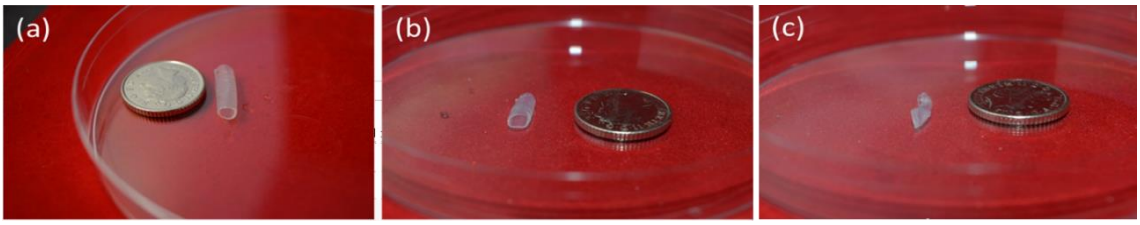

Figure 5.3 *– Fabricated (a) 8%, (b) 7% and (C) 6% (w/v) alginate hydrogel tubular structures cross-linked with 40 mM $CaCl_2$ for 25 minutes. Scale bar: 5p coin.*

As previously mentioned uniform and rigid alginate 8% alginate hydrogel structures were fabricated by exposure to 40 mM $CaCl_2$ for 25 minutes shown in Figure 5.3a. As shown in Figure 5.3b, a 7% alginate hydrogel tubular structure was also formed when cross-linked by 40 mM $CaCl_2$ for 25 minutes, however it needed to be removed from the mould with extreme care to maintain its integrity. At this stage, it was clear that lowering the alginate concentration to 6% would result in a tubular structure with poor rigidity, collapsing as shown in Figure 5.3c.

Based on the results obtained from the four experiments, the cross-linking reagent for further experiments was chosen as 100 mM $CaCl_2$ for 2 minutes (short exposure) due to its lower concentration and shorter time needed to cross-link the alginate.

5.3.2 Fabrication of alginate hydrogel tubular structure by BaCl2 cross-linking agent

This experiment was carried out to find the minimum concentration of $BaCl_2$ needed to fabricate alginate hydrogel tubular structures that are sufficiently rigid to keep their integrity once removed from the 3 mm mould bar after 2 minutes. A similar fabrication

procedure was followed as cross-linking the alginate with $CaCl_2$. Initially, the 3 mm rod mould was dipped into 8% sodium alginate and then into 10 mM, 20 mM, 30 mM, 40 mM, 50mM and 60 mM of $BaCl_2$ for 2 minutes. 2 minutes of cross-linking time was used due to the high toxicity of the $BaCl_2$, which could be harmful to the cells used during future studies. It would also be a good comparison to the alginate hydrogel tubular structures fabricated with $CaCl_2$ cross-linking reagent for 2 minutes.

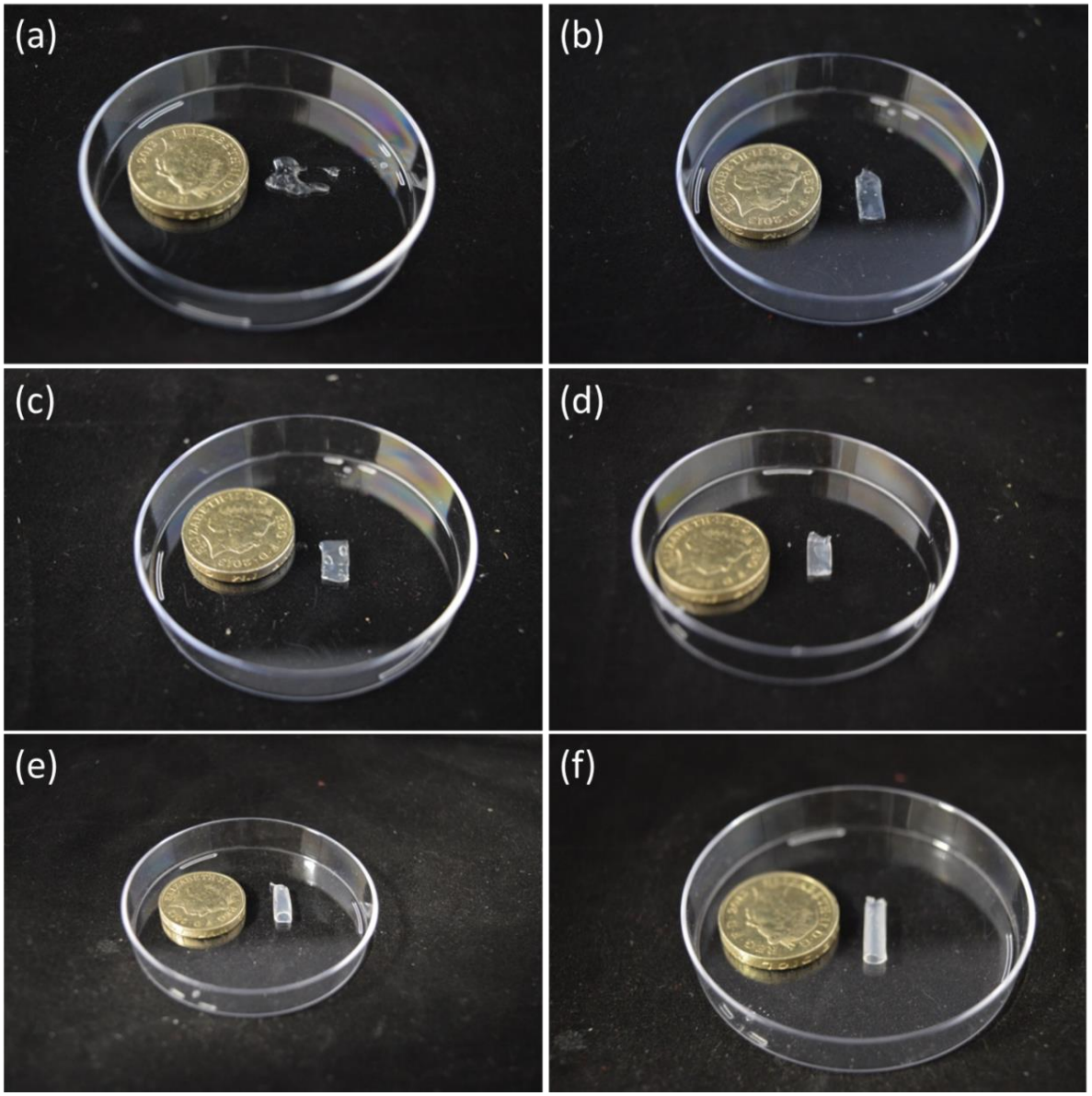

Figure 5.4 *– Fabricated alginate hydrogel tubular structures by exposure to (a) 10 mM (b) 20 mM (c) 30 mM (d) 40mM (e) 50 mM and (f) 60 mM $BaCl_2$ cross-linking reagent for 2 minutes and removed from the mould. Scale bar: 1 pound coin*

Based on the results, the 8% (w/v) sodium alginate coated on the mould's surface was not cross-linked after exposure to 10 mM of $BaCl_2$ for 2 minutes as shown in Figure 5.4a, which indicated that the $BaCl_2$ concentration was too low at this stage. On the other hand, 8% (w/v) sodium alginate cross-linked by 20 mM, 30 mM and 40 mM resulted in formation of sufficiently rigid tubular structures on the mould's surface. Once removed from the mould, however, the tubular structures were not able to keep their integrity and collapsed as shown in Figure 5.4b, Figure 5.4c and Figure 5.4d. Fabricated tubular structures cross-linked with 50 mM and 60 mM $BaCl_2$ had suitable rigidity and integrity as shown in Figure 5.4e and Figure 5.4f. The 8% sodium alginate cross-linked with 50 mM $BaCl_2$ had a minor deflection once removed from the mould;, 60 mM $BaCl_2$ resulted in a uniform and rigid tubular structure, however. A $BaCl_2$ concentration of between 50 mM to 60 mM was therefore considered to be the suitable range for cross-linking for 2 minutes.

5.4 Fabrication of alginate-gelatine tubular structures

Fabrication of alginate-only tubular structures with an optimised cross-linking condition was successfully presented in the previous section. A new experiment was designed to identify the ability of this technique to incorporate other biocompatible materials such as gelatine [27-29] with sodium alginate to fabricate tubular structures. Gelatin-alginate solution at gelatine concentration of 4% (w/v) (Gelatin from porcine skin, Type A, Sigma-Aldrich, UK) and sodium alginate at 6% was prepared in deionised water. A 3 mm rod/mould was dipped into the gelatine-alginate solution for 3 seconds to coat the mould's surface. Once the biomaterial was coated on the mould's surface, it was then dipped into the cross-linking reagents for 2 minutes (100 mM $CaCl_2$ or 55 mM $BaCl_2$) for cross-linking the sodium alginate present in the alginate-gelatin composition, forming the hollow tubular structure. As shown in Figure 5.5, the dip coating method had the ability to fabricate alginate-gelatine tubular structures that could have the potential to incorporate other biomaterials such as gelatine as well.

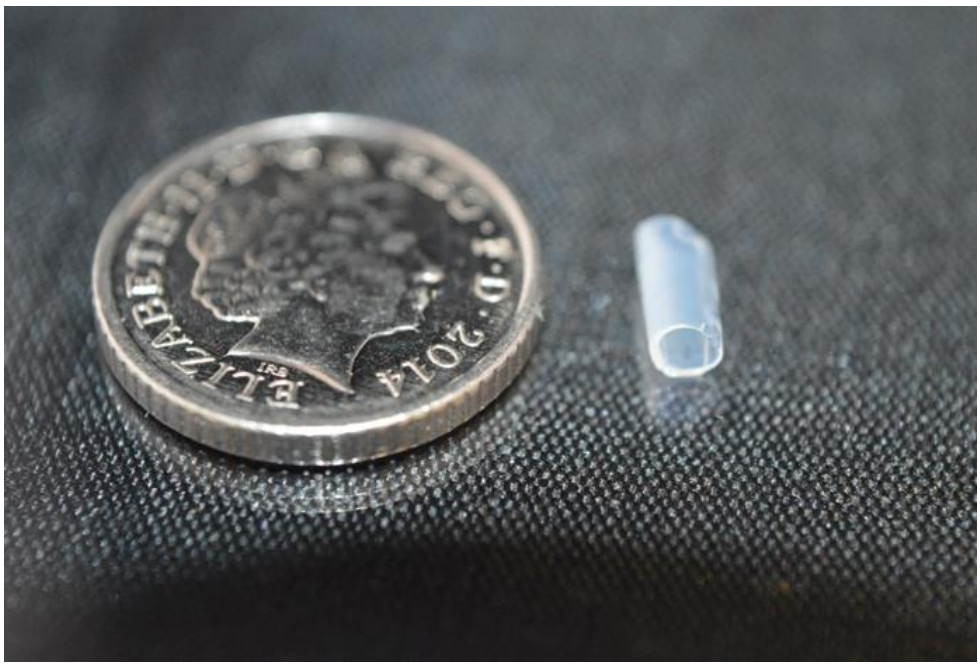

Figure 5.5 *– Fabricated alginate-gelatine tubular structure by the dip-coating approach. Scale bar: 5p coin.*

5.5 Fabrication of gelatine-only tubular structures

In order to fabricate gelatine tubular structures, gelatine-alginate tubular structures were fabricated using the dip-coating approach with the gelatine-alginate solution at concentrations of 4% (w/v) and 6% (w/v) respectively, cross-linked with 100 mM $CaCl_2$ or 55 mM $BaCl_2$ for 2 minutes. Once the gelatine-alginate tubular structure was fabricated as shown in Figure 5.6a, 400 µL of Ethylenediaminetetraacetic acid (EDTA) was added to dissolve the sodium alginate (Figure 5.6b) present within the tubular structure to leave a gelatine only tubular structure as shown in Figure 5.6c.

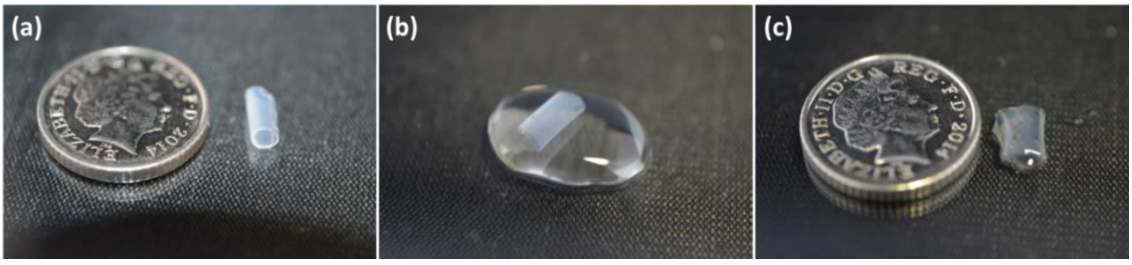

Figure 5.6 *– Fabrication of gelatine-only tubular structures processed with the dip-coating approach. (a) Initially, alginate-gelatine tubular structures were fabricated. (b) 400 µL of EDTA was added to the tubular structures to dissolve the sodium alginate present within the tubular structures to form a (c) gelatine-only tubular structure. Scale bar: 5p coin.*

The gelatine concentration at 4% (w/v) did not provide sufficient rigidity to keep the integrity of the tubular structure once the the sodium alginate was dissolved. Gelatine-alginate solutions with higher gelatine concentrations of 6%, 8% and 10% (w/v) were therefore prepared to fabricate gelatine tubular structures. The same cross-linking procedure was followed and the tubular fabricated structures can be seen in Figure 5.7. The results for 4%, 6% and 8% as shown Figure 5.7a, Figure 5.7b and Figure 5.7c respectively indicated that the tubular structure could not keep its integrity. Although at 10% the structure still collapsed, much improvement was observed in the rigidity of the tubular structure. As an example the tubes could keep their integrity within the culture medium as it would provide support for the tubular structure.

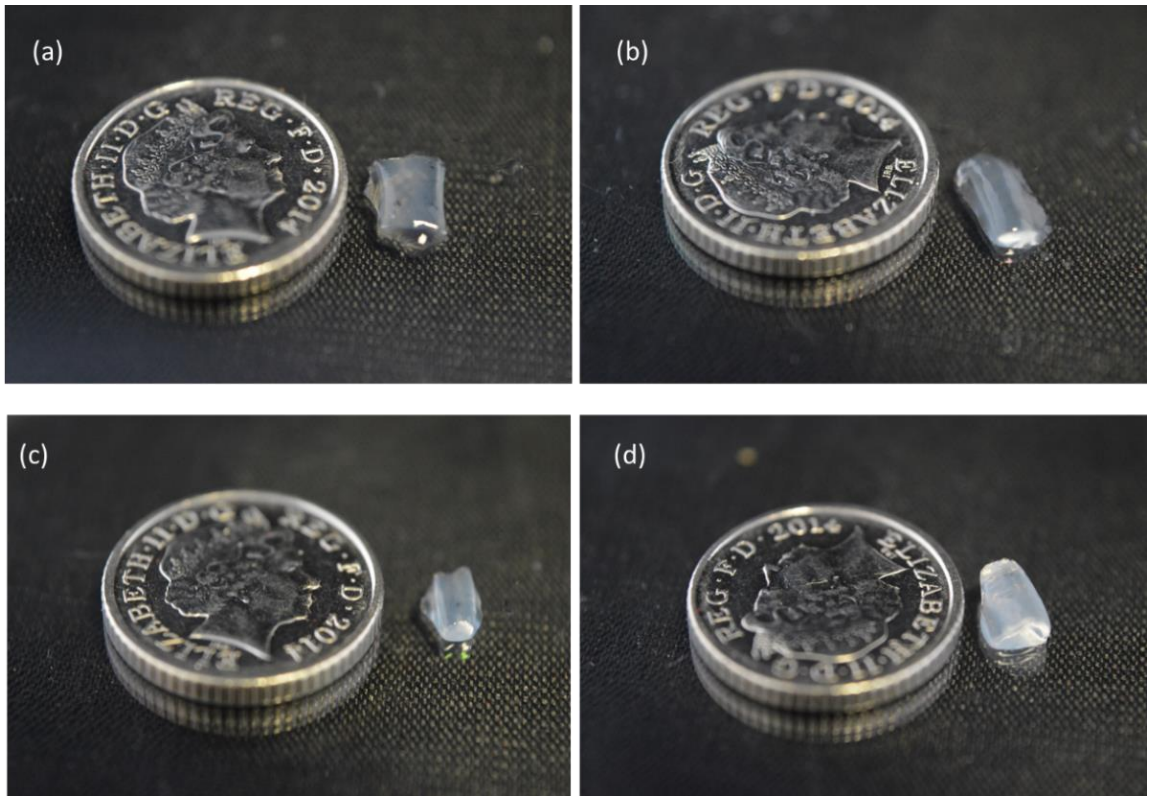

Figure 5.7 *– Fabricated gelatine tubular structures at (a) 4% (b) 6% (c) 8% and (d) 10% (w/v) via dip-coating approach. Scale bar: 5p coin.*

5.6 Fabrication of different sized alginate hydrogel tubular structures with various alginate concentrations

Tubular structures with different inner diameters ranging from 0.6 mm, 1.2 mm , 2.5 mm, 3 mm, 4 mm and 6 mm were successfully fabricated with 6 % (w/v) alginate hydrogel solution using the dip-coating method by exposing them to crosslinking

reagents as shown in Figure 5.8. The cross-linking reagents used were 100mM $CaCl_2$ solution or 55 mM $BaCl_2$ solution. The thickness of the fabricated tubes with inner diameters of 0.6 mm, 1.2 mm, 2.5 mm, 3 mm, 4 mm and 6 mm measured by calliper, were 126 ± 6 µm, 143 ± 5 µm, 171 ± 9 µm, 181.6 ± 13 µm, 206.6 ± 6 µm and 220 ± 7 µm respectively as shown in Figure 5.9. The results indicated an interesting correlation between the tube thickness and inner diameter of the tube.. To optimise the layer thickness of the tubular structures, alginate hydrogel solutions at 5%, 6%, 7% and 8% (w/v) concentrations were used to fabricate tubular structures. According to the measurements, the increase in thickness of the tubular structures was approximately linear with increasing sodium alginate concentrations. 5% alginate hydrogel concentration was the minimum concentration needed to fabricate tubular structures. Lower concentrated fabricated tubular structures had insufficient rigidity to support the integrity of the structure. It should be noted that this minimum is probably specific to the sodium alginate used in this study and that other sodium alginates with different viscosities and molecular weights may require different alginate concentrations and different concentrations of cross-linking reagents to fabricate the tubular structures. This may or may not result in a tubular structure with different wall thicknesses.

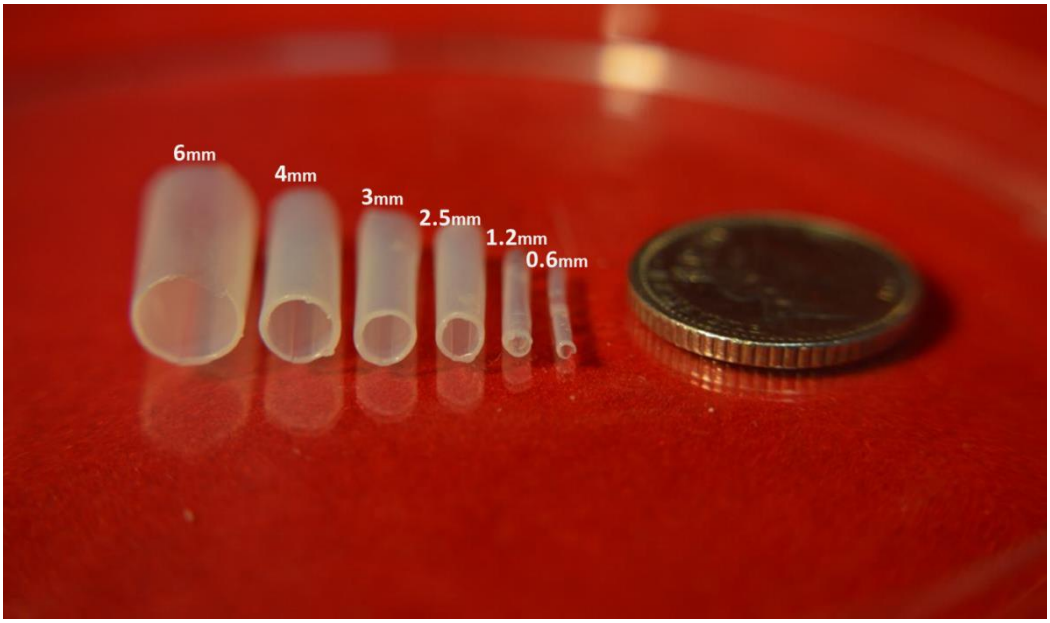

Figure 5.8 *– Alginate hydrogel tubular structures fabricated by the dip-coating method. Fabricated single layer alginate hydrogel tubular structures with descending diameters from left to right. Scale bar: 5p coin.*

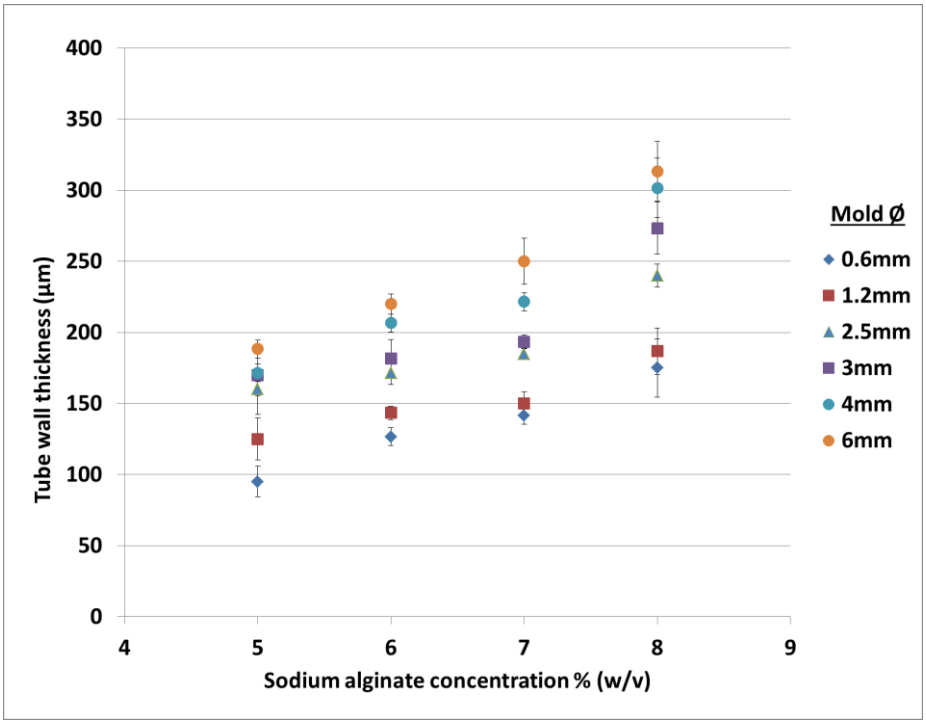

Figure 5.9 *– Sodium alginate concentration and mould diameter effect on fabricated tubular structure wall thicknesses.*

5.7 Fabrication of multi-layer alginate hydrogel tubular structures

After confirming the ability to produce single layer tubular structures, feasibility studies were performed to understand the ability of the dip-coating approach to fabricate multilayer alginate hydrogel tubular structures. To fabricate multilayer alginate hydrogel tubular structures, the mould was dipped into sodium alginate 6% (w/v) for 3 seconds and then dipped into the cross-linking reagent (100 mM $CaCl_2$ or 55mM $BaCl_2$) for 2 minutes to cross-link the sodium alginate on the mould's surface to form the first layer of the tubular structure. The cross-linked layer was then dipped into to the sodium alginate once more for 3 seconds whilst still on the mould to be coated by the second layer of sodium alginate. It was then dipped into the cross-linking reagent (100 mM $CaCl_2$ or 55 mM $BaCl_2$) for another 2 minutes to cross-link and form the second layer. This procedure could be repeated as many times as preferred to reach the number of layers within the tubular structure as desired as shown in Figure 5.10. The dip-coating approach allows the fabrication of tubes smaller than 1 mm up to various diameters, as well as the possibility to optimise the thickness of the tubes depending upon the desired application. This approach could potentially place different cell types within each layer with the ability to fine tune each layer to the desired thickness upon the application. The

tube wall thickness after the dip-coating was dependent on the wettability of the coating surface, however. Therefore the wall thickness of the secondary layer would depend on the wettability of the first coated layer and hence the thickness of the second layer may vary with different batches of material from the data presented here.

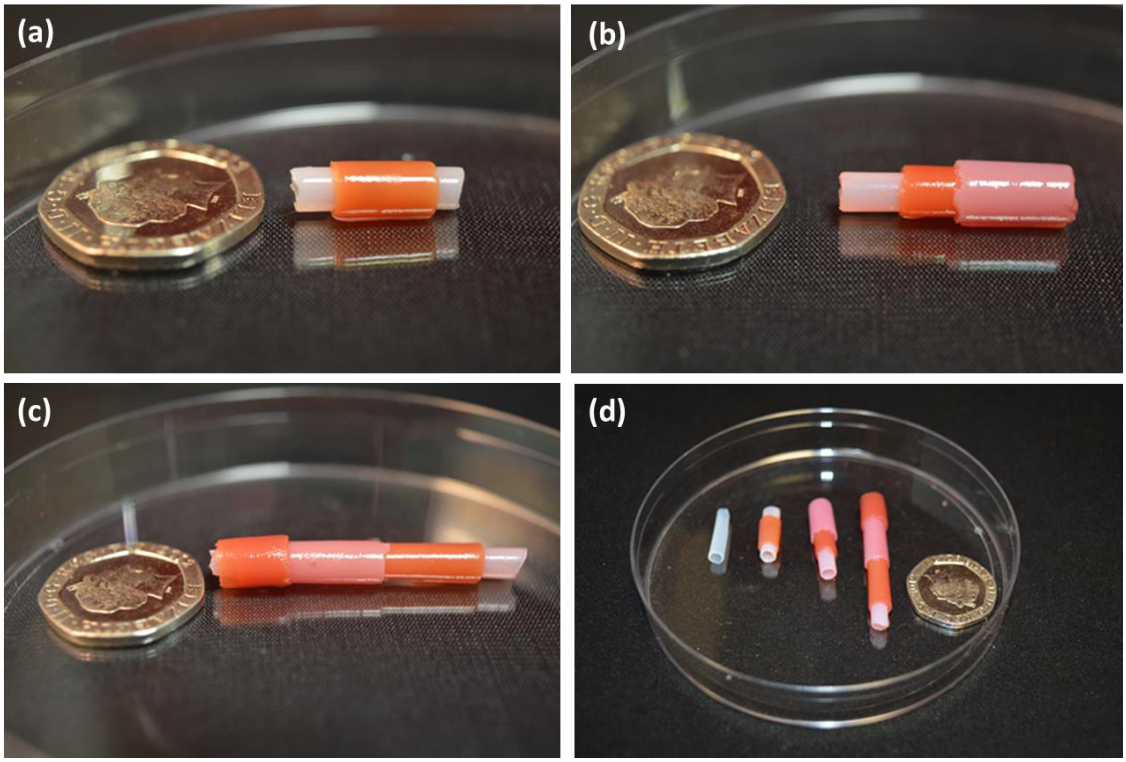

Figure 5.10 *– Fabricated multilayer alginate hydrogel tubular structures (a) Two layers, (b) three layers, (c) four layers and (d) overview of the fabricated one, two, three and four layer tubular structures fabricated via dip-coating approach. Scale bar: 20p coin.*

5.8 Flow experiment through cross-linked alginate hydrogel tubular structures

The flow experiment was designed to investigate whether the fabricated alginate hydrogel tubular structures were sealed against liquid flow. An alginate hydrogel tubular structure with 4 mm diameter was fabricated using the dip-coating protocol. 60 mL of water with red dye was prepared and loaded into the syringe. The syringe was then loaded into the syringe pump and the tubular structure was fitted with the syringe tip. The syringe pump flowrate was set to 20 mL/min for 3 minutes.

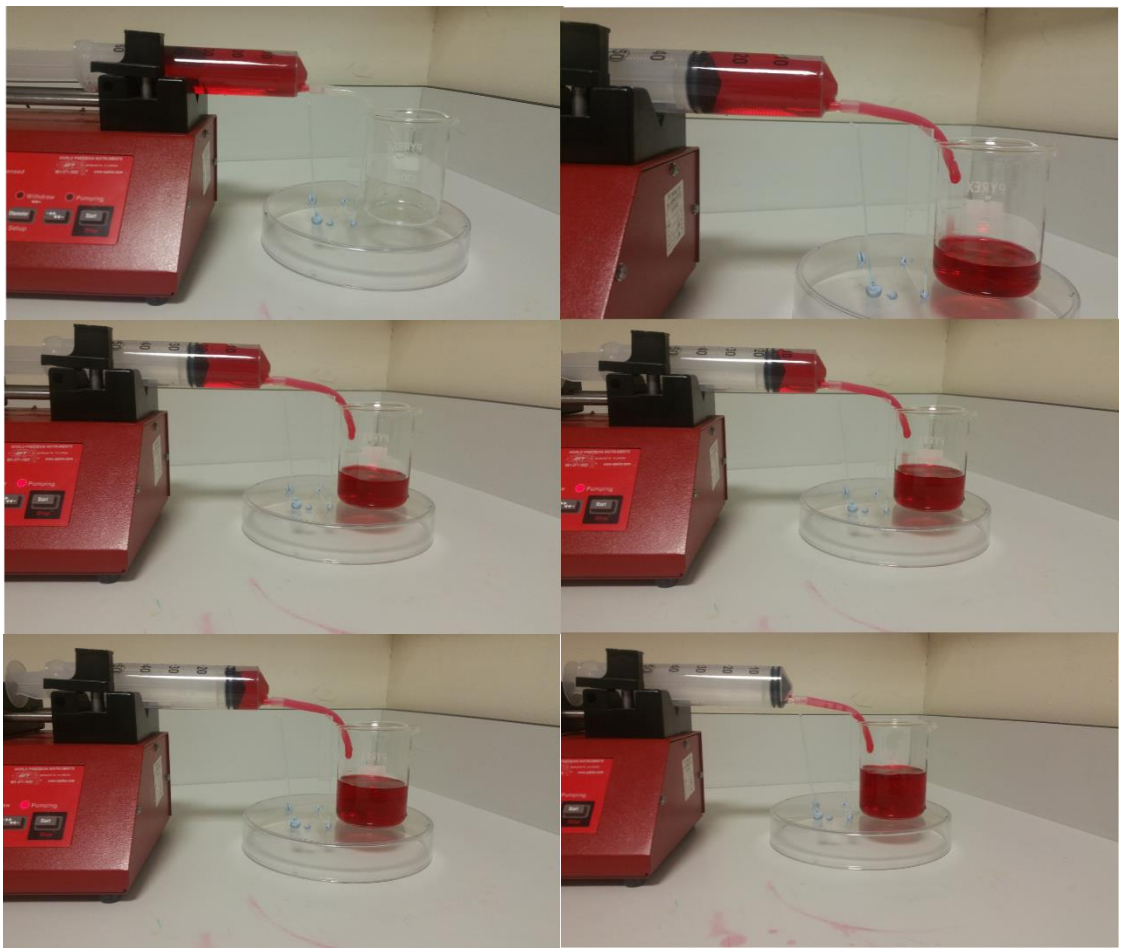

Figure 5.11 *– Water flow through a fabricated 4 mm inner diameter alginate hydrogel tubular structure.*

As shown in Figure 5.11, the tubular structure was completely sealed from the start to the end of the flow providing a safe and sealed environment for liquid flow through the tubular structure.

A similar experiment was carried out to ensure the tubular structures are fluid tight as well under water. Initially, alginate hydrogel tubular structure with 4 mm diameterwas fabricated using the dip-coating protocol. 60 mL of water with red dye was prepared and loaded into a 60 mL syringe. The syringe was then loaded into the syringe pump and the tubular structure was fitted with the syringe tip. The tubular structure then was passed through water and one end was left to discharge the water with red dye. The syringe pump flowrate was set to 20 mL/min for 3 minutes. As shown in Figure 5.12 the tubular structure was completely sealed from the start to the end of the flow and provided a safe and sealed environment for liquid flow through the tubular structure in

both water and air. Experiments based on this approach could possibly mimic blood flow through vessels.

Figure 5.12— *Flow experiment through a single layer alginate hydrogel tubular structure. Water with red dye was pumped from a syringe, through the fabricated tube to the beaker on the right. The red dye was transferred and did not leak either into water (the beaker on the left) or air (note the absence of dye on the table).*

5.9 3D fabrication of complex alginate hydrogel structure

5.9.1 3D printing branched structure and its silicone-based mould fabrication

Successful 3D fabrication of single and multiple layered tubular structures was presented in the previous section. To move to more complex 3D structures such as branched structures, the use of metal bars would not allow for removal of the cross-linked alginate or other biomaterials. Therefore the proposed idea was to fabricate a 3D mould using dissolvable material at 37 °C. This meant that once the alginate hydrogel was coated on the mould's surface and cross-linked, the mould should be dissolved when cultured at 37 °C, leaving behind the complex cross-linked alginate hydrogel structure. In order to fabricate the mould, a branched structure design was extracted from Garb-CAD, a free CAD library, and then 3D printed by MakerBot Replicator 2X ABS 3D printer as shown in Figure 5.14. Once 3D printed, a silicone mould of the branched structure was fabricated as shown in Figure 5.15. Silicone Sylgard 184 (Down Corning, UK) with a base to cross-linker ratio of 10:1 (v/v) was prepared. A 3 mm thick layer was poured into a plastic tank measuring 6 cm × 11 cm × 4 cm and was cured at 90 °C for an hour. Then the printed branched structure was placed on top of the cured layer. An uncured silicone at 17 mm layer thickness was poured into the tank containing the branch structure. The silicone was then cured at 90 °C for another hour. Once cured, a 7.6 µm thick layer of polyamide was put on the cured silicone. Another layer of uncured layer of silicon was added on top until the branch structure was covered fully

with silicone. It was left for two hours at 90 °C to cure. Once cured, the silicone was taken out. The polyamide sheet helped to keep the two main sections of the mould separate.

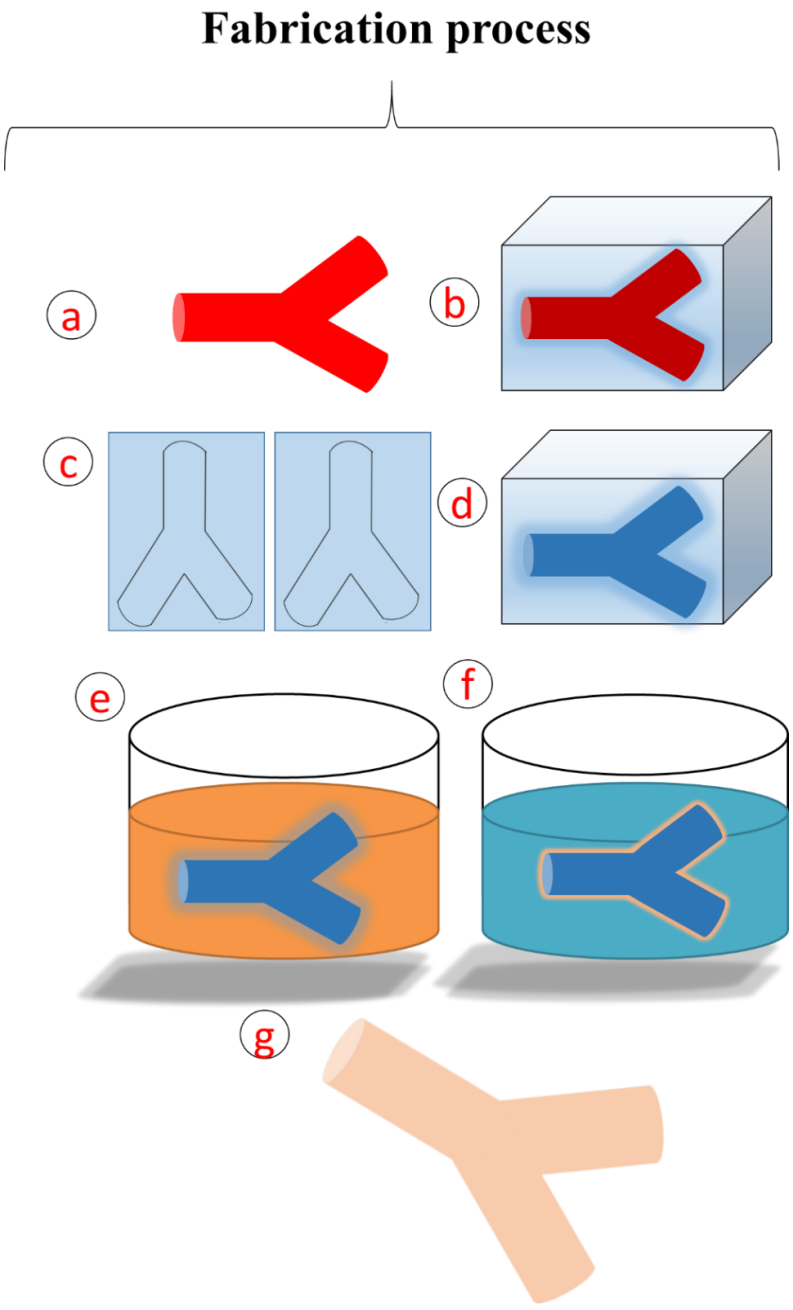

Figure 5.13 *– Schematic drawing of 3D biofabrication of complex alginate hydrogel structure via dip-coating using a dissolvable mould. (a) 3D printed solid branched structure (b) was put in an uncured silicon to form its (c) mould once the silicon was cured. (d) Water was poured into the mould and kept in the freezer overnight. Once an ice mould was formed, it was dipped in alginate hydrogel to be coated by a layer of alginate and then (f) was dipped into* $CaCl_2$ *solution until the ice melted, resulting in a (g) hollow branched structure made of cross-linked alginate hydrogel.*

Figure 5.14 *– 3D printed solid branched structured using ABS plastic by MakerBot Replicator 2X.Scale bar: 1p coin.*

Figure 5.15 *– Fabricated silicone mould for the solid branched structure. Scale bar: 1p coin.*

5.9.2 Fabrication of dissolvable mould and hollow alginate hydrogel branched structure

To understand the feasibility of this 3D fabrication approach, water at room temperature was injected into the silicon mould and was kept in the freezer at -17 °C for 3 hours. The ice mould was removed as shown in Figure 5.16 and dipped into an 8% (w/v) sodium alginate solution and then immediately dipped into a 300 mM $CaCl_2$ at room

temperature for two minutes. This dissolved the ice and cross-linked the alginate as shown in the Figure 5.17, forming a hollow branched structure.

Figure 5.16 *– Fabricated solid ice branched structure from a silicone mould. Scale bar: 50p coin.*

Figure 5.17 *– Fabricated Hollow branched cross-linked alginate hydrogel structure using solid ice mould.*

An ice mould was used to validate the feasibility of using dissolvable materials to form complex alginate hydrogel structures such as the branched structure shown in Figure

5.17. However, the use of ice could be harmful to the cells due to its low temperature, limiting the possibility of using the cells for subsequent cell studies. Therefore a biocompatible and dissolvable mould with a higher melting point, such as gelatine with a melting point of 37 °C, would be more appropriate.

5.9.3 Fabrication of a complex alginate hydrogel structure using gelatine mould

Gelatine is a highly biocompatible material and has a higher melting point than ice. To fabricate the solid gelatine mould, 20 % w/v gelatine from porcine skin was prepared in de-ionised water at 60 °C to keep the gelatine solution in a liquid state. A solid stomach at 1:2 scale was created in 3D by MakerBot Replicator 2X, similar to the branched structure shown in Figure 5.18a. A silicone mould of the solid stomach was fabricated shown in Figure 5.18b. The gelatine solution was poured into a silicone mould and left at room temperature for an hour to cool down to solidify. The solid gelatine stomach structure shown in Figure 5.18c was gently removed from the silicon mould and then dipped into 8% (w/v) sodium alginate to be coated by a layer of alginate. It was then dipped into 300 mM $CaCl_2$ solution at room temperature to cross-link the alginate to form a hollow stomach structure as shown in Figure 5.18d. Dissolving the gelatine would take more time compared to ice. However, if cell study is needed to be carried out, the cell-laden cross-linked alginate could stay coated on the gelatine due to gelatine's biocompatibility as long as both gelatine and alginate solutions are sterile. The cross-linked cell-laden alginate hydrogel could therefore possibly be incubated at 37 °C and the dissolution time of the gelatine would be insignificant.

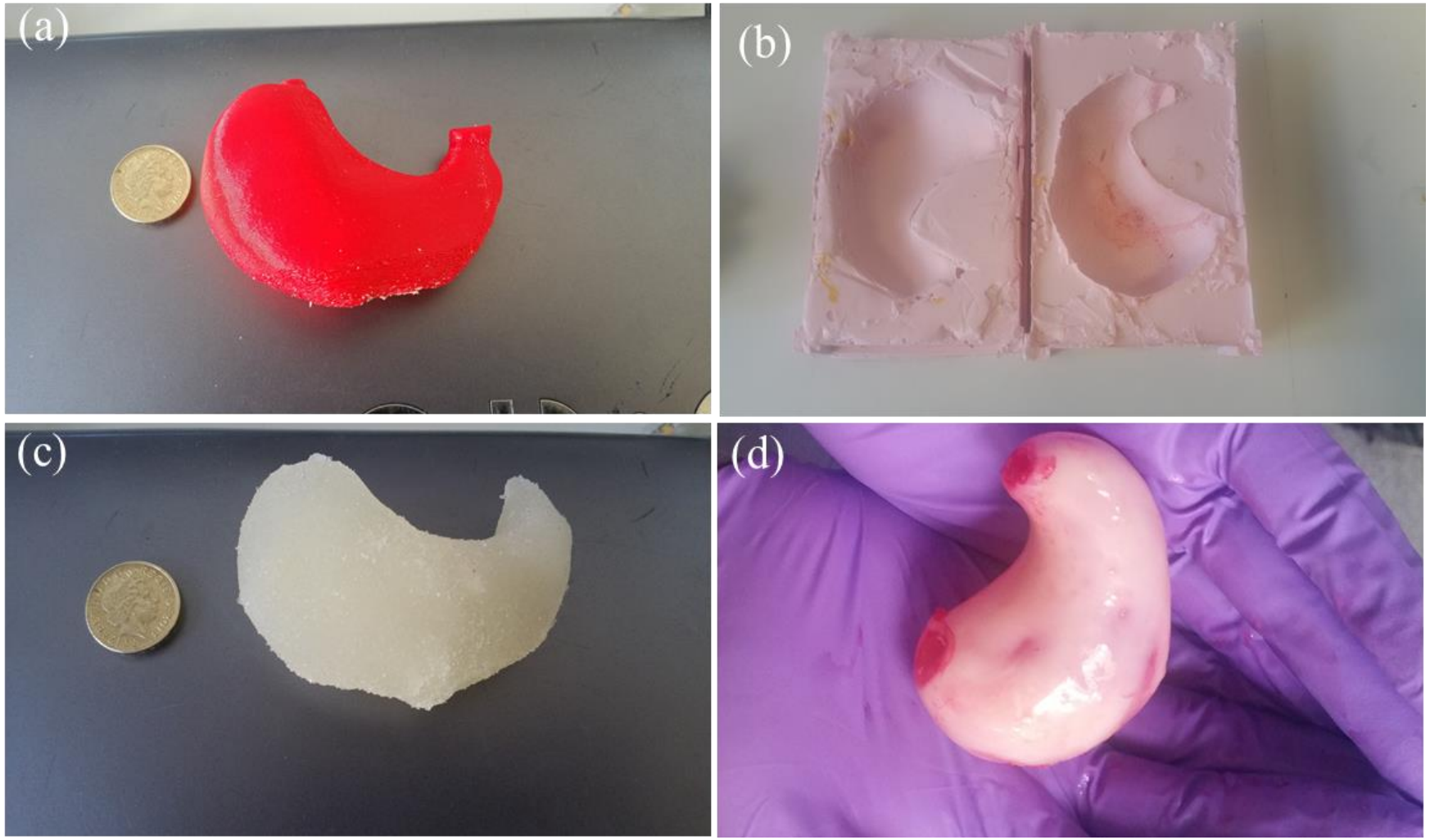

Figure 5.18 *— (a) 3D printed solid Stomach by MakerBot Replicator 2X using ABS plastic. (b) Silicone Mould fabricated using the 3D printed solid stomach. (c) Solid gelatine stomach fabricated by silicone mould. (d) Hollow stomach fabricated by the gelatine mould using alginate hydrogel.*

5.10 Conclusions

In this chapter, a new rapid 3D biofabrication technique was developed for multi-layered alginate hydrogel tubular structures, bypassing cell sheet technologies [30-33] and other complex tubular fabrication approaches [33-41] that require expensive and complicated machinery systems. Tubular structures from the submillimetre range to greater diameters with the ability to control the thickness of the tube walls can be fabricated using the dip-coating approach. This approach could incorporate other bio-materials within the alginate hydrogel to help cell biologists bypass the lengthy, complicated and expensive fabrication approaches. It would allow integration of the dip-coating method to fabricate 3D tubular structures with living cells in the preferred extracellular matrix. By making some alterations to the tube fabrication protocol, 3D fabrication of complex 3D structures such as hollow branched structure and hollow stomach was achievable.

Chapter 5 references

[1] Gies K, Kaufmann J, Pronk G J, Klippel A 2002 Unravelling novel intracellular pathways in cell-based assays *Drug Discovery Today* 7(3):179-186.

[2] Imamura Y, Mukohara T, Shimono Y, Funakoshi Y, Chayahara N, Toyoda M, Minami H. 2015 Comparison of 2D- and 3D-culture models as drug-testing platforms in breast cancer *Oncology Reports* 33:1837-1843

[3] Birgersdotter A, Sandberg R, Ernberg I 2005 Gene expression perturbation *in vitro*—A growing case for three-dimensional (3D) culture systems *Seminars in Cancer Biology* 15(5): 405-412

[4] Zhao Y, Yao R, Ouyang L, Ding H, Zhang T, Zhang K, Cheng S, Sun W 2014 Three-dimensional printing of Hela cells for cervical tumor model in vitro *Biofabrication* **6** 035001

[5] Edmondson R, Broglie J J, Adcock A F, Yang L 2014 Three-Dimensional Cell Culture Systems and Their Applications in Drug Discovery and Cell-Based Biosensors *Assay and Drug Development Technologies* 12 (4): 207–218.

[6] Bellis A D, Bernabé B P, Weiss M S, Shin S, Weng S, Broadbelt L J, Shea LD 2013 Dynamic transcription factor activity profiling in 2D and 3D cell cultures *Biotechnology and Bioengineering* 110: 563–572

[7] *Peck M, Dusserre N, McAllister TN, L'Heureux N. Tissue engineering by self-assembly. Mater Today. 2011;14:218–224.*

[8] Thadavirul, Napapaphat, Prasit Pavasant, and Pitt Supaphol. "Development of polycaprolactone porous scaffolds by combining solvent casting, particulate leaching, and polymer leaching techniques for bone tissue engineering." *Journal of Biomedical Materials Research Part A* 102.10 (2014): 3379-3392.

[9] Offeddu G S, Ashworth J C, Cameron R E, Oyen M L 2015 Multi-scale mechanical response of freeze-dried collagen scaffolds for tissue engineering applications. *Journal of the Mechanical Behavior of Biomedical Materials* 42:19-25.

[10] Chu X, Xu Q, Fenf J, Li Q, Sun X, Cao Y, Ding Y 2014 In vitro biocompatibility of polypyrrole/PLGA conductive nanofibre scaffold with cultured rat hepatocytes *Materials Research Express* 1(3):035402

[11] Bini T B, Gao S J, Tan T C, Wang S, Lim A, Hai L B, Ramakrishna S 2004 Electrospun poly(L-lactide- co -glycolide) biodegradable polymer nanofibre tubes for peripheral nerve regeneration *Nanotechnology* 15(11): 1459

[12] L'Heureux N, Paquet S, Labbe R, Germain L, Auger F A 1998 A completely biological tissue-engineered human blood vessel *FASEB* J 12 47–56

[13] Crapo P M, Gilbert T W, Badylak SF 2011 An overview of tissue and whole organ decellularization processes *Biomaterials* 32(12):3233-3243

[14] Wilson S L, Sidney L E, Dunphy S E, Rose J B, Hopkinson A 2013 Keeping an Eye on Decellularized Corneas: A Review of Methods, Characterization and Applications *Journal of Functional Biomaterials 4*(3):114–161

[15] Ghanizadeh Tabriz A, Hermida A H, Leslie N R, Shu W 2015 Three-dimensional bioprinting of complex cell laden alginate hydrogel structures. *Biofabrication* 7(4) 045012.

[16] Faulkner-Jones A, Greenhough S, King J A, Gardner J, Courtney A, Shu W 2013 Development of a valve-based cell printer for the formation of human embryonic stem cell spheroid aggregates. *Biofabrication* 5 015013

[17] Li C, Faulkner-Jones, A, Dun A R, Jin J, Chen P, Xing Y, Yang Z, Li Z, Shu W, Liu D, Duncan R R 2015 Rapid Formation of a Supramolecular Polypeptide–DNA Hydrogel for In Situ Three-Dimensional Multilayer Bioprinting *Angew. Chem. Int. Ed* 54: 3957–3961.

[18] Faulkner-Jones A, Fyfe C, Cornelissen D J, Gardner J, King J, Courtney A, Shu W 2015 Bioprinting of human pluripotent stem cells and their directed differentiation into hepatocyte-like cells for the generation of mini-livers in 3D *Biofabrication* 7 044102

[19] Gudapati H, Yan J, Huang Y, Chrisey D B 2014 Alginate gelation-induced cell death during laser-assisted cell printing. *Biofabrication* 6:035022

[20] Yamaguchi S, Ueno A, Akiyama Y and Morishima K 2012 Cell patterning through inkjet printing of one cell per droplet *Biofabrication* **4** 045005

[21] Kang K H, Hockaday L A, Butcher J T 2013 Quantitative optimization of solid freeform deposition of aqueous hydrogels *Biofabrication* 5(3):035001

[22] Hochleitner G, Jungst T, Brown T D, Hahn K, Moseke C, Jakob F 2015 Additive manufacturing of scaffolds with sub-micron filaments via melt electrospinning writing. *Biofabrication* 2015;7:035002

[23] Ouyang L, Yao R, Mao S, Chen X, Na J, Sun W. 2015. Three-dimensional bioprinting of embryonic stem cells directs highly uniform embryoid body formation *Biofabrication* **7**:044101

[24] Groll J, Boland T, Blunk T, Burdick J A, Cho D W, Dalton P D, Derby B, Forgacs G, Li Q, Mironov V A, Moroni L, Nakamura M, Shu W, Takeuchi S, Vozzi G,Woodfield T B, Xu T, Yoo J J, Malda J 2016 Reappraising the definition of an evolving field *Biofabrication* 8(1): 013001

[25] Kang H W, Lee S J, Ko I K, Kengla C, Yoo J J, Atala A 2016 A 3D bioprinting system to produce human-scale tissue constructs with structural integrity. *Nature Biotechnology* 34(3):312-319

[26] Mørch Ý A, Donati I, Strand B L 2006 Effect of Ca2+, Ba2+, and Sr2+ on Alginate Microbeads *Biomacromolecules* 7(5):1471-1480

[27] Stevens, K. R., N. J. Einerson, J. A. Burmania and W. J. Kao (2002). "In vivo biocompatibility of gelatin-based hydrogels and interpenetrating networks." Journal of Biomaterials Science, Polymer Edition 13(12): 1353-1366.

[28] Lai, J.-Y. (2010). "Biocompatibility of chemically cross-linked gelatin hydrogels for ophthalmic use." Journal of Materials Science: Materials in Medicine 21(6): 1899-1911.

[29] Rathna, G. V. N. (2008). "Gelatin hydrogels: enhanced biocompatibility, drug release and cell viability." Journal of Materials Science: Materials in Medicine 19(6): 2351-2358.

[30] Sekine, H., T. Shimizu, J. Yang, E. Kobayashi and T. Okano (2006). "Pulsatile Myocardial Tubes Fabricated With Cell Sheet Engineering." Circulation 114(1 suppl): I-87-I-93.

[31] Othman R, Morris G.E, Shah D.H, Hall S,Hall G, Wells K, Shakesheff K.M , Dixon E.J. (2015). "An automated fabrication strategy to create patterned tubular architectures at cell and tissue scales." Biofabrication 7(2): 025003.

[32] Matsuda, N., Shimizu, T., Yamato, M. and Okano, T. (2007), Tissue Engineering Based on Cell Sheet Technology. Adv. Mater., 19: 3089–3099. doi:10.1002/adma.200701978

[33] Kubo, H., T. Shimizu, M. Yamato, T. Fujimoto and T. Okano (2007). "Creation of myocardial tubes using cardiomyocyte sheets and an in vitro cell sheet-wrapping device." Biomaterials 28(24): 3508-3516.

[34] A. Wang, Q. Ao, W. Cao, C. Zhao, Y. Gong, N. Zhao, et al. Fiber-based chitosan tubular scaffolds for soft tissue engineering: fabrication and in vitro evaluation Tsinghua Science and Technology, 10 (4) (2005), pp. 449–453.

[35] Yuan, B., Jin, Y., Sun, Y., Wang, D., Sun, J., Wang, Z., Zhang, W. and Jiang, X. (2012), A Strategy for Depositing Different Types of Cells in Three Dimensions to Mimic Tubular Structures in Tissues. Adv. Mater., 24: 890–896. doi:10.1002/adma.201104589

[36] Sakai S, Liu Y, Mah E J and Taya M (2013) Horseradish peroxidase/catalase-mediated cell-laden alginate-based hydrogel tube production in two-phase coaxial flow of aqueous solutions for filament-like tissues fabrication *Biofabrication* **5** 015012

[37] A. Wang, Q. Ao, W. Cao, C. Zhao, Y. Gong, N. Zhao, et al. Fiber-based chitosan tubular scaffolds for soft tissue engineering: fabrication and in vitro evaluation Tsinghua Science and Technology, 10 (4) (2005), pp. 449–453.

[38] Johnson, L. M., C. A. DeForest, A. Pendurti, K. S. Anseth and C. N. Bowman (2010). "Formation of Three-Dimensional Hydrogel Multilayers Using Enzyme-Mediated Redox Chain Initiation." ACS Applied Materials & Interfaces 2(7): 1963-1972.

[39] Praveen, S., M. O. Sara, B. João and F. M. João (2015). "Assembly of cell-laden hydrogel fibre into non-liquefied and liquefied 3D spiral constructs by perfusion-based layer-by-layer technique." Biofabrication 7(1): 011001.

[40] Hume, P. S., Bowman, C. N., & Anseth, K. S. (2011). Functionalized PEG hydrogels through reactive dip-coating for the formation of immunoactive barriers. *Biomaterials*, *32*(26), 6204–6212. http://doi.org/10.1016/j.biomaterials.2011.04.049

[41] Onoe, H., T. Okitsu, A. Itou, M. Kato-Negishi, R. Gojo, D. Kiriya, K. Sato, S. Miura, S. Iwanaga, K. Kuribayashi-Shigetomi, Y. T. Matsunaga, Y. Shimoyama and S. Takeuchi (2013). "Metre-long cell-laden microfibres exhibit tissue morphologies and functions." Nat Mater 12(6): 584-590.

Chapter 6 - Biological studies based on dip-coating approach

6.1 Introduction

In the previous chapter, rapid fabrication of tubular structures made of alginate hydrogel was demonstrated using the dip-coating approach, as well as the composition of the alginate hydrogel with other biomaterials. Rapid fabrication of complex 3D structures such as a branched structure and a stomach were demonstrated using the dip-approach, as well using a dissolvable mould. In this chapter the biological studies cover sterilisation methods other than the Gamma sterilisation used for 3D bioprinting in chapter 4. The methods were used to sterilise the alginate to investigate cell attachment on alginate hydrogel based on the different sterilisation methods. Madin-Darby canine kidney cells (MDCKII cells) and mouse dermal embryonic fibroblast cells were fabricated into tubular structures using different biomaterials and various cross-linking conditions over 6 days of culture. The cell viability was subsequently tested. Cell function within the tubular structures fabricated by the dip-coating approach was tested using the human embryonic kidney cells (tHEK). In addition, new biomaterial compositions were tested to enhance the cells' attachments on the biomaterial's surface using MDCKII cells, mouse dermal fibroblast cells, U87-MG cells and Human fibroblast cells.

6.2 Cell culture

All cell lines used in this study were cultured in 5.0 % CO_2 at 37.0 °C. Human embryonic kidney 293 cells containing a tetracycline responsive red fluorescence protein (tHEK) were kindly donated by Dr. Elise Cachat (Centre for integrative physiology, Edinburgh University, UK) and cultured in Dulbeccos Modified Eagle Medium (DMEM, Sigma D5796) with 5 % Fetal Bovine Serum (Biosera, FB-1090/500). Mouse dermal embryonic fibroblasts that were kindly donated by Mrs. Audrey Peter (College of Medicine & veterinary Medicine, Edinburgh University, UK) were cultured in Minimum Essential Medium (MEM, Sigma M5650) supplemented with 5 % Fetal Bovine Serum and 1 % L-Glutamine (Invitrogen, 25030-081).

Human glioma U87-MG cells, originally purchased from European Collection of Cell Cultures (ECACC) (Public Health England, UK), were seeded at the density of 0.5 × 10^6/mL in 6-well plates and were allowed to attach and acquire normal morphology. Then the cells were transduced using a lentiviral vector which expresses enhanced green

fluorescent protein (EGFP) under control of the SFFV promoter. After transduction, cells were seeded in 96-well plates at a cell density of 0.7 cells per well, allowing the selection of a single transduced cell population which were replicated for 2 weeks until a stable clone GFP1-U87-MG line was generated. U87-MG cells were cultured in minimum essential medium (MEM) supplemented with 10 % (v/v) fetal bovine serum (FBS), L-Glutamine, non-essential amino acids (NEAA), and sodium pyruvate. All culture medium components were from Life Technologies. During experimental procedures, medium was supplemented with penicillin/streptomycin (100 UI/ml and 100 µg/ml). After printing, cells were maintained at 37 °C and with 5 % CO_2 in 10 cm petri dishes (Fisher Scientific, UK). The culture media were changed every 2 days.

6.3 Fabrication of sterilised 2D Alginate sheets to culture MDCKII cells

I8% (w/v) sodium alginate solution (Product number W201502, Sodium Alginate, Sigma-Aldrich, Gillingham, UK) was prepared in deionized water. An ultrasonic bath was used overnight at 60 °C to ease the mixing process. 100 mM $CaCl_2$ solution (Product number 223506, $CaCl_2$ dehydrate, Sigma-Aldrich, Gillingham, UK) was prepared in deionised water as the cross-linking reagent. Two sets of sheets were prepared for culture purposes.

400 µL of alginate was poured on a 60 mm petri dish and was spin coated. 100 mM $CaCl_2$ was poured on the alginate layer and was kept there for 2 minutes. Once the alginate was cross-linked, it was cut into 1 cm × 1 cm sheets using a razor and kept in a 50 mM $CaCl_2$ solution to keep its shape.

In addition to sheets that were not sterile, three different sterilisation techniques were used to sterilise the alginate sheets before cell seeding:

1. Autoclaving: The sheets were autoclaved for 2 hours at 120 °C.

2. UV radiation: The sheets were transferred to distilled water and incubated at room temperature overnight in a tissue culture hood under UV radiation.

3. Chloroform: The chloroform was added to deionised water so that it formed a bottom layer and did not mix; this was done in a fume hood. The sample was then left overnight in a fume hood so that the chloroform evaporated through the water and alginate to sterilise the sample. All samples were washed with medium (minimal essential medium,

fetal bovim serum (FBS) and 1% Penicillin/streptomycin) before transferring to cell culture treated six-well plates.

Once the sterilisation process was performed the alginate sheets were transferred into a 6 well plate and 0.3 $\times 10^6$ MDCKII cells in 5 mL of medium were added into each well. The cultures were then left for 5 days at 37 °C, 5% CO_2 before imaging.

6.3.1 Fabrication of 2D alginate sheets with rat collagen type 1

0.67 mL of 0.4% (w/v) collagen type 1 from rat tail dissolved in 20 mM acetic acid (Product number C3867, Sigma-Aldrich, Gillingham, UK) was added to 1.33 mL of 8 % (w/v) sodium alginate and mixed with an ultrasonic bath at room temperature for 2 hrs. This resulted in a solution consisting of 0.133% (w/v) collagen and 6% (w/v) sodium alginate. 400 µL of the solution was placed on a 60 mm Petri dishes and was spin coated. 100 mM $CaCl_2$ was added for 2 minutes to cross-link the alginate sheet. Once cross-linked the sheet was cut into smaller sheets of 1 cm × 1 cm and was kept in 50 mM $CaCl_2$ solution to keep its shape. The sheets with rat collagen used the same procedure of cell seeding as was performed on the alginate only sheets. The images shown in Figure 6.1 represent the results based on a 5-day culture with different sterilisation processes.

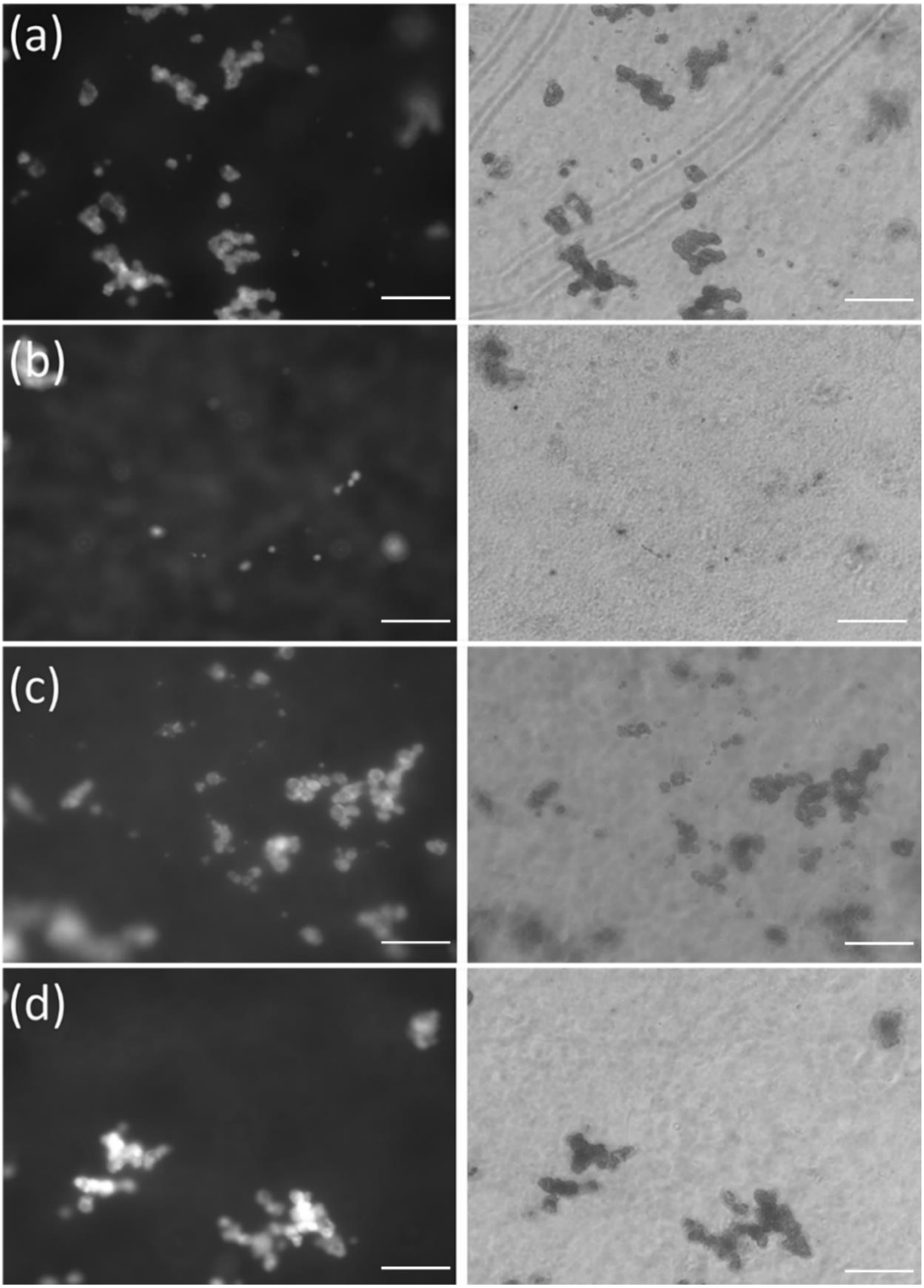

Figure 6.1 *– Seeded MDCK cells on a (a) non sterile cross-linked alginate sheets and sterile cross-linked alginate sheets by (b) autoclave, (c) UV radiation and (d) Chloroform. Scale bar: 100 µm.*

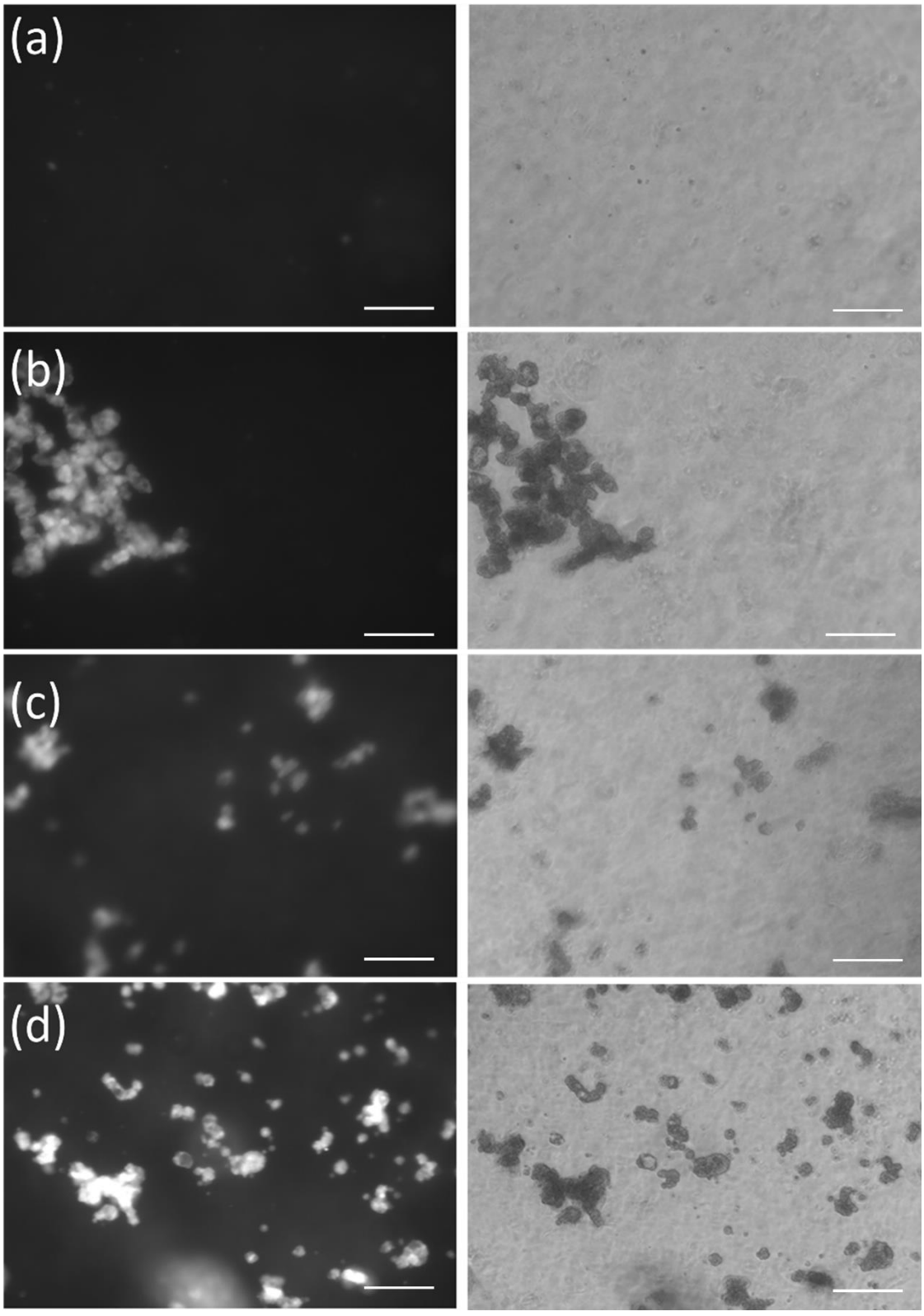

Figure 6.2 *– Seeded MDCK cells on a (a) non sterile cross-linked alginate-collagen sheets and sterile cross-linked alginate-collagen sheets by (b) autoclave, (c) UV radiation and (d) chloroform. Scale bar: 100 µm.*

6.4 Increase in concentration of rat-collagen in alginate-rat collagen 2D sheets

Based on the results shown in Figure 6.1 and Figure 6.2, the collagen seems to be enhancing adhesion of MDCK II cells to the cross-linked alginate hydrogel sheets. Therefore to improve the cell attachment, an increase in collagen concentration could be beneficial. To increase the concentration of collagen, 0.12 g of sodium alginate was directly added to 2 mL of 0.4% (w/v) collagen. This resulted in a solution with 0.4% (w/v) collagen and 6% (w/v) sodium alginate. An ultrasonic bath at room temperature was used to reduce the mixing process duration to 1 hr. Once the solution was ready, it was dispensed on the centre of a 12 mm hydrophilic Petri dish and then spin coated. 100 mM $CaCl_2$ solution was poured on the gel for 2 minutes to cross-link the sodium alginate. The calcium was removed and the cross-linked sheet was cut into identical pieces of 1 cm × 1cm and kept in a 50 mM $CaCl_2$ solution to keep their shapes. The sheets then were sterilised by autoclave, chloroform and UV radiation as per the protocol in section 6.1. The sheets were then moved to the bottom of a 6 well plate culture dish. 0.3×10^6 MDCKII cells in 5 mL culture medium were seeded on the well plates. The images shown in Figure 6.3 show the adhesion of MDCKII cells on alginate-collagen sheets after 5 days of culture.

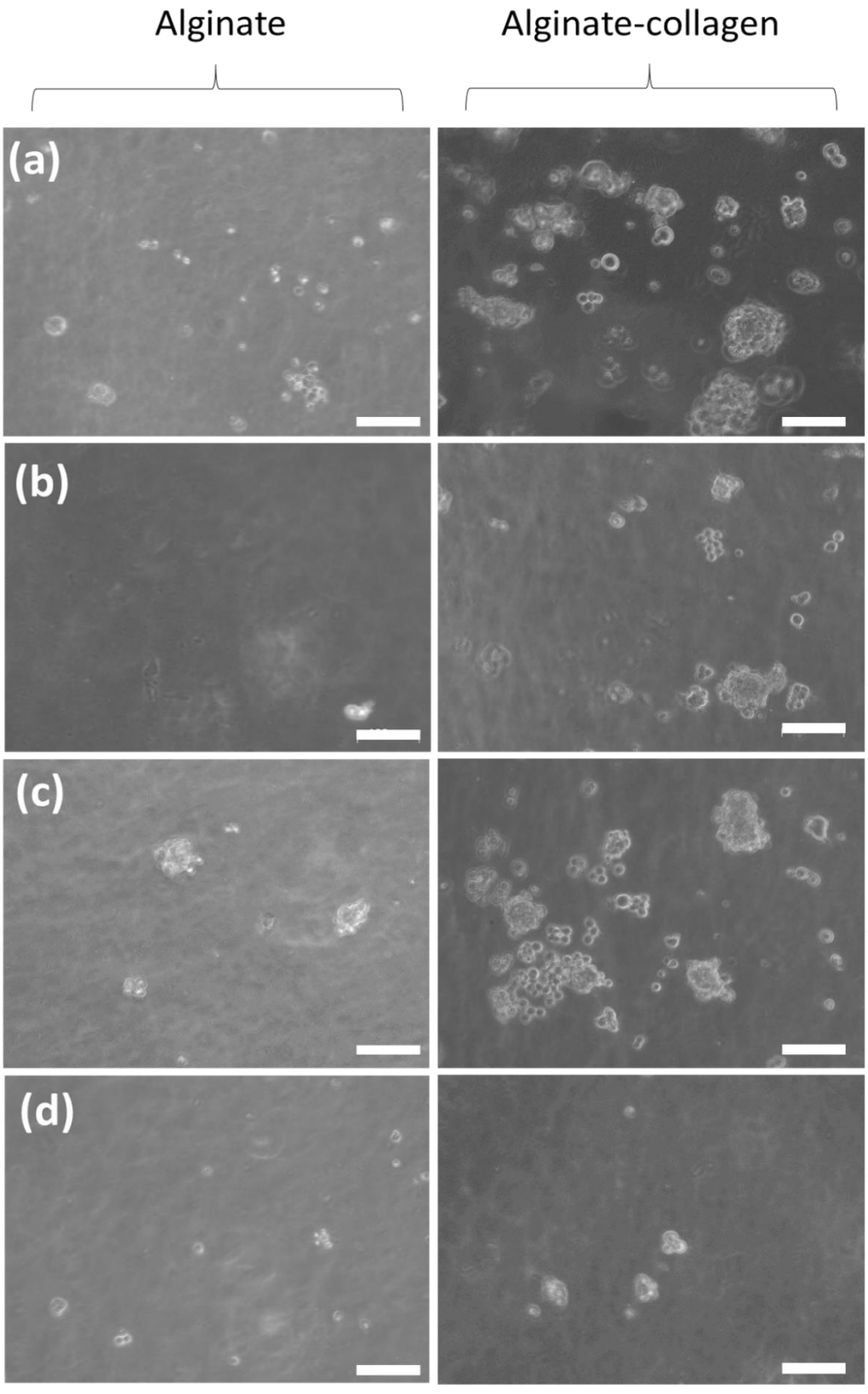

Figure 6.3 *– MDCKII cells seeded on (a) non sterile cross-linked alginate and alginate-collagen sheets and seeded cells on cross-linked alginate and alginate-collagen sterilised by (b) UV radiation, (c) chloroform and (d) autoclaving.*

Alginate sterilisation by chloroform resulted in better adhesion of the cells to the cross-linked alginate sheet and alginate-collagen sheets compared to the other sterilisation methods. However, the formation of clusters on top of the hydrogel sheet was not acceptable and a better morphology was required. A similar alginate sterilisation method as used previously in chapter 4 for bioprinting of U87-MG cells was therefore was used for further studies in this chapter due to the formation of tissue-like structures within the gel.

6.5 Fabrication of 3D hydrogel tubular structures encapsulated with MDCKII cells

Sodium alginate at 8% (w/v) and collagen type 1 from rat tail were used as scaffold biomaterials for this 3D biofabrication process. 100 mM $CaCl_2$ and 55 mM $BaCl_2$ (Product number 34290, $BaCl_2$, Sigma-Aldrich, Gillingham, UK) were used as the cross-linking reagents. Metal bars used for cell experiments were purchased from OK International and the metallic parts were extracted from the needles (TE718150PK, OK International). Sodium alginate 8% (w/v) was sterilised by Gamma radiation (IBL-637 CIS-BioINternational gamma irradiator, France) with 10 Gy at the rate of 1 Gy/min. 0.5 mL of MDCKII cells, at a concentration of 8×10^6 cells/ mL were suspended each with 1 mL of 8 % w/v sodium alginate solution, resulting in a 6 % w/v sodium alginate solution with a cell concentration of 2.67×10^6 cells/mL respectively. Similarly, 0.4 % (w/v) collagen solution was prepared containing 8 % (w/v) sodium alginate and sterilised by Gamma radiation with 10 Gy at the rate of 1 Gy/min. 0.5 mL of MDCKII cells with a concentration of 8×10^6 cells/mL were separately added, resulting in a 0.26 % (w/v) collagen and 6 % (w/v) sodium alginate solution at a cell concentration of 2.67×10^6 cells/mL. Stainless steel metal bars with a range of diameters were chosen as the mould for tubular structure fabrication due to their suitable wettability. . The metal bars were first kept in ethanol overnight to make them sterile. As shown in Figure 6.4, the mould was first dipped into a 6% (w/v) sodium alginate solution containing cells or dipped into collagen- alginate solution containing cells for about 3 seconds and then removed immediately. A thin layer of the cell-laden hydrogel was left coated on the surface of the metal bar. The coated surface of the metal bar was then dipped into the filtered cross-linking reagents (100 mM CaCl2 or 55mM BaCl2) for 2 minutes to cross-link the sodium alginate. The cross-linked cell-laden hydrogel was then gently pulled out by tweezers from one end of the metal bar mould, leaving a hollow tubular structure

of cross-linked cell-laden hydrogel. Cell-laden tubular hydrogel structures were fabricated using a metal bar with a 1.2 mm diameter.

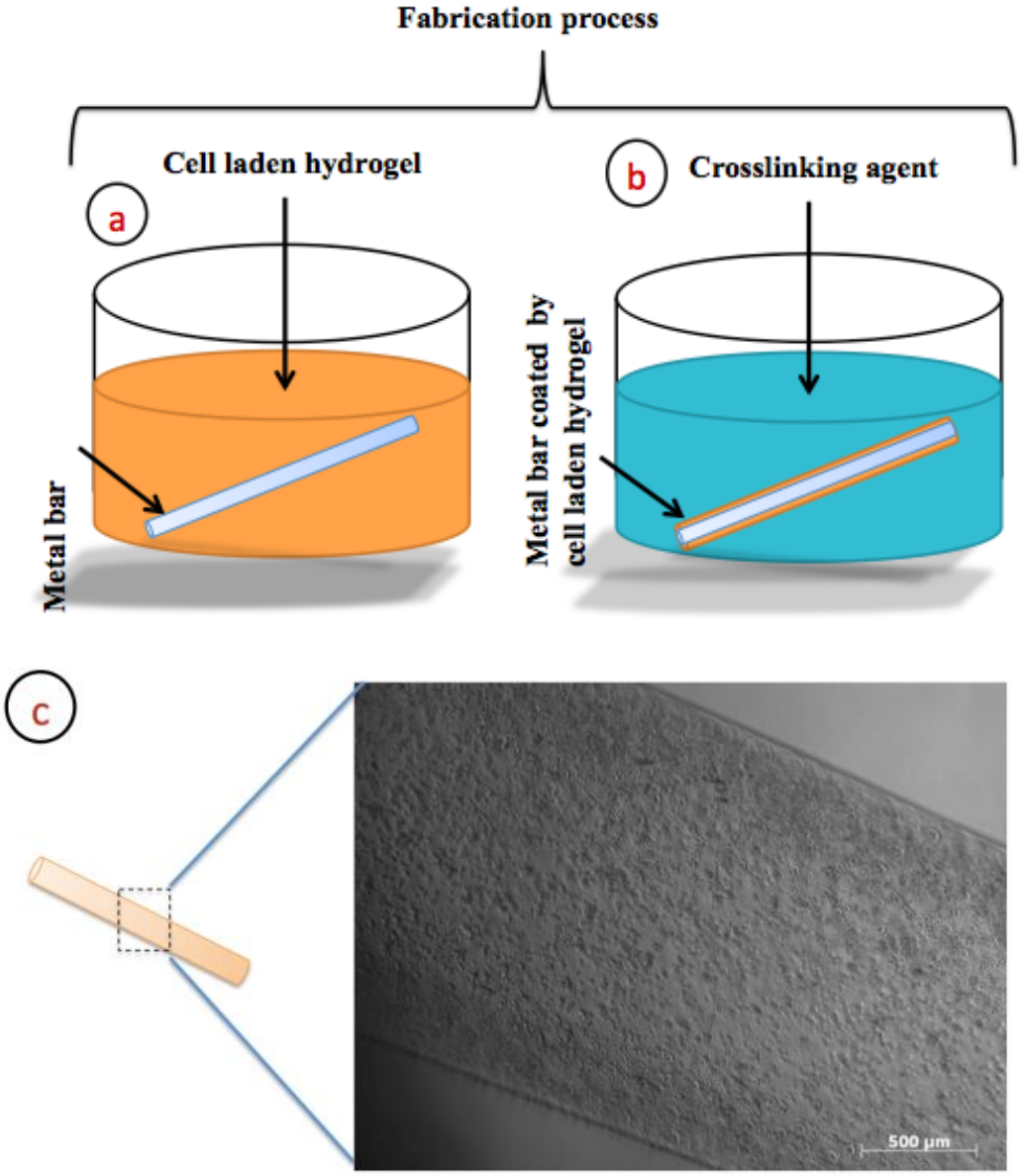

Figure 6.4 – *Schematic drawing of the alginate hydrogel tubular structure fabrication process, (a) a metal bar mould dipped in 6% (w/v) sodium alginate to coat the surface with a thin layer of cell-laden alginate hydrogel, followed by (b) the exposure to 55mM $BaCl_2$ or 100mM $CaCl_2$ to fully cross-link the sodium alginate layer for 2 minutes and (c) the cross-linked alginate layer is be pulled out from the mould as a hollow tube. (d) An optical image of a fabricated cell-laden alginate hydrogel tub. Scale bar: 500 µm.*

6.6 MDCK cell viability within the fabricated tubular structures

Fabricated cell-laden tubular structures under four different conditions were cultured for 5 days and viability of the cells was examined every day.

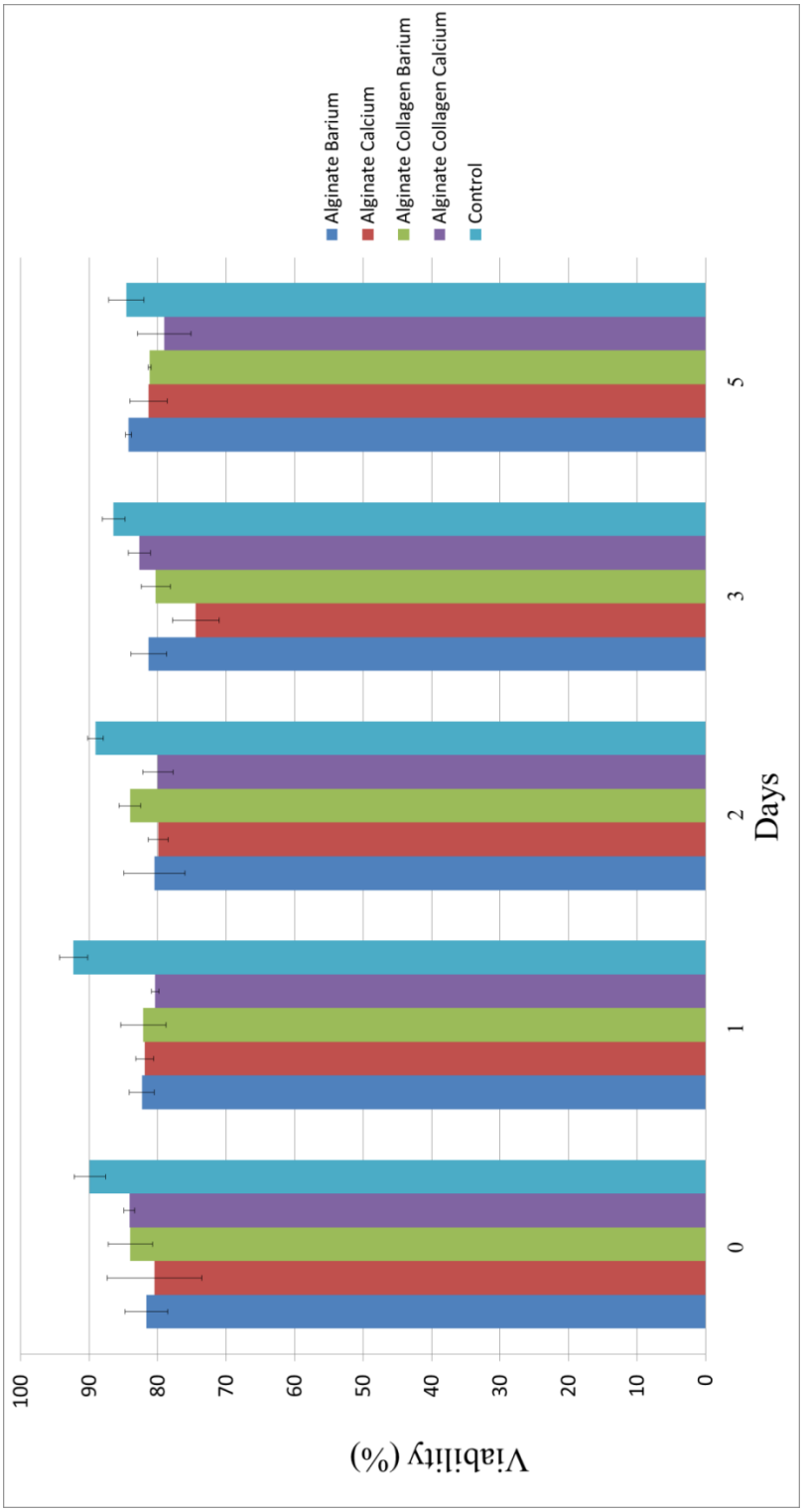

Figure 6.5 *— MDCKII cell viability within the tubular structures fabricated with the dip-coating approach under 4 different conditions from day 0 to day 5*

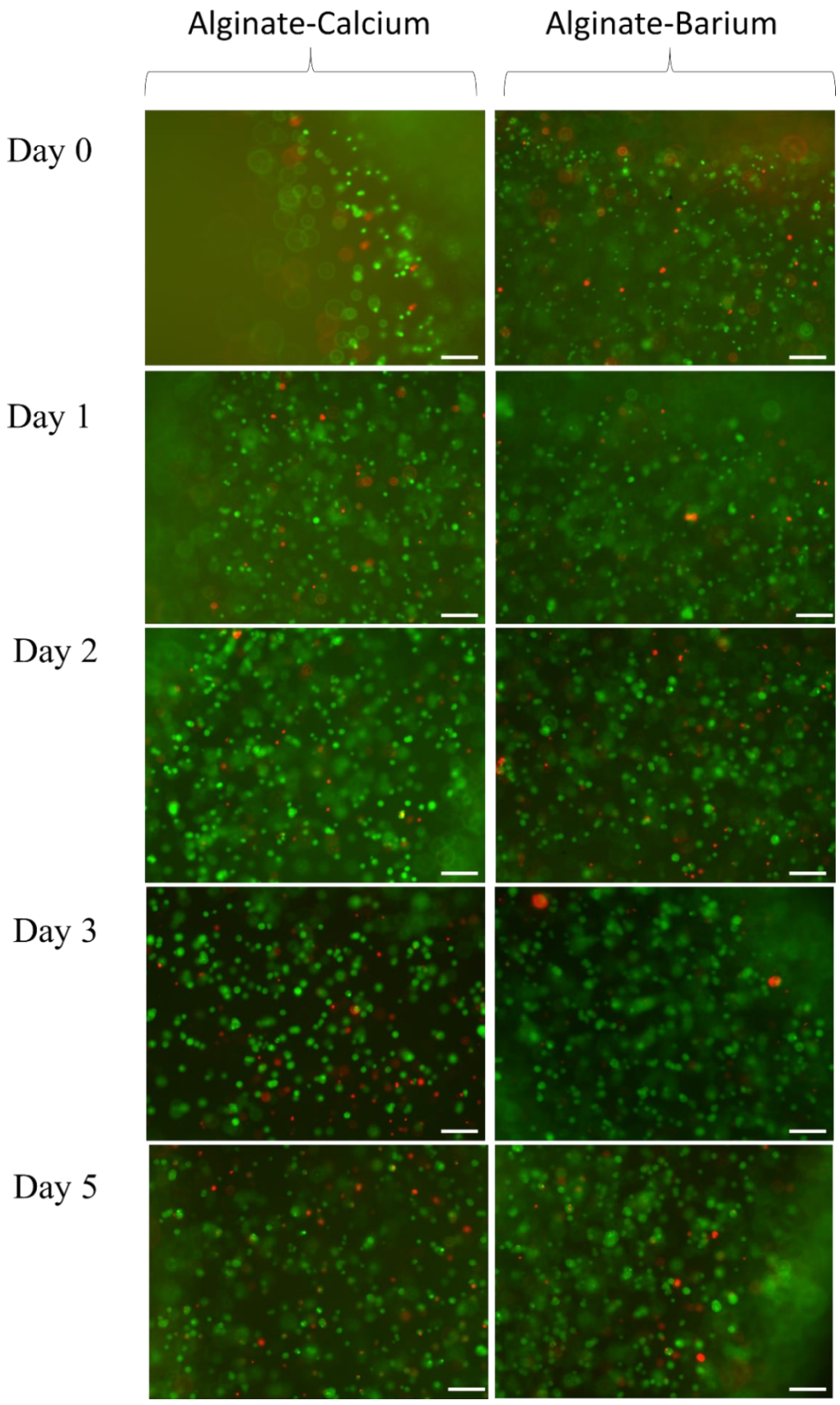

Figure 6.6 *– MDCKII cells cultured throughout 5 days within alginate hydrogel tube walls cross-linked by 100 mM $CaCl_2$ or 55 mM $BaCl_2$.Green stain indicates live cells and red stain indicates dead cells. Scale bar: 100 µm.*

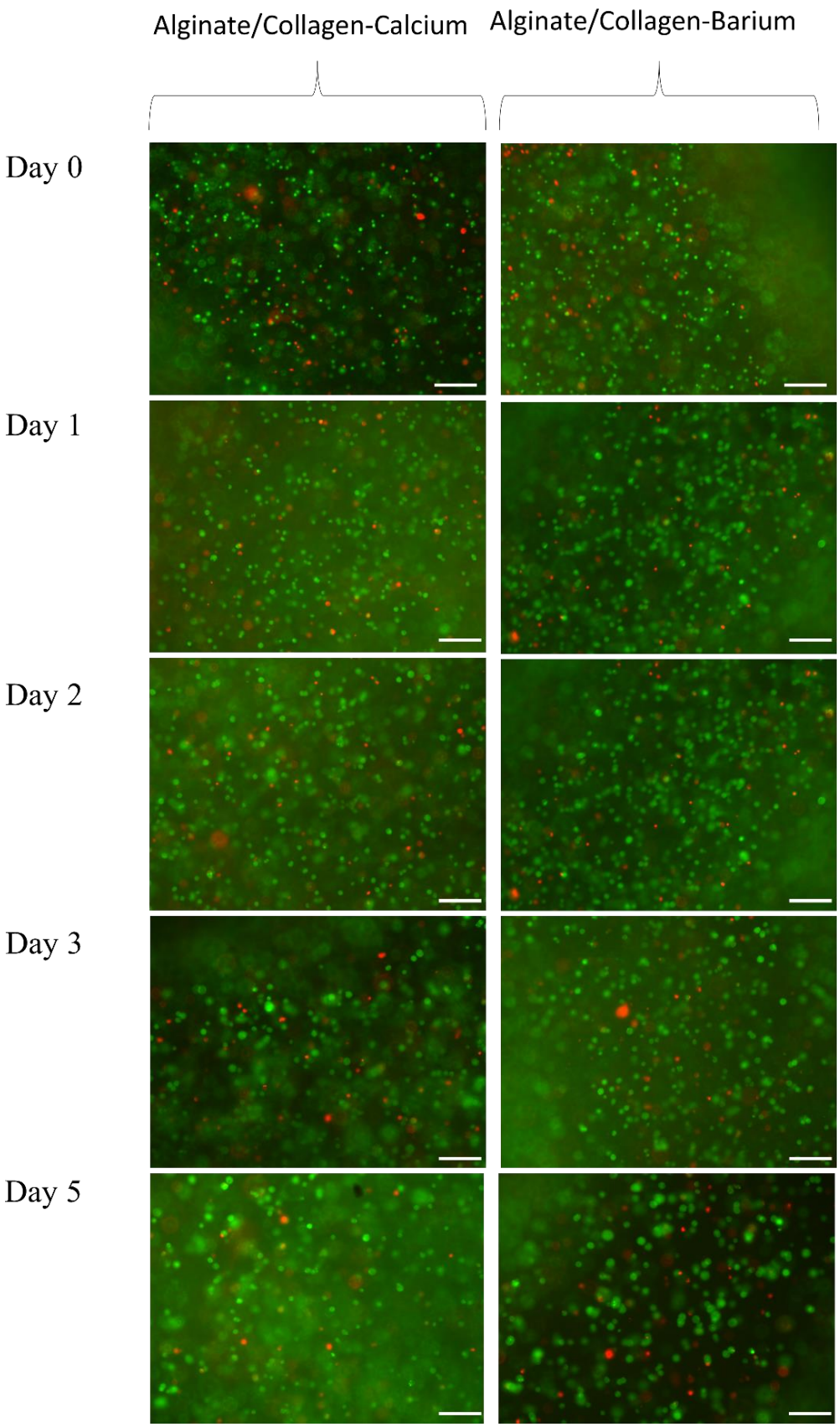

Figure 6.7 *– MDCKII cells cultured throughout 5 days within alginate-collagen hydrogel tube walls cross-linked by 100 mM* $CaCl_2$ *or 55 mM* $BaCl_2$*. Green stain indicates live cells and red stain indicates dead cells Scale bar: 100 µm.*

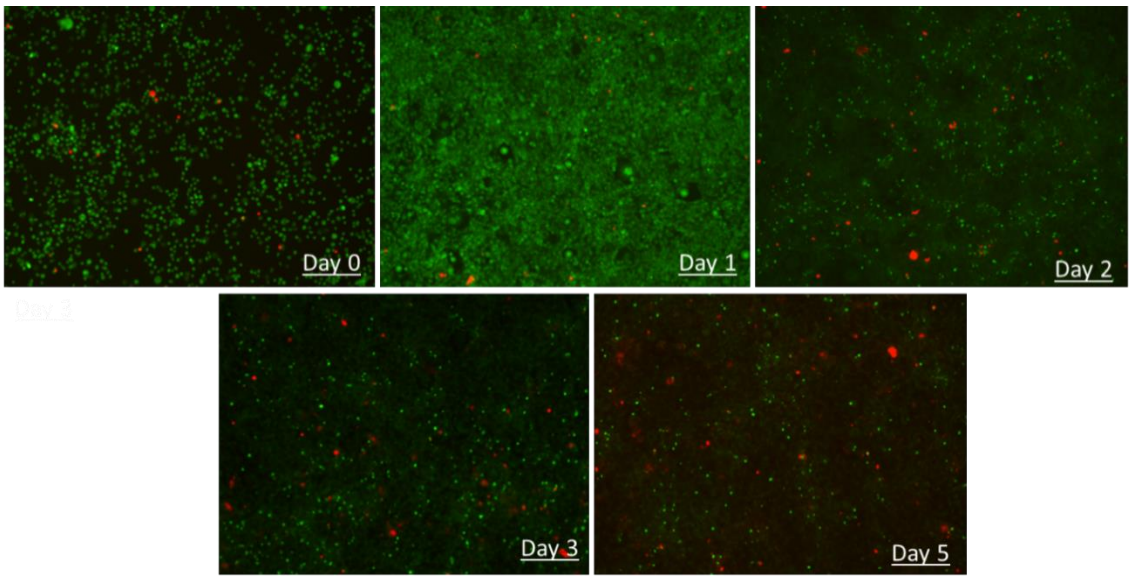

Figure 6.8 *– MDCKII cell culture throughout 5 days on a 6 well plate culture dish. Green stain indicates live cells and red stain indicates dead cells Scale bar: 100 µm*

The viability data were analysed using Image J, which suggested the cell survival rate within the tubular structures is generally above 80% for all four different fabrication conditions after the fabrication process. By comparing it with normal MDCKII cell culture, it appeared that the fabrication process is very gentle on cells and can sustain a high cell viability after fabrication. After 5 days of culture, MDCKII cells maintained cell viability of over 75% based on the four different fabrication conditions. Although the cell viability was lower than for the bioprinting approach in chapter 4, the viability relative to the control was high: above 90% for all days at all four different conditions.

6.7 Fabrication of 3D hydrogel tubes with mouse dermal embryonic fibroblast, viability assay and imaging

Sodium alginate at 8% (w/v) and collagen type 1 from rat tail were used as scaffold biomaterials for this 3D biofabrication process. 100 mM $CaCl_2$ and 55 mM $BaCl_2$ sterile solutions prepared in de-ionised water were used as the cross-linking reagents. Sodium alginate 8% (w/v) was sterilised by Gamma radiation with 10 Gy at the rate of 1 Gy/min. 0.5 mL of cells, at concentration of 8×10^6 cells/ mL were suspended each with 1 mL of 8 % (w/v) sodium alginate solution, resulting in a 6 % (v/w) sodium alginate solution with cell concentration of 2.67×10^6 cells/mL. Similarly, 0.4% (w/v) collagen solution was prepared containing 8% (w/v) sodium alginate and sterilised by

Gamma radiation with 10 Gy at the rate of 1 Gy/min. 0.5 mL of mouse dermal embryonic fibroblast cells with concentration of 8×10^6 cells/mL were separately added, resulting in a 0.26 % w/v collagen and 6 % w/v sodium alginate solution at a cell concentration of 2.67×10^6 cells/mL. 1.2 mm stainless steel metal bars were used for the fabrication process. Precisely same fabrication process was followed to produce the cell-laden tubular structures. The cell-laden tubular structures containing mouse embryonic dermal fibroblasts were cultured for 6 days. A LIVE/DEAD® Cell Vitality Assay Kit (L34951, Life Technologies) was used according to the manufacturer's protocol. The medium was briefly replaced with fresh medium containing 500 nM c_{12}-resazurin and 10 nM SYTOX Green before incubating at 37 °C, 5 % CO_2 for 15 minutes. The viability was assessed on day 1, 3, and 6. Confocal images of mouse embryonic dermal fibroblast cells were taken on a Nikon A1R FLIM confocal microscope. Z-Stacks (range of 176 µM, 5 µM steps) of each sample were captured using a Nikon A1R FLIM confocal microscope. Images were analysed using Imaris software to investigate the viability of the cells encapsulated within the tube walls fabricated by 1.2 mm mould over day 1, day 3 and day 6 of culture.

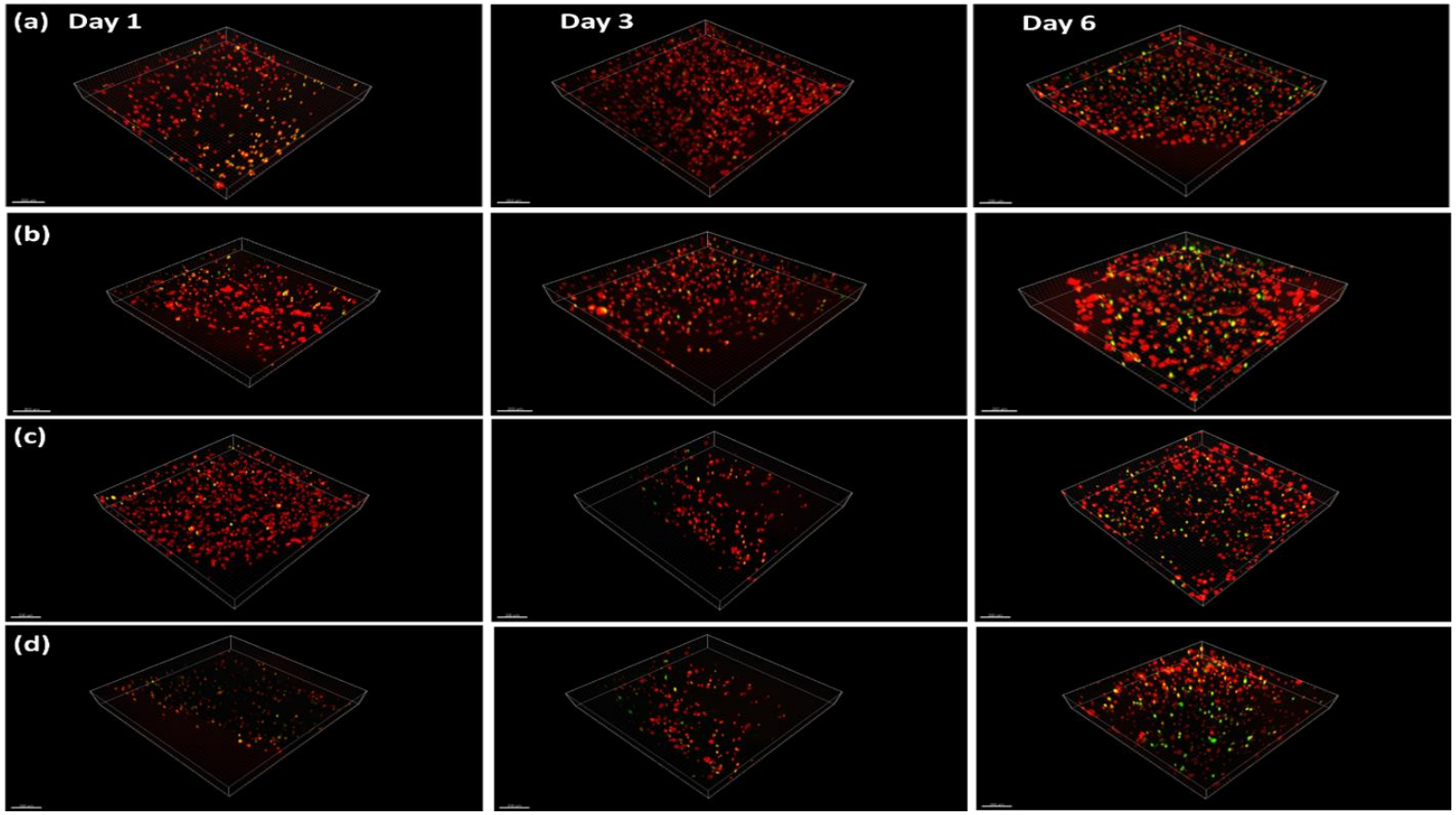

Figure 6.9 *– Mouse fibroblast cell lines cultured within the tube walls of (a) alginate hydrogel cross-linked by Calcium (b) alginate hydrogel cross-linked by barium (c) alginate-collagen cross-linked by calcium and (d) alginate-collagen cross-linked barium over 6 days. Red stain indicates live cells and green stain indicates dead cells. Scale bar: 100 µm.*

6.8 Cell viability in alginate and collagen-alginate hydrogel tubular structures

Tubular structures containing mouse dermal fibroblast cells were fabricated using the dip coating method by cell-laden alginate hydrogel cross-linked with 100 mM $CaCl_2$ or 55 mM $BaCl_2$ solution as well as cell-laden Alginate-Collagen hydrogel mixture cross-linked with 100 mM $CaCl_2$ or 55 mM $BaCl_2$ solution. Cell viability was monitored through 6 days of culture for each condition. The results suggested that the cells within alginate hydrogel tubes cross-linked with 55 mM $BaCl_2$ had the highest viability of 84 ± 2.4 % followed by collagen-alginate crosslinked by 55 mM $BaCl_2$ showing cell viability of 81 ± 7.4 %. Cell viability in alginate hydrogel cross-linked by $CaCl_2$ was 78 ± 3.1 % and alginate-collagen crosslinked by $CaCl_2$ was 72 ± 4.4% as shown in Figure 6.10. The results showed a good viability after 6 days of culture within the tubular structures for all conditions. However, the slight decrease in viability in collagen-alginate mixture cross-linked by 100 mM $CaCl_2$ and 55 mM $BaCl_2$ could be due to the lower PH level of the collagen, which created a harsher environment for the cells to survive in. By neutralising the collagen the cell viability might have been enhanced and better cell viability could be recorded. The ability to incorporate other biomaterials with alginate to fabricate tubular structures potentially allows for a better extracellular matrix to be created or an even harsher environment could be used for the cells depending upon the desired applications.

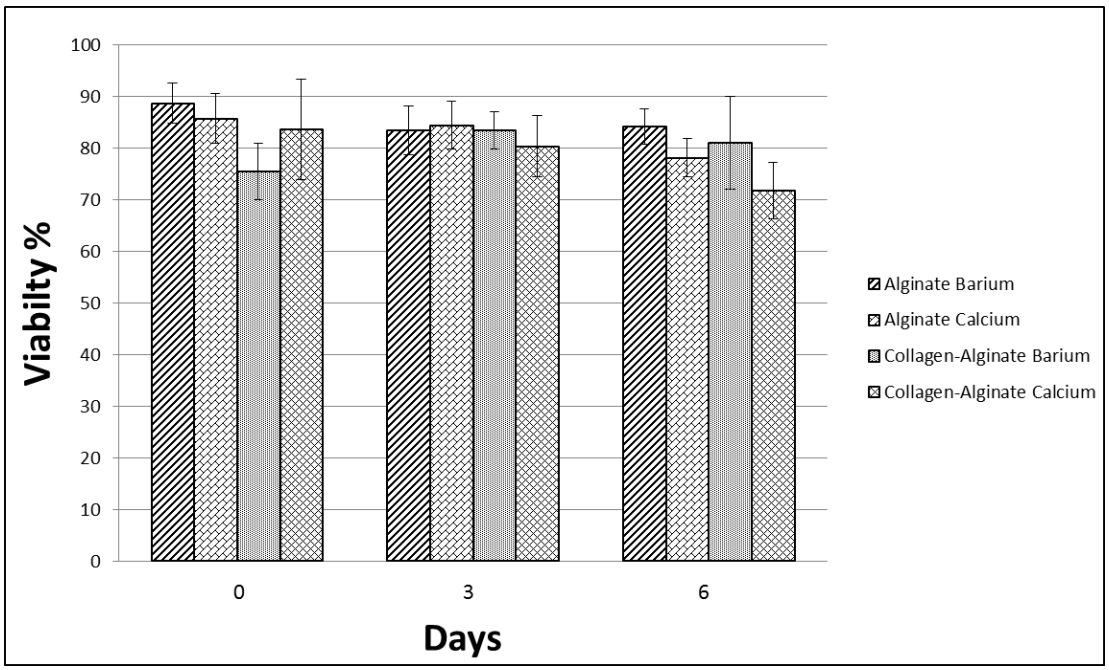

Figure 6.10 *– Viability of the mouse embryonic dermal fibroblast cells within the fabricated tube walls over 6 days of culture in two different bio-inks cross-linked by 100 mM $CaCl_2$ and 55 mM $BaCl_2$ for 2 minutes.*

6.9 3D cell growth in alginate and collagen-alginate hydrogel tubular structures

Confocal images of the mouse dermal fibroblast cells were taken for the four different conditions of fabrication at day 1, day 3 and day 6 as shown in Figure 6.9. Three random 300 µm × 300 µm × 50 µm areas within each tubular structure were selected to evaluate the cell number using Imaris software. The results shown in Figure 6.9 indicate that for all four conditions the cells had grown and proliferated in parts of the gel, which started the basis of cell to cell interaction and the formation of small clusters within the fabricated tube walls. The results showed that the fabricated gel had good permeability and porosity, allowing nutrients and oxygen to penetrate into the gel as well as allowing waste to be extracted from the gel. These optimum conditions created an extracellular matrix suitable for cell growth while supporting cell to cell interaction in some parts of the gel. Figure 6.11 summarises the cell density within the tubular structures fabricated in four different conditions throughout 6 days in culture. The cell density was considerably higher in alginate cross-linked with $BaCl_2$ and cell viability results also indicated the highest viability was achieved in alginate cross-linked with $BaCl_2$ over 6 days of culture.

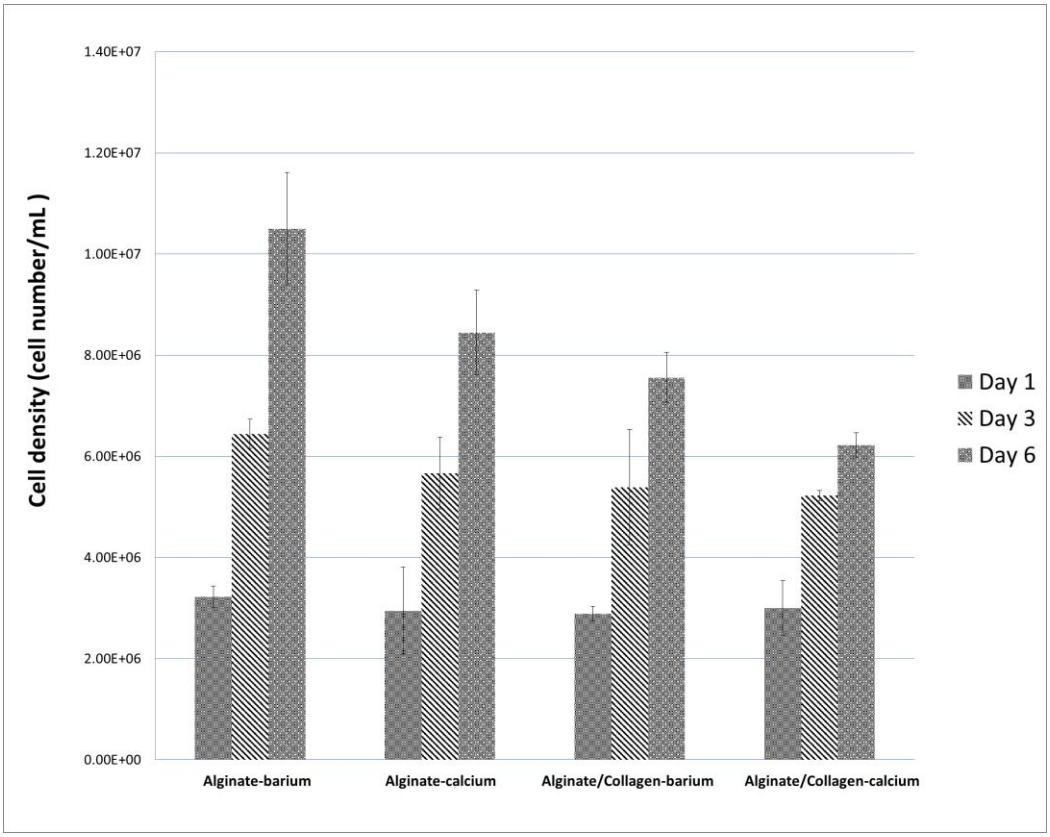

Figure 6.11— *Fibroblast cell density within the tubular structures fabricated by four different conditions at day 1, day 3 and day 6*

6.10 Fabrication of 3D hydrogel tubes with tHEk cells and inducing tHEk cells with tetracycline and imaging

Sodium alginate 8% (w/v) was sterilised by Gamma radiation with 10 Gy at the rate of 1 Gy/min. 0.5 mL of human embryonic kidney 293 cells containing a tetracycline responsive red fluorescence protein (tHEK), at a concentration of 8×10^6 cells/ mL was suspended with 1 mL of 8% (w/v) sodium alginate solution, resulting in a 6 % v/w sodium alginate solution with a cell concentration of 2.67×10^6 cells/ mL. Similarly, 0.4 % (w/v) collagen solution was prepared containing 8% (w/v) sodium alginate and was sterilised by Gamma radiation with 10 Gy at the rate of 1 Gy/min. 0.5 mL of tHEK cells with a concentration of 8×10^6 cells/mL were separately added, resulting in a 0.26% (w/v) collagen and 6% (w/v) sodium alginate solution at a cell concentration of 2.67×10^6 cells/mL. Tubular structures containing tHEK cells within the tube walls were fabricated using 1.2 mm rods as per the fabrication protocol and incubated for 24 hrs. The medium was then replaced with fresh medium containing tetracycline at a concentration of 1 µg/mL. The structures were then incubated for a further 48 hrs. Images of the induced tHEK cells were captured after 72 hours using a Zeiss Axiovert Immunofluorescence microscope.

6.11 Responsiveness of cells to small molecules

To validate whether the walls of the tube allow cells to access small signalling molecules and whether they show normal gene expression responses to these, a tHEK cell line that activates expression of Red Fluorescent Protein (RFP) in response to tetracycline was used [1-3]. The tHEK cells were cultured for 24 hrs within the fabricated tube walls, again made using the four methods of tube manufacture (with and without collagen, and using either $CaCl_2$ or $BaCl_2$ to cross-link). The cells were then cultured for a further 48 hrs in the presence or absence of tetracycline. Cells cultured with no tetracycline could be detected but showed no red fluorescence (Figure 6.12a, c, e, g and i). Cells exposed to tetracycline showed a robust induction of RFP expression in all four conditions (Figure 6.12b, d, f, h and j).

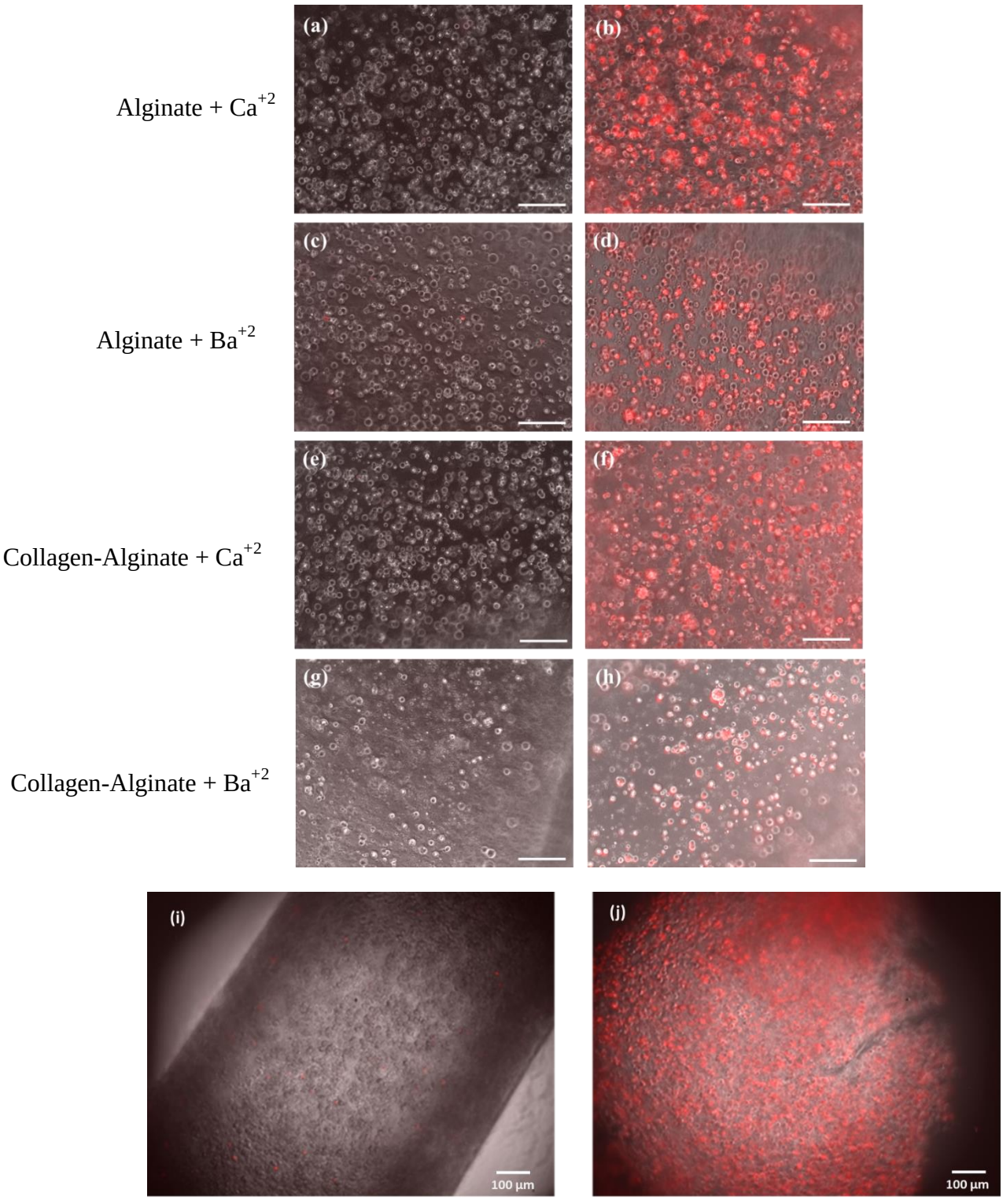

Figure 6.12 *– Responsiveness of cells in the wall to small signalling molecules. (a,c,e and g) show tHEK cells cultured in tubes made from, and cross-linked by, the reagents indicated, but not exposed to tetracycline. (b,d,f and h)_show tHEK cells in tubes made the same way but then exposed to tetracycline for 72h. Red fluorescent protein is robustly induced. (i) and (j) show low-magnification images of the tubes containing cells before and after induction with tetracycline .*

6.12 Incorporation of gelatine to increase cell attachment of MDCKII cells

Gelatine (gelatine from porcine skin, Sigma-Aldrich, Gillingham, UK) was introduced to further investigate whether this would improve the attachment of the cells to the biomaterial [4-9]. Alginate, gelatine and alginate-gelatine solutions were coated onto a 12 well plate. The alginate used in this study was at a concentration of 6% (w/v) and was cross-linked with 55 mM of $BaCl_2$ for 2 minutes. The gelatine coated onto the well plate had a concentration of 6% (w/v) and was kept for 30 minutes to solidify. The gelatine-alginate coated composition with a final gelatine concentration of 6% (w/v) was cross-linked with 55 mM $BaCl_2$. The coated well plates were then sterilised by gamma radiation with 20 Gy at the rate of 2 Gy/min. 1 mL of MDCKII cells in medium with a cell concentration of 0.3×10^6 cells/mL was added to each well plate and cultured for 2 days in the incubator at 37 °C. Images of MDCKII cells on the alginate, gelatine, and alginate-gelatine compositions were taken at day 1 and day 2 of culture.

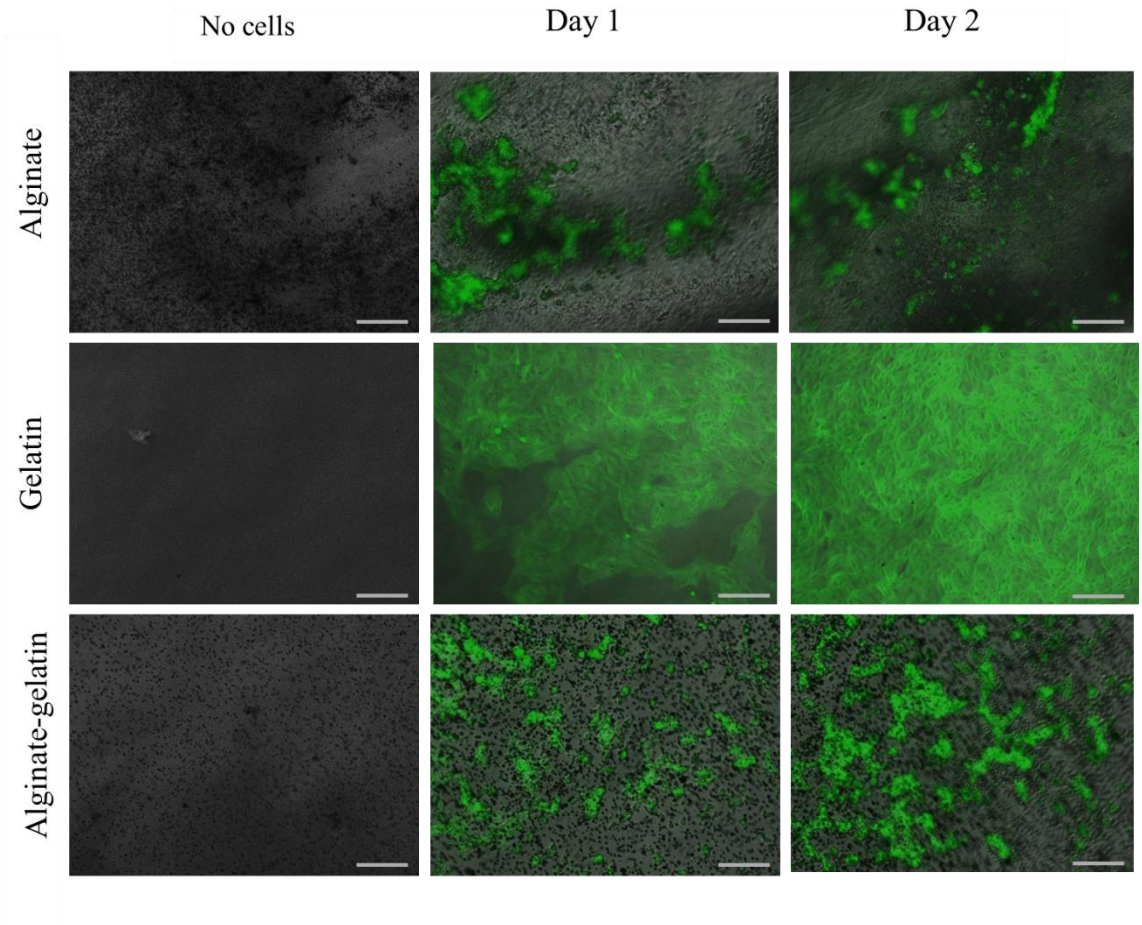

Figure 6.13 *– MDCKII cells cultured on alginate, gelatin and alginate-gelatin composition 2D sheets for two days. Scale bar: 100 µm.*

As shown in Figure 6.13, MDCK cells cultured for two days on cross-linked alginate sheets did not show a suitable morphology on day 1 and day 2, as cells formed clusters on top of the cross-linked alginate sheets. On the other hand, cells did form a suitable morphology on solidified gelatine sheets at day 1 and kept the same morphology at day 2. Cells on cross-linked alginate-gelatine sheets showed better morphology compared to the alginate sheets, but not better than the gelatine sheets at day 1. At day 2 of culture, cells showed better morphology on alginate-gelatine compared to day 1.

6.13 Incorporation of gelatine to enhance cell attachment of mouse dermal embryonic fibroblast

To confirm the previous morphology experiments on MDCKII cells, mouse dermal embryonic fibroblast cells were tested and similarly added on alginate, alginate-gelatine and gelatine 2D sheets at 1 mL with a cell concentration of 300,000 cells/mL. Cells were cultured for two days at 37 °C in the incubator and were imaged on day 1 and day 2.

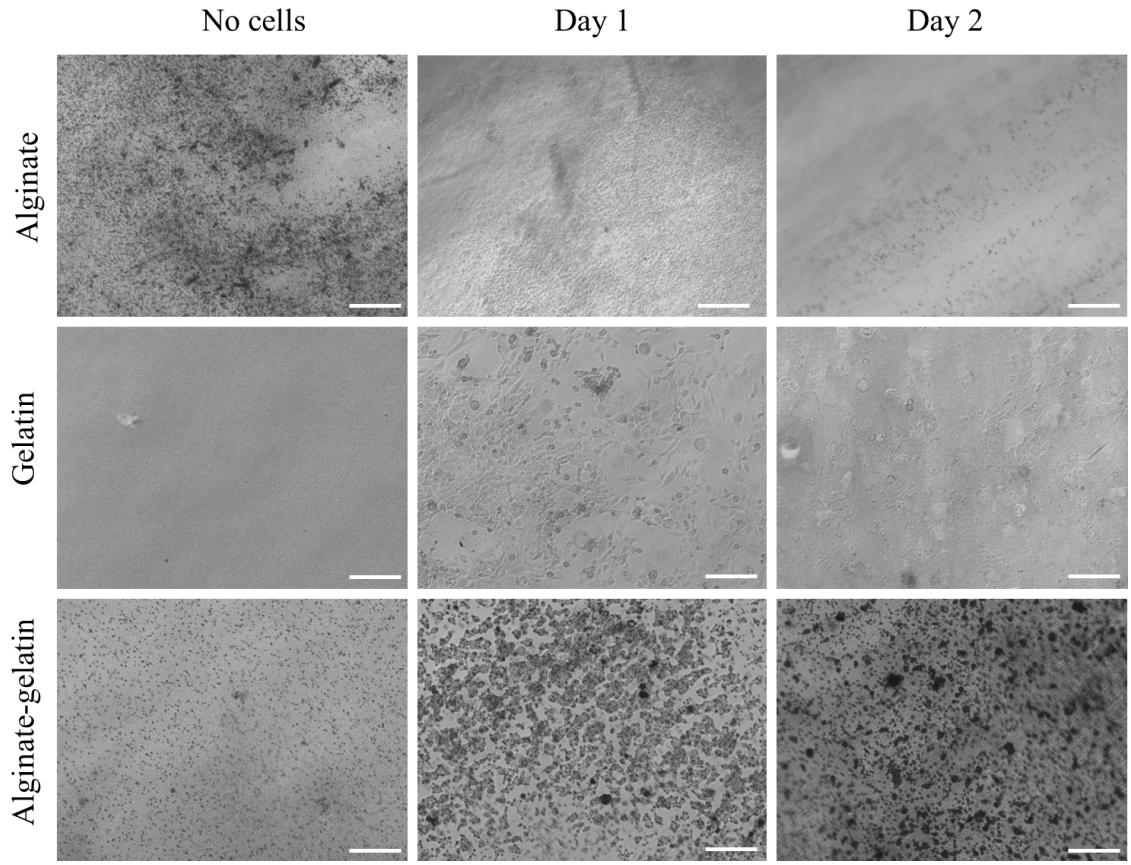

Figure 6.14 *– Mouse dermal embryonic fibroblast cells cultured on alginate, gelatine and alginate-gelatine composition 2D sheets for two days.*

Similar to MDCKII cells, mouse dermal embryonic fibroblast cells showed the better morphology at day 1 and day 2 when cultured on gelatine. Cells did not form a suitable morphology on cross-linked alginate sheets at day 1 and 2, and cells showed a much better morphology on cross-linked alginate-gelatine sheets compared to cross-linked alginate sheets. The results indicated the tubular fabrication method is potentially capable of keeping the cells alive within the tubular structures. By fine tuning the biomaterial, other cell types could potentially form a monolayer on either the inner or the outer surface of the tubular structures.

6.14 U87-MG and mouse fibroblast cells seeding on alginate-gelatine tubular structures

To further investigate the attachment of cells from 2D to 3D, alginate–gelatine tubular structures were fabricated. 6% (w/v) gelatine solution was prepared in de-ionised water

at 37 °C and sodium alginate powder was added to the gelatine solution. This was mixed, resulting in a final concentration of 6% (w/v) gelatine w/v and 6% (w/v) sodium alginate. A metal bar with a 4 mm diameter was used to fabricate tubular structures using the dip-coating approach at 37 °C. Tubular structures were cross-linked in 55 mM $BaCl_2$ for 2 minutes. To sterilise the tubular structures, they were kept in ethanol overnight. U87-MG cells and mouse fibroblast cells introduced to the tubular structures at a concentration of 0.3×10^6 cells/mL and were cultured in the incubator at 37 °C and 5% CO_2 for 6 days. Images of the U87-MG cells and mouse fibroblast cells seeded inside the tubular structures were taken on day 0, 1, 4 and 6.

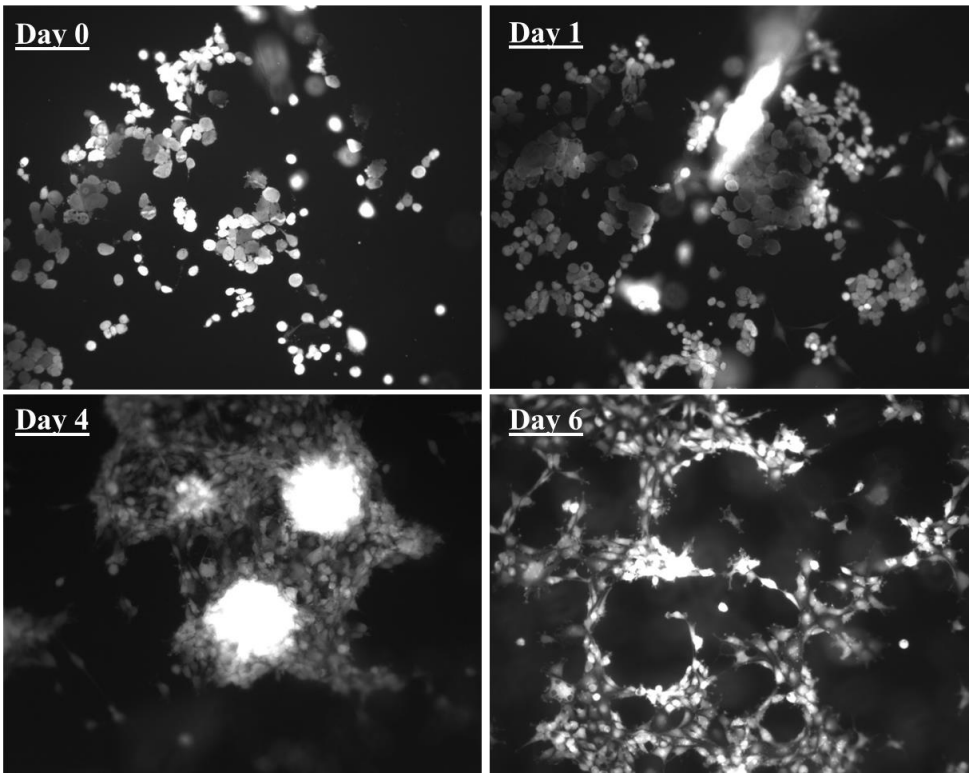

Figure 6.15 *– U87-MG cells seeded inside alginate-gelatine tubular structures and cultured for 6 days.*

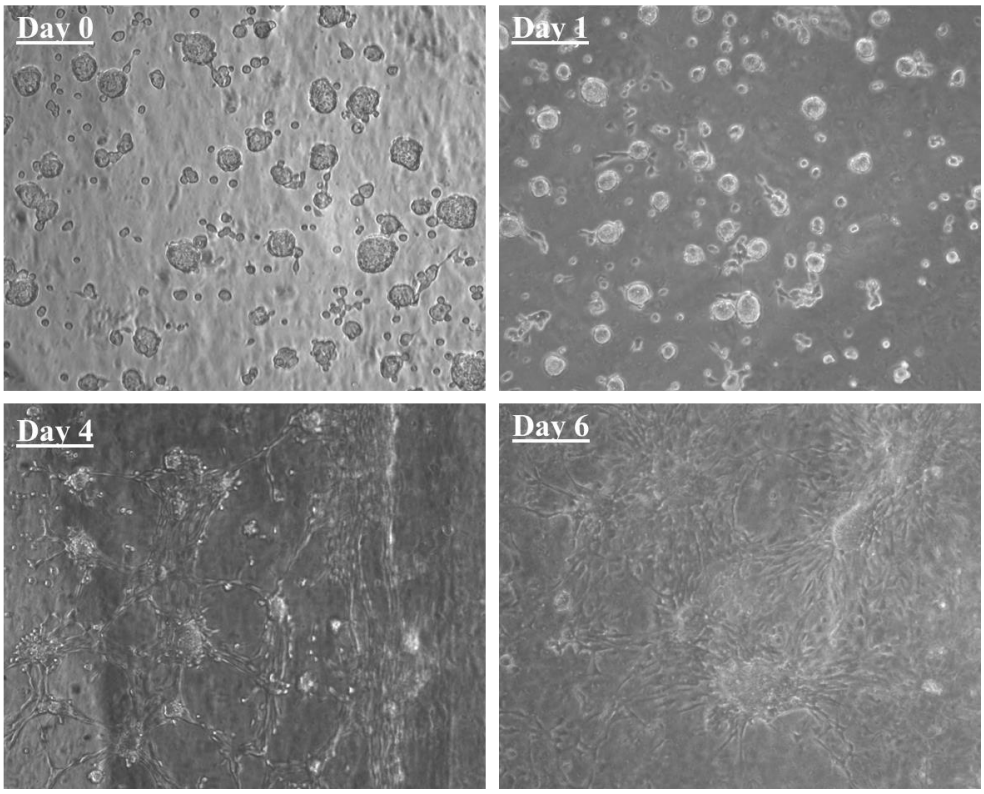

Figure 6.16 *– Mouse fibroblast cells seeded inside alginate-gelatine tubular structures and cultured for 6 days.*

U87-MG cells, as shown in Figure 6.15, were attached to the inside of the alginate-gelatine tubular structures at day 0, but the cells did not have a good morphology. At day 1 the cells had started to grow and form colonies on the surface of the tubular structures, and the clusters grew larger at day 4 but the morphology was still poor. However, at day 6 cells started to form normal morphology inside the tubular structures and cell clusters were not visible anymore.

Seeded fibroblast cells inside the alginate–gelatine tubular structures as shown in Figure 6.16 formed small cell clusters at day 0 and day 1 and normal morphology was not visible. At day 4 these small clusters had started to interact with each other to form a better morphology on the surface of the tubular structures. At day 6, there were no more clusters visible inside the tubular structures and normal cell morphology is noticeable.

6.15 Addition of gelatine nanofibres and micro-carriers to enhance cell attachment

To increase cell attachment within the tubular structures, gelatine nanofibres and microcarriers were introduced. 1 mL of gamma-sterilised 8% (w/v) sodium alginate was

mixed with 0.1 g of sieved gelatine nanofibres (beads smaller than 100 µm) fabricated in accordance with the protocol [10], 0.1 g of non-sieved gelatine numbers (beads greater than 100 µm), 0.1 g of microcarriers and 0.05 g of microcarriers with 0.5 g of non-sieved microcarriers. The compositions were mixed with 0.5 mL of U87-MG cells in a culture medium with a concentration of 10×10^6 cells/mL, resulting in an approximately 6% (w/v) alginate with 10% (w/v) of the support matrix having a cell concentration of 3.67×10^6 cells/mL. Tubular structures were fabricated with the dip-coating approach with a 1.2 mm mould bar cross-linked by 55 mM $BaCl_2$ and cultured for 2 days in the incubator at 37° C and 5.0% CO_2.

6.15.1 Gelatine nanofibre fabrication to enhance cell attachment

10 g of gelatine powder (gelatine from porcine skin, product code 10011968154, Sigma Aldrich UK) was mixed with 20 mL of de-ionised water. 40 mL of acetic acid was added to the water-gelatine solution and was gently stirred for 5 minutes. 32 mL of ethyl acetate was added to the solution and stirred gently for 5 another minutes. The final solution was then incubated for 12 hrs at 37 °C.

Once incubated for 12 hours 3 mL of the water-acid based gelatine solution was loaded into a 5 ml syringe and electro spun for 24 hrs at 0.06 ml/hr by 12.5 kV/8 cm with a 500 µm tip.

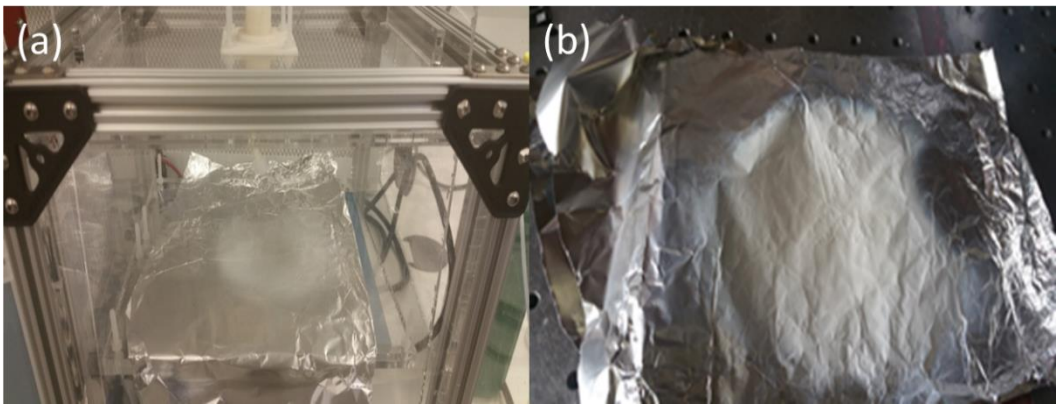

Figure 6.17 *– (a) water-acid based gelatine solution after 4 hrs and (b) after 24 hrs of electrospinning*

The fabricated fibrenanofibres then were removed from the top of aluminium foil and ground using an electric grinder and sieved with 100 µm sieve in order to produce small beads of fibrenanofibres. Fabricated nanofibres had diameters ranging from 50 nm to

250 nm. Once the nanofibres were ground, a 100 µm sieve was used to separate the beads that are smaller than 100 µm.

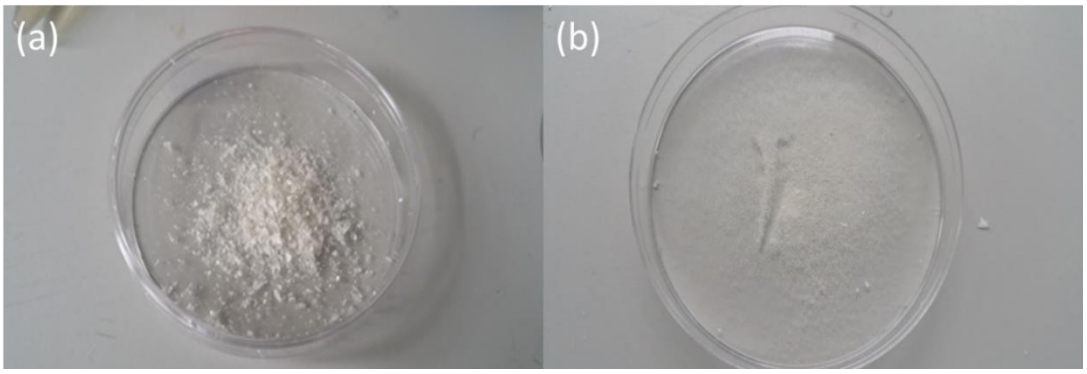

Figure 6.18 *– (a) water-acid based gelatine solution after 4 hrs and (b) after 24 hrs of electrospinning*

Samples were taken from electrospun gelatine nanofibres, transferred to the gold sputter coating instrument and vacuumed before SEM examination. Vacuumed sputter coating was performed at 2.5 kV and 20 mA for 45 seconds, resulting in gold layers on the samples a few nanometre thick. Sputter coated samples then were taken to SEM for imaging. Images were taken at 5 kV with magnifications of 3000, 5000, 20000 and 50000 as shown in Figure 6.19.

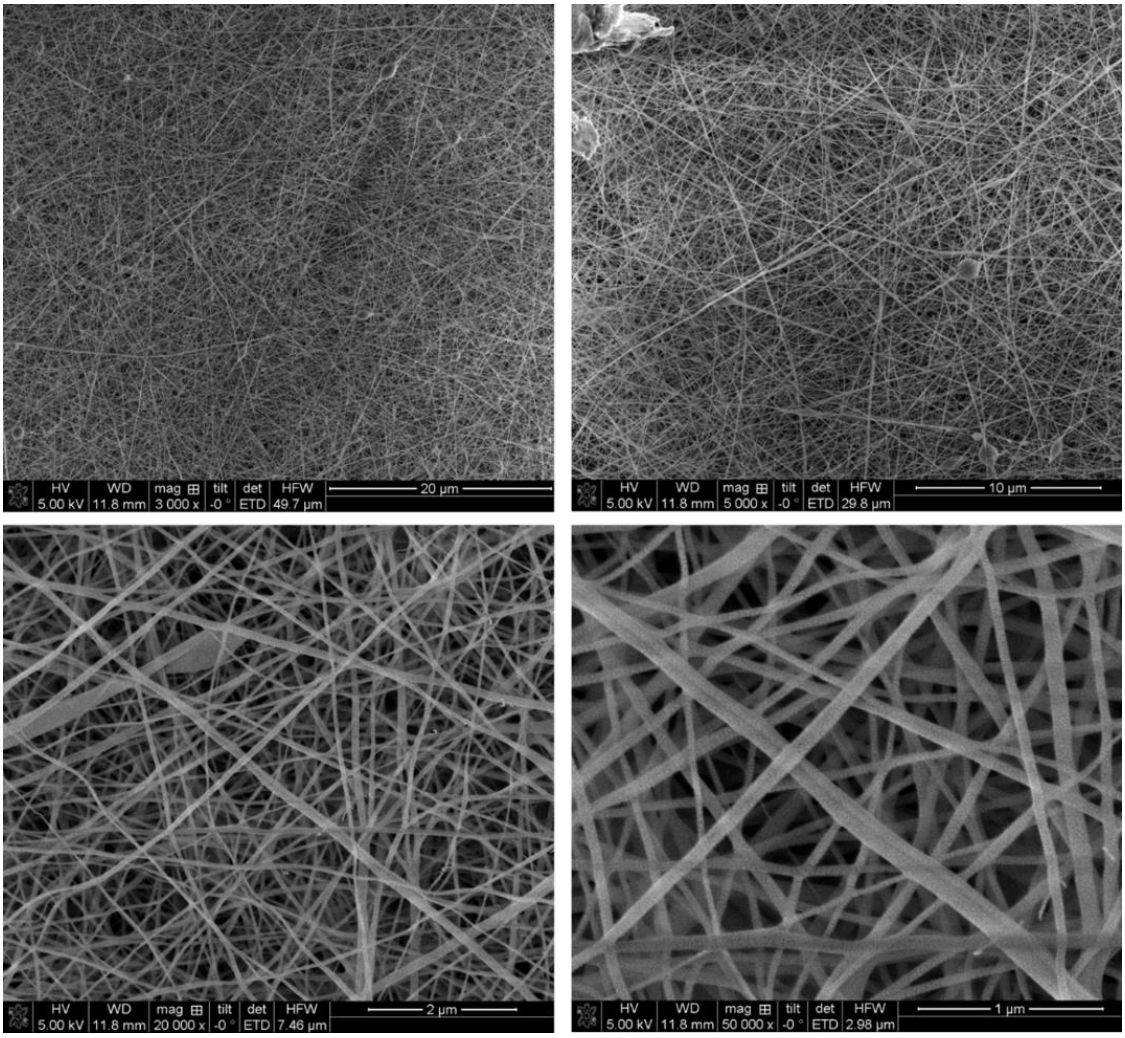

Figure 6.19— *SEM images of gelatine nanofibres taken at 5 KV with 3000, 5000, 20000 and 50000 magnifications.*

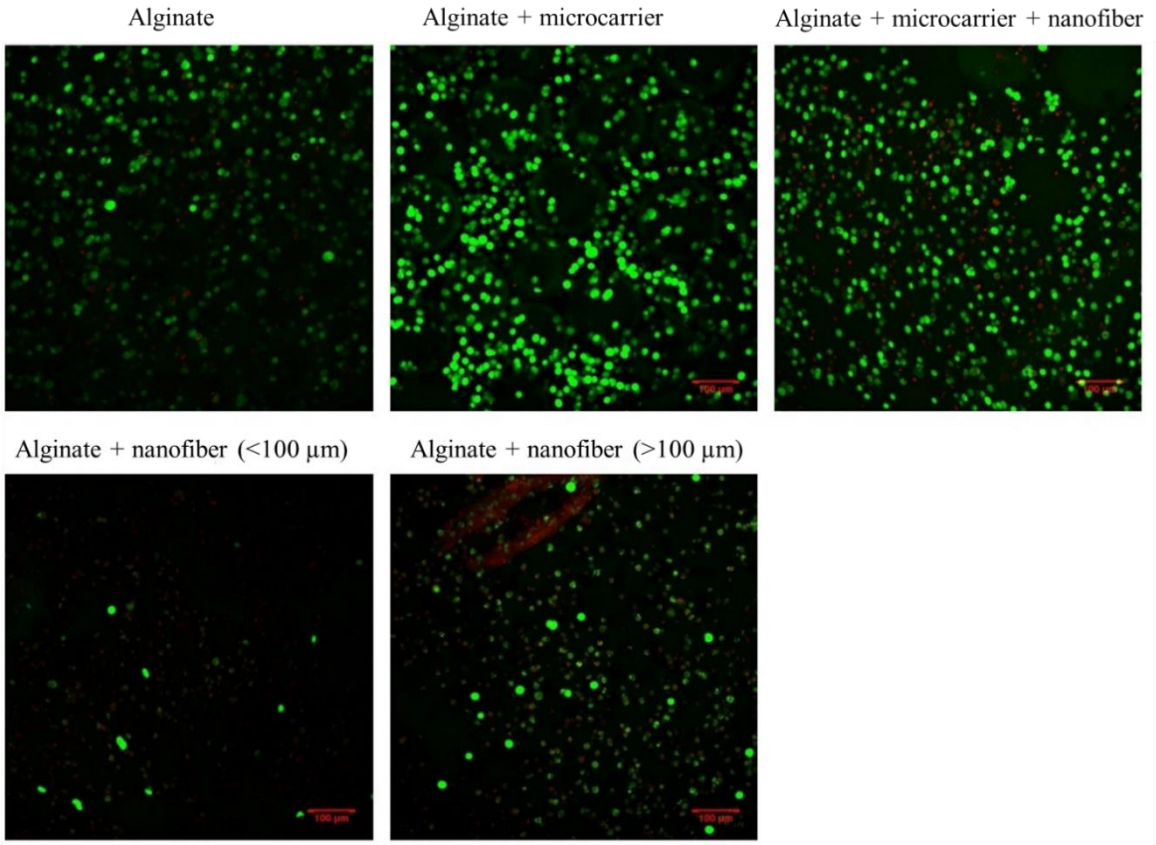

Figure 6.20 *– U87-MG cells encapsulated within tubular structures fabricated using the dip-coating approach. The bio-ink compositions were; alginate, alginate-microcarrier, alginate-microcarrier-nanofibre, alginate-nanofibre (beads smaller than 100 µm) and alginate-nanofibre (beads greater than 100 µm).*

The addition of gelatine nanofibres to alginate resulted in a very low cell viability. This could be due to the possible existence of acid residues within the gelatine nanofibres, which is harmful to cells. On the other hand, the addition of microcarriers to alginate improved the cell attachment compared to the alginate only and alginate-gelatine nanofibre-microcarrier compositions.

6.16 Acknowledgments

This chapter was completed in collaboration with Christopher G. Mills, Jamie A. Davis and John J. Mullins from Edinburgh University. Human embryonic kidney 293 cells containing a tetracycline responsive red fluorescence protein, Mouse Dermal Fibroblast cells, and Madin-Darby canine kidney cells were provided by them. Cell culture and imaging were performed by Christopher G. Mills at Edinburgh University. Miguel A.

Hermida and Nicholas R. Leslie from Heriot Watt University provided U87-MG cells and Human Fibroblast cells including culture and imaging.

6.17 Conclusions

In this chapter biological studies were carried out based on the dip-coating approach. This approach could incorporate other bio-materials within the alginate hydrogel to help cell biologists to bypass the lengthy, complicated and expensive fabrication approaches and integrate the dip-coating method to fabricate 3D tubular structures with living cells in their preferred extracellular matrix. The fabrication method was gentle on live cells while maintaining high cell viability over 6 days within the tubular structures. This provided a platform for cells to freely interact with small molecules such as the tetracycline used as a demonstration here. By introducing other biomaterials cooperated with alginate it was possible to enhance the cell attachment within the tubular structures as well as the capability to form cell monolayers on the inner or outer surface of the tubular structures.

This method shows promising potential for fabricating tubular structures that are better models of anatomy than 2D cultures. These may be suitable for a range of tubular tissues including embryonic kidney, lymph vessels, blood vessels, trachea, and intestine.

Chapter 6 references

[1 Wong, H.-L., M.-X. Wang, P.-T. Cheung, K.-M. Yao and B. P. Chan (2007). "A 3D collagen microsphere culture system for GDNF-secreting HEK293 cells with enhanced protein productivity." Biomaterials 28(35): 5369-5380.

[2] Cachat, E., Liu, W., Martin, K. C., Yuan, X., Yin, H., Hohenstein, P., & Davies, J. A. (2016). 2- and 3-dimensional synthetic large-scale *de novo* patterning by mammalian cells through phase separation. *Scientific Reports*, *6*, 20664.

[3] Ouyang L, Yao R, Chen X, Na J and Sun W (2015) 3D printing of HEK 293FT cell-laden hydrogel into macroporous constructs with high cell viability and normal biological functions *Biofabrication* **7**015010

[4] Yang, C., Frei, H., Rossi, F. M. and Burt, H. M. (2009), The differential *in vitro* and *in vivo* responses of bone marrow stromal cells on novel porous gelatin–alginate scaffolds. J Tissue Eng Regen Med, 3: 601–614

[5] Sarker B, Singh R, Silva R, Roether JA, Kaschta J, Detsch R, et al. (2014) Evaluation of Fibroblasts Adhesion and Proliferation on Alginate-Gelatin Crosslinked Hydrogel. PLoS ONE 9(9): e107952.

[6] Rosellini E, Cristallini C, Barbani N, Vozzi G, Giusti P (2009) Preparation and characterization of alginate/gelatin blend films for cardiac tissue engineering. J Biomed Mater Res A 91: 447–453

[7] Nguyen T-P, Lee B-T (2012) Fabrication of oxidized alginate-gelatin-BCP hydrogels and evaluation of the microstructure, material properties and biocompatibility for bone tissue regeneration. J Biomater Appl 27: 311–32

[8] Tobias, Z., Bapi, S., Aldo, R. B., & Rainer, D. (2015). Evaluation of an alginate–gelatine crosslinked hydrogel for bioplotting. Biofabrication, 7(2), 025001.

[9] Sarker, B., Rompf, J., Silva, R., Lang, N., Detsch, R., Kaschta, J., . . . Boccaccini, A. R. (2015). Alginate-based hydrogels with improved adhesive properties for cell encapsulation. International Journal of Biological Macromolecules, 78, 72-78. doi: http://dx.doi.org/10.1016/j.ijbiomac.2015.03.061

[10] Song, J.-H., H.-E. Kim and H.-W. Kim (2008). "Production of electrospun gelatin nanofibre by water-based co-solvent approach." Journal of Materials Science: Materials in Medicine 19(1): 95-102.

Chapter 7 - Conclusions and future work

In this thesis, two different approaches were developed for the 3D biofabrication of complex cell-laden hydrogel structures with sodium alginate as the main hydrogel. The first approach involved a novel extrusion-based bioprinting approach where cell-laden alginate hydrogel structures were bioprinted through a three step alginate hydrogel cross-linking process (primary, secondary and tertiary). This was done through use of $CaCl_2$ and $BaCl_2$ providing a novel 3D bioprinting platform to deliver a sufficiently viscous alginate bio-ink for printability whilst minimising the shear stress applied to the cells during the printing process. The three-step cross-linking process not only led to robust and stable structures of the cross-linked alginate but also exhibited suitable controllability over its degradation time. This allowed cells to stay viable, proliferate and grow to form their own extracellular matrix within the hydrogel after 9 days. Co-printing of two different alginate hydrogels was also demonstrated, indicating the ability to co-print two different cell types. The summary of this work is shown in figure 7.1.

The other method for the biofabrication of complex cell-laden alginate hydrogel was the micro dip-coating approach. This created a very simple, rapid and straight-forward platform with the ability to incorporate other biomaterials to create a suitable environment for desired applications. Tubular structures were fabricated by this method and it was possible to control the thickness of tubular structures by adjusting the alginate hydrogel concentration. This method is capable of producing ultrafine tube diameters down to 100 µm, as well as multi-layered alginate hydrogel tubular structures. Different cell types were used to create tubular structures and viability results showed this approach is gentle on cells, allowing them to proliferate, grow and function. Swapping the solid metal bar mould for a bio-compatible 3D printed dissolvable mould allowed real size complex hollow organ structures such as a stomach and branched structures to be rapidly fabricated. The summary of this work is shown in figure 7.2.

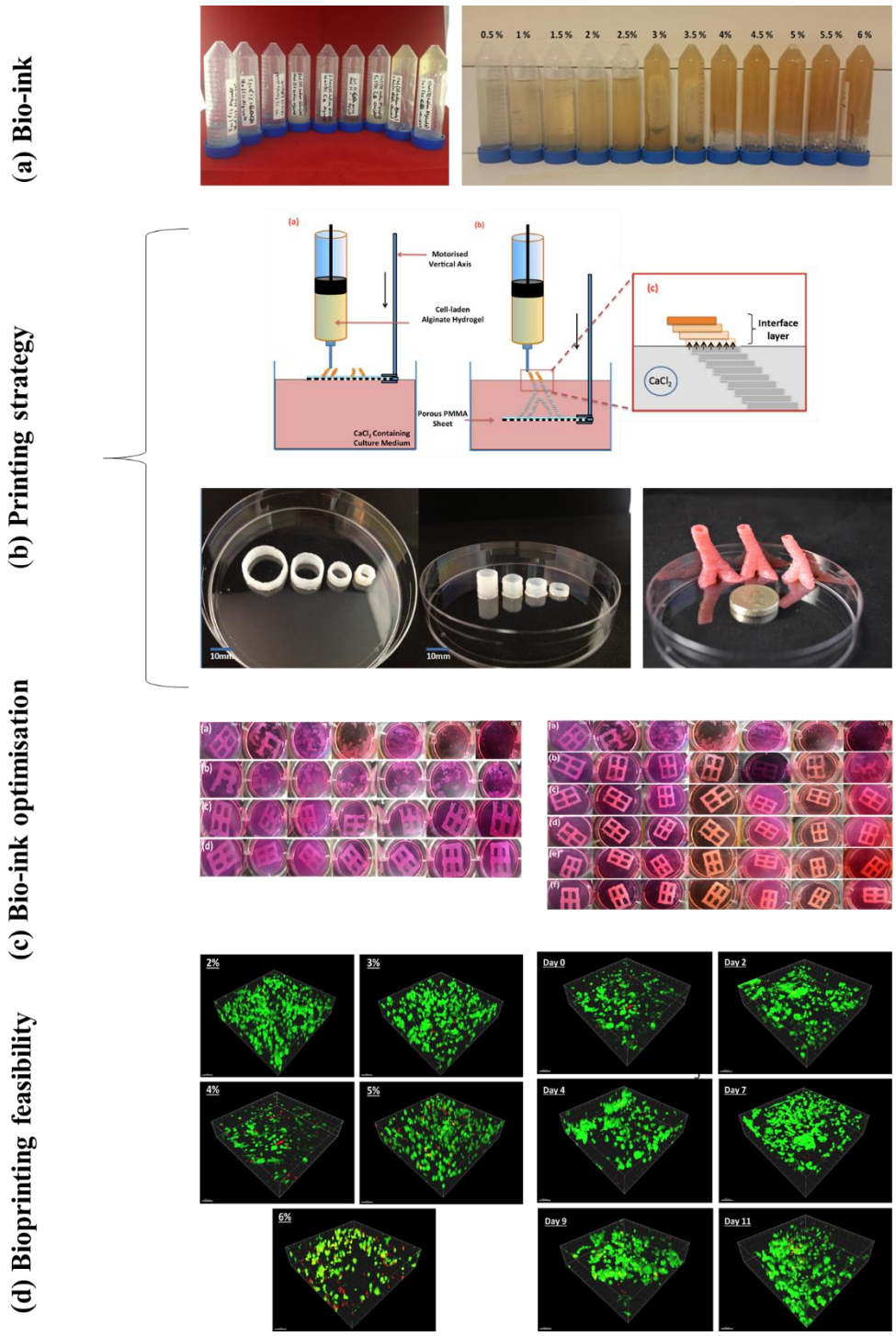

Figure 7.1 *– The completed milestones in order to bioprint live cells into a complex 3D structures while keeping the cell viability high over 10 days.*

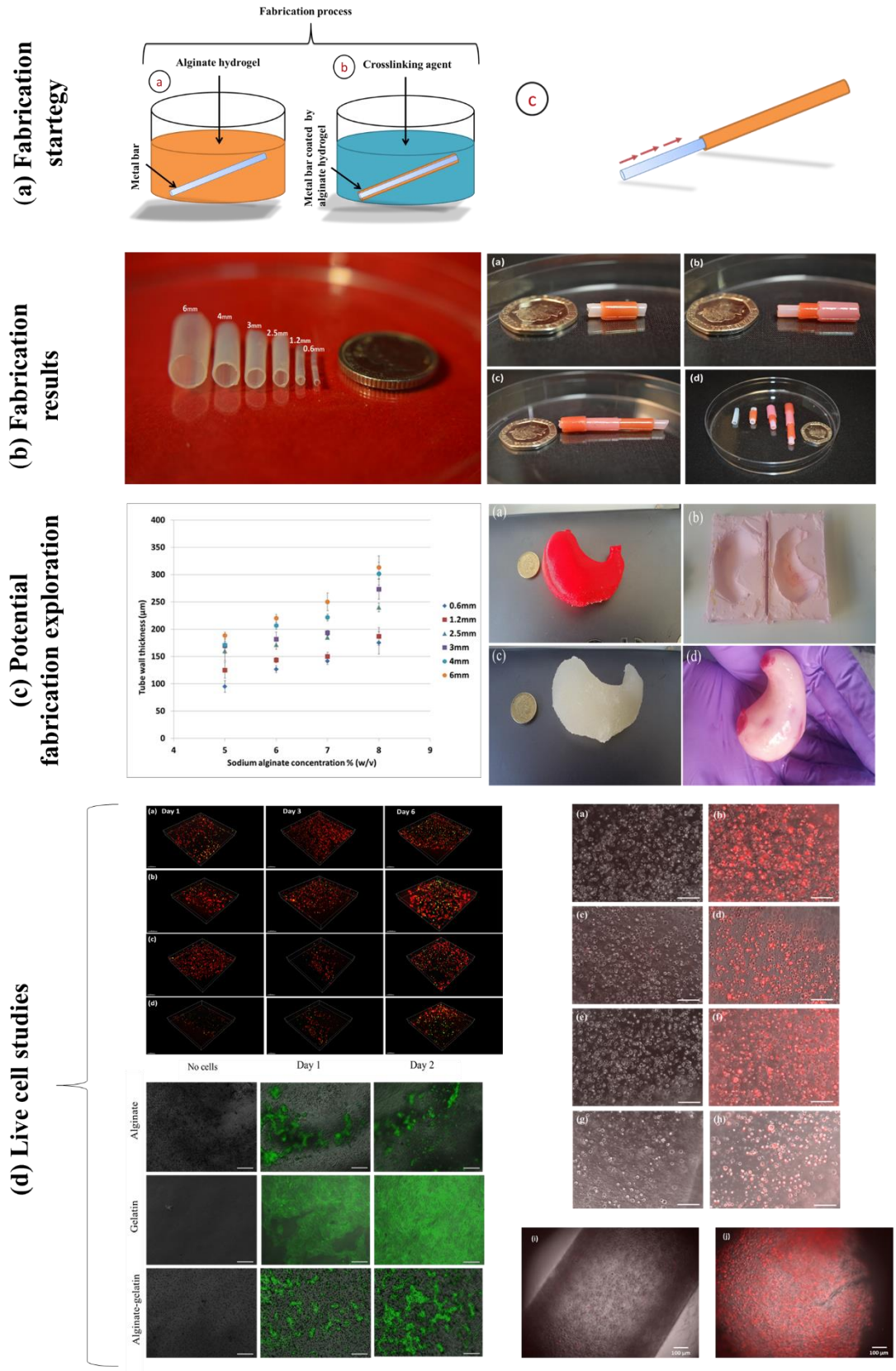

Figure 7.2 *– The completed milestones in order to validate a new rapid biofabrication approach to produce tubular and complex structures through dip-coating by keeping the cells viable and maintaining their normal function.*

Future work on bioprinting

Despite being capable of producing complex cell-laden hydrogels with both methods, there are several improvements needed to allow both methods to achieve their full capability to meet a variety of applications in tissue engineering. The recommendations for future improvements are as follows.

- The printing XYZ resolution needs to be improved. Structures with wall thicknesses smaller than 100 µm or even single cell resolution need to be printed in order to get closer to physiological conditions. To achieve this goal a smaller printing tip must be used; however the current bioprinter's X-Y-Z resolution is limited to 100 µm and therefore new step/servo motors are needed to replace the current servo motors. By decreasing the tip diameter, cells will be under a higher shear stress. Cell studies therefore need to be carried out to evaluate the significance of this change after bioprinting.

- Different types of alginate hydrogel with different molecular weights or even a different composition of alginate with other biomaterials such as gelatin, collagen and chitosan should be tested and printed in order to enhance the cell attachment to the gel and encourage faster cell proliferation within the gel. There is a wide range of alginate hydrogels available, with different viscosities and molecular weights. However, partial cross-linking studies of these hydrogels needs to be performed and printing configurations need to be fine-tuned and adjusted for each hydrogel.

- Despite the ability to co-print two types of hydrogels, cell studies were not carried in this instance. Therefore different cell types need to be printed and cell to cell interaction between the two cell types need to be investigated. The idea can simply be performed by printing two lines merging together each containing a different cell type. The addition of other print heads to make printing more than two cell types possible. The addition of different print heads such as a valve head could be helpful due to some cells being very sensitive to the bio-extrusion process, particularly stem cells.

Future work on rapid biofabrication via dip-coating

- The fabrication method is a manual process and automating the process would be helpful to the fabrication procedure to generate more precise tubular structures with reproducible results. Manual fabrication will encounter many human errors; automating the dip-coating process can minimise fabrication errors such as tube wall thickness variations. For example, by using a rotary system the wall thickness distribution can be even throughout the entire tubular structure.

- The bio-ink used for fabrication was limited to one type of alginate hydrogel. The use of other alginate hydrogels with different molecular weight could perhaps produce better results and lower concentrations of cross-linking reagents could be needed. Due to the different viscosities of these hydrogels the tube wall thickness could differ from the presented data and new studies must be carried out in this regard.

- Gelatine, collagen and gelatine nanofibres were used with alginate to investigate the cell behaviour in these compositions. Other biomaterials such a chitosan, different types of collagens and gelatines could be tested with alginate to produce better data and allow for comparison between compositions.

- Cell studies need to be carried out on the multi-layered tubular structure fabrication to understand cell to cell interactions between the layers, as this approach has the potential to generate or mimic blood vessels. For example, part of a blood vessel consists of fibroblast and smooth muscle cells; in theory these cells can be placed into two different layers by the dip-coating approach. The layers consisting of the smooth muscle cells can use alginate-gelatine hydrogel and endothelial cells can then be seeded in the inner wall to form monolayers on the surface. Also, a more systematic study into 3D complex fabrication protocol and cell studies is highly recommended. This may include the use of different hydrogels, mechanical testing and biocompatibility.